Title
Plant-Microbe-Mineral Interactions Control Carbon Persistence in Soil

Author
Neurath, Rachel Anne

Publication Date
2020

Peer reviewed|Thesis/dissertation

Plant-Microbe-Mineral Interactions Control Carbon Persistence in Soil

By

Rachel Anne Neurath

A dissertation submitted in partial satisfaction of the

requirements for the degree of

Doctor of Philosophy

in

Environmental Science, Policy, and Management

in the

Graduate Division

of the

University of California, Berkeley

Committee in charge:

Professor Mary K. Firestone, Chair
Professor Garrison Sposito
Dr. Jennifer Pett-Ridge

Summer 2020

Abstract

Plant-Microbe-Mineral Interactions Control Carbon Persistence in Soil

by

Rachel Anne Neurath

Doctor of Philosophy in Environmental Science, Policy, and Management

University of California, Berkeley

Professor Mary K. Firestone, Chair

Soils store more carbon (C) than the atmosphere and biosphere combined, yet the fundamental mechanisms that regulate this vast pool of C remain elusive. Soil C and associated organic molecules are critical to soil fertility, water holding capacity, and the global C balance. Plants, particularly plant roots, are the primary source of C in soil. The fate of that C depends largely on the composition and activity of the soil microbial community, which transforms and cycles C. However, when C associates with soil minerals or is isolated in soil aggregates, C may be physically protected. Mineral-associated C can be thousands of years old, but mineral-associated C can also rapidly turnover. We examined how interactions between plants, soil microbial communities, and minerals control the persistence of C in soil.

Plants release C into soil as rhizodeposits during plant growth. After plants die, detrital litter is incorporated into soil organic matter (OM). The rhizosphere, or zone of root influence, is a zone of dynamic release of low molecular weight C compounds and a hotspot of microbial activity. The detritosphere, which we define as soil with dead plant litter, has more chemically complex C substrates and a microbial community distinct from the rhizosphere. A typical mineral in planted surface soil likely experiences times when a root grows past, and after the plant senesces, the surrounding soil shifts from a rhizosphere zone to a detritosphere zone. In ecosystems with Mediterranean-type climates with distinct wet growing seasons and dry seasons with little plant growth, shifts from plant growth to plant decay are largely seasonal. The impact of oscillation between a rhizosphere-dominated system and a detritosphere-dominated system on mineral-associated C chemistry and persistence is unknown. We designed two experiments to compare between a rhizosphere-dominated system and a detritosphere-dominated system, with controls allowing comparison to bulk soil with no added plant C.

In both the rhizosphere and detritosphere, mineral type controlled total C accumulation. We placed quartz, ferrihydrite-coated quartz, and kaolinite specimen minerals in soil microcosms with ^{13}C-labeled *Avena barbata* rhizosphere soil, ^{13}C-labeled *A. barbata* litter detritosphere soil, and unlabeled bulk soil. These specimen minerals represent a range of surface reactivity and surface area, and had no detectable C at the start of the experiments. We also used a density-gradient centrifugation method to separate native minerals from the soil that already had associated C from the field. The specimen minerals provided a snapshot of a single season of

plant growth and decay, while the native minerals were a natural analog to minerals in the field. All specimen minerals accumulated C, but in the rhizosphere, the ferrihydrite accumulated the most C, while in the detritosphere, the kaolinite accumulated the most C by mineral mass. Mineral type mattered, but so did the C source. It was the interaction between the two that controlled the total quantity of C.

Carbon association with minerals was dynamic. Unlike the specimen minerals, native minerals did not significantly accumulate or lose total C in either the rhizosphere or detritosphere soil. However, we saw evidence for C exchange with these minerals, as well as with the specimen minerals, by comparing trends in C accumulation with ^{13}C enrichment. We detected no significant difference in total C between minerals incubated in the rhizosphere compared with those incubated in bulk soil, and between minerals incubated in the detritosphere compared with those incubated in bulk soil. In the rhizosphere, kaolinite minerals did not accumulate C after 1 month incubation, but the percent root-derived ^{13}C increased after 1 month. This suggests dynamic C exchange. Other evidence for dynamic C exchange in the rhizosphere were rapid changes in mineral-associated C chemistry and exchange of old C for ^{13}C labeled root-derived C on the native minerals, despite no significant change in total C. Based on a mixing model that determined what fraction of C on the minerals was from the growing roots, we calculated that C turnover on native minerals could be 6.0 mg C per g mineral per year or greater. In the detritosphere, we also see evidence for dynamic C exchange, but to a much lesser degree than in the rhizosphere. Based on a mixing model that determined what fraction of C on the minerals was from added litter, we calculate that C turnover on native minerals could be 0.2 mg C per g mineral per year or greater. While there was no significant treatment effect on total C, treatment did impact mineral-associated C chemistry.

Both C source (rhizosphere, detritosphere, or bulk soil) and mineral type interacted to define the composition of mineral-associated C. This was particularly evident at the microscale, which we analyzed with a combined NanoSIMS-STXM/NEXAFS approach. We also found that mineral size, morphology, and ability to form microaggregates, in addition to mineral surface reactivity, influenced mineral-associated C chemistry. In the detritosphere, microaggregate formation may play a particularly important role in protecting litter that is only marginally degraded, including litter-derived C compounds such as phenolic C. We found that a portion of all mineral-associated C was lipids.

Lipid classes varied by both mineral type and C source. Lipidomic analysis suggested that many of these lipids were microbial, particularly fungal storage lipids and microbial membrane lipids. Evidence suggested that the lipid-rich fungal order *Mucorales* and bacterial order *Streptomyces* may play an important role in mineral-associated lipid formation. In the rhizosphere, fungal hyphae, likely arbuscular mycorrhizal fungi (AMF), acted as a conduit of root-derived C to the minerals, accounting for a significant fraction of total ^{13}C associated with the minerals.

We found that it was the interaction of plant C source, microbial community, and mineral type that ultimately controlled the fate and potential persistence of mineral-associated C. While we observed similar trends in the rhizosphere and detritosphere, such as the importance of mineral type and evidence of dynamic C association, we also found important distinctions between the two systems. In the rhizosphere, we see evidence for rapid exchange of C with minerals in the

presence of a growing root. Here, minerals with high surface reactivity, such as ferrihydrite, may accumulate more C because they lose less C. Other minerals with lower surface reactivity may lose more C due to microbial degradation and reaction with organic acids from the root. While adjacent to a growing root, the chemistry of mineral-associated C shifts to more oxidized C characteristic of microbially-processed compounds, reflecting the high microbial activity of the rhizosphere. In the detritosphere, C exchange with minerals appears slower. Aggregation was important in determining both total C and chemistry, particularly for kaolinite. If a new root grew by a mineral, we expect that any C not strongly bound chemically or physically through aggregation may be more likely to exchange with new root-derived C. Certain microbial orders may play an important role in impacting the fate of C. AMF, as conduits of root-derived C to mineral, and lipid-rich microbes such as the fungal order *Mucorales* and the bacterial order *Streptomyces*, show promise to enhance C association and persistence on minerals. The temporal and spatial oscillation between bulk, rhizosphere, and detritosphere soil in natural surface soil systems necessitates a holistic view of C contribution from different sources, and the resulting microbe-mineral interactions that control C fate and persistence.

This dissertation is dedicated to my daughter, Esme

Table of Contents

Introduction

The dynamics that control carbon (C) turnover govern the storage capacity of soil, which holds more C than the atmosphere and biosphere combined. As anthropogenic C emissions increase the atmospheric greenhouse gases that drive climate change, an enigmatic question emerges: *can soils offset climate change by storing more C?* To approach this question, we must better understand the mechanisms of soil C storage and persistence.

Plant roots are the dominant source of C in soil, allocating C captured from the atmosphere to the soil. Roots may release C during active growth, primarily as low molecular weight organic compounds, or after death as detrital root litter. Soil microorganisms are the primary drivers of C transformation in soils, consuming and breaking down plant-derived C. Microbial community composition and functional capacity may have important implications for the rate and type of C transformations. When microbes die, microbial "necromass" is incorporated into soil organic matter (OM). It is possible that compositional differences in microbial bodies may lead to chemically distinct OM. Soil OM, including necromass, as well as living microbes, may associate with soil minerals. A portion of this mineral-associated C persists for thousands of years, but recent work shows that not all mineral-associated C is protected. Why some mineral-associated C persists and some does not remains a central question in the field of soil C dynamics, and has important implications for climate change prediction and management, as well as soil fertility and microbial community ecology.

Traditionally, studies of soil OM association with minerals examine the transformation and association of plant litter. More recently, the importance of the rhizosphere, or zone of root influence, has come into focus. In most surface soils, particularly grassland and agricultural soils, the environment experienced by an individual mineral likely periodically changes from a rhizosphere-dominated system when a root is growing past, to a detritosphere-dominated system as that root dies and root litter begins to decompose. The oscillation between rhizosphere-dominated and detritosphere-dominated is particularly pronounced in ecosystems with distinct growing seasons, such as a grassland in a Mediterranean-type climate. In the growing season, a large fraction of surface soil may be in the rhizosphere, but in the summer, annual grasses senesce, and the soil is dominantly a detritosphere system. The impact of random and/or seasonal oscillation between a rhizosphere-dominated system and a detritosphere-dominated system on mineral-associated C chemistry and persistence is unknown.

In Chapter 1, we modeled the rhizosphere with soil microcosms planted with *Avena barbata*. Along the root face, we placed bags of four mineral types chosen both because they were the dominant mineral types in our soil and also because they represented a spectrum of surface areas and reactivities. We placed the same mineral types in unplanted control microcosms to represent the bulk soil. We labeled the microcosms with $^{13}CO_2$ to trace the fate of ^{13}C that was photosynthesized by the plant and transferred to the soil system. Our objectives were (1) to determine the influence of active roots on soil OM association with mineral surfaces, (2) to determine the influence of mineral type, and (3) to explore the role of microorganisms in transformation of mineral-associated OM.

In Chapter 2, we focused on the detritosphere, looking at what has been hypothesized as a critical period for C movement and transformation within soil: wet-up. In a Mediterranean-type climate, the first rainfall after a months-long dry season, called wet-up, causes a sudden dramatic increase in soil water potential, microbial resuscitation and activity, and CO_2 release from the soil. Focusing on the wet up period immediately following a long summer drought allows us to explore C transformation and fate from decomposing litter in the absence of growing roots. We examined how (i) mineral type, and (ii) the presence of root litter influenced microbial colonization of minerals and mineral-OM associations.

In Chapter 3, we examined soil minerals at the nano- to microscale to look at the heterogeneity and spatial distribution of mineral-associated C in the rhizosphere and detritosphere. Rhizosphere minerals were selected from the 2 month harvest in the rhizosphere experiment in Chapter 1. Detritosphere minerals were selected from the 3 month harvest in the detritosphere experiment in Chapter 2. The detritosphere minerals were the same four mineral types used in Chapter 1, but here they were placed in soil microcosms with ^{13}C labeled *Avena barbata* root litter. As in the rhizosphere experiment, we also placed minerals in a bulk soil control with no ^{13}C label. Using a coupled NanoSIMS-STXM/NEXAFS approach, we sought to trace the distribution of plant-derived ^{13}C on minerals and determine whether that ^{13}C was transformed en route to the mineral surface. We sought to answer (i) how a microscale view of mineral-OM heterogeneity differed from a bulk analysis of mineral-OM, (ii) whether ^{13}C root-derived C underwent transformation prior to association with minerals, and (iii) how the composition of mineral-associated C varied between the rhizosphere and detritosphere.

Acknowledgements

My dissertation is the product of the wisdom and support of a large group of mentors, colleagues, friends, and family. First, my major professor and chair of my dissertation committee, Mary Firestone, thank you for accepting a geologist with no microbiology experience in your lab. I do not know how I could have done it without your guidance and support along the way. Your ability to ask just the right question, drawing on an impressive depth and breadth of knowledge, has shown me science at its very best. I feel profoundly lucky for the privilege of working with you. It has been a long and winding path to get my PhD, and I am grateful you always believed in me. I can only hope that as I move forward as a scientist, I can bring forward what I have learned from you.

Jennifer Pett-Ridge, thank you for your encouragement early on in my PhD, and for your wonderful mentorship as a Lawrence Graduate Scholar for four years and beyond. I learned so much working with you. Thank you for making me a better scientist and a better writer.

Peter Nico, I could not have written the third chapter of my dissertation without your guidance and expertise. Thank you for teaching me everything I know about STXM/NEXAFS. Your geochemical expertise not only strengthened my dissertation, but also helped cultivate my interest in soil chemistry, which I am excited to continue to pursue as a postdoc.

Gary Sposito, thank you for your wisdom as chair of my qualification committee and your mentorship throughout my dissertation. Your work on the chemistry of soils provided an invaluable foundation for my dissertation research, and I appreciate all your advice along the way. Thank you, also, to Celine Pallud for your advice and guidance on my qualification committee.

I would not be here without the amazing support of the Firestone Lab. Thank you, in particular, to Ilexis Jacoby, Rina Estera, and Don Herman. You have all helped so much not only with the complex logistics of running two huge experiments, but also as incredible wells of wisdom and advice. To my fellow graduate students, postdocs, and former Firestoners, thank you for all your support and camaraderie, Evan Starr, Heejung Cho, Anne Kakouridis, Alexa Nicolas, Yoni Sher, Nameer Baker, Sarah Baker, Ella Sieradzki, Alex Greenlon, and Shengjing Shi. Thank you to the former undergraduates who helped me with my research, and for the great fun of being your mentor, Ilexis Jacoby, Divya Raghu, and Evan Layefsky.

It was a real privilege to work as a Lawrence Graduate Scholar at Lawrence Livermore National Laboratory during my PhD. Thank you to Peter Weber for sharing your knowledge and enthusiasm for NanoSIMS. Christy Ramon, thank you not only for all your logistical support, but also for always asking how I was doing. Thank you for the carpools and NanoSIMS advice, Xavier Mayali and Erin Nuccio. Thank you to Dinesh Adhikari for your help with STXM analysis.

I had the opportunity to work with incredibly talented and knowledgeable scientists at Lawrence Berkeley National Laboratory and the Pacific Northwest National Laboratory during my PhD.

Thank you to Amrita Bhattacharyya for helping teach me how to do STXM analysis, for the long nights at the ALS beamlines, and for your friendship. Thank you to the dedicated beamline scientists, Matthew Marcus and Hendrik Ohldag. Thank you, Andrew Lipton, for taking the time to teach me about ^{13}C-NMR and helping host my visit at PNNL. Thank you to everyone at PNNL who helped me with FTICR-MS analysis: Malak Tfaily, Ljiljana Pasa-Tolic, Allison Thompson, and Rosalie Chu. Thank you Jennifer Kyle for all your help with lipidomic analysis.

Thank you to all my professors and mentors who helped guide me and shape me as a scientist before I started my PhD. Bob Newton at Smith College, thank you for getting me started on this journey. The lessons you taught me as an undergraduate are still the most vivid, and I'll never forget how supported I felt when you spent hours helping me practice for my first scientific conference. Joop Varekamp at Wesleyan University and Lisa Gilbert at Williams College, thank you for the opportunity to conduct such exciting research as an undergraduate. Andy Friedland at Dartmouth College, thank you for getting me hooked on soils during my masters' research. It was really the foundation for the questions I pursued in my dissertation. Thank you for all your encouragement and support.

I am extraordinarily lucky to have an incredible family who have been so supportive throughout my dissertation, as in my whole life. Thank you to my parents, Karen and Paul, for your constant love and encouragement, and for always fostering my curiosity. Thank you to my amazing sister, Sarah, for your support and creative perspective. Thank you to my grandparents, Connie and Bob, for your unfailing love, and for teaching me at a very young age, while I sat at your kitchen table by a poster of the periodic table, that everything is made of chemicals. Thank you to my wonderful parents-in-law, Kathy and Jeff, for welcoming me into your family. And thank you to Claire and Natasha, who have been the most incredible friends since we were six years old.

Above all, thank you to my husband, Jesse, and our daughter, Esme. Jesse, it is hard to believe we met at the start of my PhD. I would not be here without your love, support, and of course your sense of humor. Esme, you amaze me every day. My love for you two is infinite…and increasing.

1

Root carbon interaction with soil minerals is dynamic, leaving a legacy of microbially-derived lipids

1.1 ABSTRACT

Minerals bind the oldest, most persistent soil carbon and mineral characteristics appear to play a critical role in soil organic matter (SOM) association. We hypothesized that carbon source and soil microorganisms (the transformers of SOM) also influence mineral-SOM associations. We incubated permeable bags of minerals in soil microcosms with and without plant roots (*Avena barbata*). Mineral bags contained quartz, ferrihydrite, kaolinite, or native soil minerals isolated as the heavy fraction of a density gradient separation. We followed plant-derived C by growing plants in $^{13}CO_2$; soil microcosms were harvested at three plant growth stages, after which, we analyzed total carbon, ^{13}C, and carbon chemistry (^{13}C-NMR, FTICR-MS, and lipidomics). While C accumulation was rapid and mineral-dependent, the amount that accumulated was not significantly affected by the plant treatment. However, the rhizosphere left a distinct legacy on the chemistry of the mineral-associated SOM. Minerals incubated in the rhizosphere were associated with a more diverse array of compounds from different C functional groups (carbonyl, aromatics, carbohydrates, lipids) than those in the bulk soil C. However, these diverse rhizosphere-derived compounds may represent a "transient fraction" of mineral SOM, more rapidly exchanging with minerals. Our work suggests that lipids may persist on minerals, and most of these lipids are microbially derived with a large fraction of fungal lipids.

1.2 INTRODUCTION

Plant roots are the primary mediators of C transfer into soil (Finzi et al. 2015, Paul 2016, Sokol et al. 2019a), allocating C captured from the atmosphere to the soil system (Kuzyakov and Domanski 2000). Root C is then transformed within the soil, where it may be respired back to the atmosphere or stored as soil organic matter (SOM) (Rasse et al. 2005). Association with soil minerals offer a degree of protection for SOM (Torn et al. 1997, Trumbore 2000, Kogel-Knabner et al. 2008, Schmidt et al. 2011, Kleber et al. 2015b), however the residence time of this SOM varies widely (Heckman et al. 2018b), due to a complex interplay of soil processes(Bailey et al. 2019). Why some mineral-associated C persists and some does not is a central question in the field of soil C dynamics (Stockmann et al. 2013), with important implications for soil health, fertility, and microbial community ecology (Lal 2004a, b, Schimel and Schaeffer 2012, Tang and Riley 2015).

In grassland ecosystems, most surface soils are periodically or continually in the zone of root influence, or rhizosphere (Gregory 2006). As plant roots transfer organic compounds to the soil, the fate of this C is determined by (i) microbial community composition and activity (Schimel and Schaeffer 2012, Cotrufo et al. 2013, Dwivedi et al. 2017), (ii) the chemical form of the C (Kleber 2010), (iii) where within the soil physical environment it is located (Dungait et al. 2012), and (iv) the soil mineral sorption capacity (Dwivedi et al. 2017, Creamer et al. 2019). Affecting all of these is proximity to the root itself. More than just a C source, root growth physically and

chemically alters the soil environment (Roose and Fowler 2004, Roose and Schnepf 2008), with implications for the fate of soil C.

The rhizosphere is the nexus of plant-soil-microbe interactions (Hinsinger et al. 2009, Philippot et al. 2013). Plant roots exude of a diverse array of C substrates (Lynch and Whipps 1990, Bertin et al. 2003, Farrar et al. 2003, Jones et al. 2009, Finzi et al. 2015, Zhalnina et al. 2018). These substrates can associate with minerals (e.g. ligand exchange, van der Waals, ionic bridging, co-precipitation and complexation, hydrophobic interactions (Kleber et al. 2007, Sposito 2008)), but many root exudates are rapidly metabolized and transformed by microorganisms (Schweinsberg-Mickan et al. 2012, Kaiser et al. 2015). Microorganisms also interact with minerals, associating with mineral surfaces for protection from predation and desiccation, access to nutrients and energy sources, and as a platform for biofilm formation (Ehrlich 1996, Banfield Jillian and Hamers Robert 1997, Banfield et al. 1999, Uroz et al. 2009, Hutchens et al. 2010, Kleber et al. 2015a, Uroz et al. 2015). These microorganisms transform SOM directly via metabolic activity or indirectly via microbial byproducts and microbial alteration of the soil physiochemical environment (Six et al. 2006). Microorganisms not only transform SOM, which may become mineral-associated, but are also themselves a part of that mineral-associated SOM (Kallenbach et al. 2016, Creamer et al. 2019, Sokol et al. 2019b).

The rhizosphere is dynamic and complex and harbors a rhizosphere microbial community that is distinct from that of the bulk soil (Philippot et al. 2013, Kuzyakov and Blagodatskaya 2015), less phylogenetically diverse but more active. Rhizosphere microbial communities are interconnected and undergo succession through the plant growing season (Philippot et al. 2013, Shi et al. 2015b, Nuccio et al. 2016, Shi et al. 2016). While plant growth provides a C source and stimulates microbial activity (Shi et al. 2011, Shi et al. 2015b), root production of organic acids, such as oxalic acid, can release organo-metal complexes from minerals surfaces (Keiluweit et al. 2015). Thus, roots influence both C association with minerals and also C loss from minerals. We hypothesized that plant growth results in altered composition and quantity of mineral-associated SOM. However, the influence of mineral type on mineral-associated SOM quantity (Torn et al. 1997), composition (Kaiser et al. 2012), and persistence (Kleber et al. 2005, Mikutta et al. 2006, Kleber 2010, Torn et al. 2013, Kleber et al. 2015b) is well-documented. We expect that any plant-growth influence would take place in the context of these mineral influences.

In soil microcosms, we incubated four mineral types to represent a spectra of surface areas and reactivities. These minerals were placed in soil microcosms with or without (bulk soil control) a growing *Avena barbata* rhizosphere for a single growing season (2.5 months). All microcosms were incubated in a chamber with labeled $^{13}CO_2$ to trace the fate of plant-derived C. Our objectives were (1) to determine the influence of active roots on SOM association with mineral surfaces, (2) to determine the influence of mineral type on the quantity and composition of mineral-associated SOM, and (3) to explore the role of microorganisms in transformation of mineral-associated SOM. We found that while mineral type drove the total quantity of mineral-associated SOM, it was the combined effect of mineral type and exposure to root growth that defined the chemical composition of mineral-associated SOM.

1.3 MATERIALS AND METHODS

1.3.1 Experimental Design

The study soil and plant type were chosen to represent a typical Mediterranean-type grassland ecosystem, with a fertile Alfisol soil and the slender oat grass *Avena barbata*. Both the soil and *A. barbata* seeds used in the soil microcosms were collected from Little Buck Field (38.992938° N, 123.067714° W) at the Hopland Research and Extension Center (HREC), Hopland, CA, in March, 2014, just before the start of the California summer dry season. This field site is well characterized (Sudderth et al. 2012), and the microbial community has been studied in numerous experiments (Shi et al. 2011, Shi et al. 2015b, Nuccio et al. 2016, Shi et al. 2016, Starr et al. 2018, Starr et al. 2019, Nuccio et al. 2020, Pett-Ridge et al. 2020 (in press)). The soil, a fine-loamy, mixed, active, mesic Typic Haploxeralf (Sudderth et al. 2012), was sieved to <2 mm in the field, dried to 1.1 VWC, and stored at 4°C. Field soil had a field bulk density of 1.2 g-cm-3, a pH of 5.36 ± 0.03 (n = 10), and 23.27 ± 2.28 mg-g^{-1} (n = 3) total carbon (C). The soil mineralogy was dominated by quartz, ferrihydrite, and kaolinite with some feldspar and mica (**SI Methods**). *A. barbata*, a naturalized species of slender oat grass, is the dominant grass in Little Buck Field, a managed pasture that is regularly grazed by sheep. Seeds were collected in the field, dried, and scarified before germination.

Microcosms (2.9 x 11.5 x 25.3 cm) were filled with soil to field bulk density (1.2 g-cm^{-3}) (**SI Figure 1.1**). Before filling the microcosms, perforated tubing was inserted along one face of the microcosm (**SI Figure 1.1a**) to allow for even watering in the soil and in 12 microcosms, a volumetric water content (VWC) sensor (Decagon, EC5) was buried at approximately 10 cm depth. Along the opposite face of the microcosm, a 2 mm width sidecar panel was inserted to keep that area of the microcosm free of soil and roots. We had two treatment types: (1) a *rhizosphere treatment*, with actively growing *A. barbata* planted in the soil microcosm, and (2) a *bulk soil treatment*, which was left unplanted. For the rhizosphere treatment, four germinated *A. barbata* seedlings were planted in each microcosm, simulating field density (**SI Figure 1.1b**). Microcosms were then tilted at 45°, with the sidecar facing downward, for one month (**SI Figure 1.1c-d**). Due to the geotropism, roots grew along the sidecar panel face (**SI Figure 1.1e**). During this time, VWC was maintained at 14%, the average for Hopland soil during the growing season, using an automated watering system.

After one month of plant growth, microcosms were opened along the sidecar face and the sidecar panel was removed, leaving a 2 mm gap. Nylon mesh bags (18 μm mesh, 5 x 5 x 0.2 cm dimensions) were filled with one of four mineral types: quartz sand ("Quartz"), ferrihydrite-coated quartz sand ("Ferrihydrite"), 50:50 by mass mixture kaolinite and quartz sand ("Kaolinite"), or the heavy density fraction (>1.75 g-cm^{-1}) ("Native Minerals") of Hopland soil (**Figure 1.1, SI Fig. 1.1f**). Mineral preparation is described in the **SI Methods**. The minerals added reflect the dominant mineral types present at our field site (determined by XRD, see **SI Methods**). All but the "Native Minerals" were specimen minerals. The Native Minerals were density fractionated from field soil. We mixed kaolinite with quartz to prevent formation of large kaolinite aggregates and allow more permeability than pure kaolinite alone. Additionally, SEM imaging revealed that in the heavy density fraction, most kaolinite was associated with larger minerals that resembled quartz, rather than isolated. As described in the **SI Methods**, our ferrihydrite preparation also was designed to more closely represent a ferrihydrite coating in natural samples. We added trace amounts of aluminum and silicon and aged the synthesized

ferrihydrite slurry before coating the quartz. Each mineral bag was filled to field bulk density for Little Buck Field. The mineral types selected represent a range of surface area and reactivity, from quartz with low surface area and low reactivity to kaolinite with high surface area and moderate surface reactivity to ferrihydrite, an amorphous iron oxy-hydroxide, with moderate surface area and high surface reactivity (**SI Table 1.1**).

Mineral bags were harvested after 1, 2, and 2.5 months incubation, at which point *A. barbata* had reached senescence (**Figure 1.1, Supp. Fig. 1.1g**). At harvest, both minerals and soil were weighed, dried (65°C), and weighed again to obtain soil moisture content. Plant biomass was also weighed and dried. Five microcosms were selected from each harvest timepoint for analysis. Minerals from these microcosms, along with soil, were subdivided and the portion for DNA extraction was removed (Whitman et al. 2018). The dried minerals and soil were stored at 4°C until analysis.

1.3.2 Total C and Isotope Ratio Mass Spectrometry

To measure total C accumulation on mineral surfaces, bulk soil and in roots, we used Elemental Analysis (EA) coupled to an IsoPrime 100 Isotope Ratio Mass Spectrometer (IRMS) (Isoprime Ltd, Cheadle Hulme, UK), to measure total C and N simultaneously with ^{13}C. Peach leaf standards (NIST SRM 1547) were run to ensure accuracy and duplicates for precision. Samples were then analyzed for ^{13}C enrichment through IRMS. *Avena fatua* roots, labeled with a range of ^{13}C atom%, were ground and used as additional IRMS standards.

1.3.3 Scanning Electron Microscopy and BET Surface Area

Minerals were imaged using Scanning Transmission Electron Microscopy (SEM) at Lawrence Livermore National Laboratory (FEI, Inspect F) before and after incubation in soil microcosms. Mineral samples were mounted and gold-coated before imaging. Images were acquired at 5 kV energy. The surface area of the minerals was determined before and after incubation in soil microcosms by Brunauer-Emmett-Teller (BET) analysis with N_2 gas at Lawrence Berkeley National Laboratory.

1.3.4 ^{13}C-Nuclear Magnetic Resonance Mass Spectrometry

Major chemical classes of mineral-associated organic matter were identified by ^{13}C-Nuclear Magnetic Resonance Mass Spectrometry. Finely ground samples were packed in a 5 mm optical density ceramic rotor and analyzed on 500 MHz solid-state ^{13}C-NMR (Oxford) at the Environmental Molecular Sciences Laboratory (EMSL) at the Pacific Northwest National Laboratory (PNNL). Standards of potassium bromide and Adamantine were run at 5,000 Hz. Next, a soil standard, "Pahokee Peat" (IHSS, Standard Sample), collected from Florida and sieved to <53 μm, was run. The low C concentrations on our samples required long ^{13}C-NMR experiments, thus we ran pooled samples (n=3) for each minerals type rather than replicates. Due to the interference of iron in the Ferrihydrite and a low signal-to-noise ratio in the Quartz, we were unable to obtain suitable ^{13}C-NMR spectra from those mineral types (**SI Figure 4)**.

1.3.5 Fourier Transform Ion Cyclotron Resonance Mass Spectrometry and Lipidomics

FTICR-MS and lipidomics analysis of mineral samples extracted with water (FTICR-MS) and then chloroform/methanol (lipidomics (Tfaily et al. 2019)) was conducted at the Environmental Molecular Sciences Laboratory (EMSL). Analyses were conducted on dried mineral samples

from the 2-month time point. We ran 3 biological replicates of each sample. Total lipid extracts were analyzed in both positive and negative modes, and lipids were fragmented using higher-energy collision dissociation and collision-induced dissociation. Confident lipid identifications were made using LIQUID (Lipid Quantitation and Identification) (Kyle et al. 2017). Aligned features were manually verified and peak apex intensity values were exported for statistical analysis. Identified lipids were selected by manually evaluating the MS/MS spectra for diagnostic and corresponding acyl chain fragment ions. In addition, the precursor isotopic profile, extracted ion chromatogram, and mass measurement error along with the elution time were evaluated. All LC-MS/MS runs were aligned and gap-filled using the identified lipid name, observed m/z, and the retention time using MZmine 2 (Pluskal et al. 2010). Each ionization type was aligned and gap-filled separately. Aligned features were manually verified and peak apex intensity values were exported for statistical analysis.

1.3.6 Sequential Extraction

To characterize the bonds between mineral surfaces and associated SOM, we performed a series of sequential extractions, adapted from Heckman *et al.* (Heckman et al. 2018a): (1) a water extraction was used to remove weakly mineral-associated soluble SOM (e.g. Van der Waals, dipole-dipole forces); (2) 0.1 M tetra-sodium pyrophosphate extraction (Ross and Wang 1993) for organic-metal complexes and base soluble C; and (3) 0.25 M hydroxylamine (Ross and Wang 1993, Courchesne and Turmel 2008) for non-crystalline and poorly crystalline iron and aluminum and associated C. We conducted sequential extractions on 3 biological replicates of each sample. For the sequential extractions, 40 mL extraction reagent was added to 3 g mineral sample, vortexed, shaken overnight, centrifuged and the supernatant decanted and passed through a 0.2 μm Whatman GX/D syringe filter. The residual minerals were rinsed with sterilized MiliQ water three times. The filtered supernatant was analyzed by ICP-MS (Perkin-Elmer Elan DRC II). Oven dried minerals were analyzed for total C and ^{13}C by EA and IRMS as described above.

1.3.7 Mixing Model

To calculate the relative contribution of total C on mineral surfaces from the actively growing *A. barbata* plant, we used a mixing model (**Eq. 1.1**). In our mixing model, the two pools of C were the *A. barbata* root and the bulk soil:

$$E_M = E_R \cdot f_R + E_B \cdot f_B \qquad \textbf{Eq. 1.1}$$

Where E_M is the atom% enrichment of the mineral, E_R is the atom% enrichment derived from the *A. barbata* root, f_R is the fraction of C from the root, E_B is the atom% enrichment derived from the bulk soil, and f_B is the fraction of C from the bulk soil. In our equation, $f_R + f_B = 1$.

Bulk soil had a natural abundance ^{13}C of 1.074 ± 0.001 atom%. Plant roots were pooled, ground, and analyzed by IRMS to calculate an average enrichment of 7.191 ± 0.398 SE atom% ^{13}C.

1.3.8 Statistics

Carbon concentrations are reported with standard error (n=5). We used a partially-nested mixed effects model according to Doncaster and Davey (Doncaster and Davey 2007) to analyze the total C results and IRMS results. We conducted analysis of variance (ANOVA) on these data,

using the nlme package(Pinheiro et al. 2019) in R v.3.5.1 (R Core Team, 2018) on log-transformed data to maintain assumptions of normality. To conduct pairwise comparisons, we used the emmeans package (Lenth 2019) in R. We performed non-metric multidimensional scaling (NMDS) analysis using presence/absence data and Jaccard distances on FTICR-MS data to determine group differences in R using the package ftmsRanalysis (Bramer and White 2018). To determine whether the differences illustrated in the NMDS plot were significant, we ran a permutational multivariate ANOVA (PERMANOVA) analysis in R using the adonis function in the vegan package(Oksanen et al. 2019). We performed principal coordinate analysis (PCoA) with a Bray-Curtis dissimilarity matrix on the lipidomic data to determine sub-class differences in R using the vegan package (Oksanen et al. 2019). To determine whether the differences in the PCoA plot were significant, we ran a PERMANOVA analysis in R using the adonis function in the vegan package(Oksanen et al. 2019).

1.4 RESULTS AND DISCUSSION

1.4.1 Mineral type controls total C accumulation on minerals

All specimen minerals (Quartz, Kaolinite, and Ferrihydrite) had no detectable C prior to incubation. Carbon accumulated on all specimen mineral types in all treatments (**Figure 1.2 a, SI Fig. 1.3**). In SEM images, we see visual evidence of C accumulation on minerals (**SI Fig. 1.2**). This C accumulation was rapid; the majority of C association with minerals occurred in the first month. While total C associated with kaolinite and quartz leveled off at 1mo incubation, the enrichment of the C (atm%) associated with the minerals continued to increase until 2 to 2.5 months. Total C concentration varied significantly by mineral type ($p<0.0001$). When expressed as total C per gram mineral, the most C was associated with Ferrihydrite (1.3 ± 0.3 mg C- g^{-1} for rhizosphere at 2.5 months) (**Figure 1.1a**). However, when normalized to BET-measured surface area (**SI Table 1.1**), Quartz had the highest concentration of total C per square meter mineral surface (11.4 ± 1.6 mg C- m^{-2} for rhizosphere at 2.5 months) (**SI Figures 1.3-4**). This near reversal in trend reveals an important distinction in how measured total C is presented. Here, we focus on total C per gram mineral. We did not find a significant plant vs. bulk treatment effect for total C across all minerals ($p=0.250$) (**SI Figure 1.4**).

Carbon concentrations on specimen minerals were more than an order of magnitude lower than the Native Minerals, with an average total C of 0.6 ± 0.1 mg C- g^{-1} for the specimen minerals in the rhizosphere versus 17.0 ± 1.0 mg C- g^{-1} for the Native Minerals (**SI Figure 1.4**). For our specimen minerals (Quartz, Ferrihydrite, and Kaolinite), we assume at the end of the growing season, we are far from "carbon saturation" (Six et al. 2002, Stewart et al. 2007, Castellano et al. 2015). Considering that the Native Minerals have likely resided in the soil for thousands of years or more (Baisden et al. 2002), the C concentrations on the specimen minerals suggest that C accumulation over time is rapid on fresh mineral surfaces, but slows down over time. Indeed, in the short 2.5 months of our study, we observed a linear rate of C accumulation on Ferrihydrite. Quartz and Kaolinite minerals had rapid initial C accumulation followed by a leveling off. The Native Minerals did not accumulate a significant amount of additional total C in either rhizosphere or bulk soil treatment compared with their initial total C concentration ($p = 0.101$). Our study observes a single plant growing season, and therefore offers critical snapshot of C accumulation and exchange on a mineral surface.

Rhizosphere-derived C contributed a significant portion of the C on mineral surfaces (21.2% ± 5.5% for Ferrihydrite, 42.6% ± 4.6% for Kaolinite, and 13.9% ± 3.4% for Quartz at 2.5 months, and 6.2% ± 0.4% for the Native Minerals at 2 months) based on a ^{13}C mixing model (**Eq. 1.1**). However, the rhizosphere treatment had no significant effect on total C present on the minerals. Thus over the timescale of a single plant growing season, while there was evidence of plant-derived C on the minerals based on ^{13}C tracing, the addition of root C to the microcosms did not result in more total C on the minerals, as compared to minerals incubated in the bulk soil. This finding suggests the importance of considering not only C association with minerals, but also C desorption. When assessing the persistence of mineral-associated C, the interaction of C on and C off the minerals is a critical variable.

A possible explanation for the absence of a rhizosphere effect on total C is that, while the total C stock is the same, the fluxes of C are different. To illustrate, the stock of mineral associated C at time *t,* ($\boldsymbol{M_t}$), is equal to the stock of mineral associated C at time zero, ($\boldsymbol{M_0}$), plus the amount sorbed during time interval Δt, ($\boldsymbol{\Delta t \cdot S_t}$), minus the amount desorbed during time interval Δt, ($\boldsymbol{\Delta t \cdot D_t}$):

$$\boldsymbol{M_t = M_0 + \Delta t(S_t - D_t)} \qquad \textbf{Eq. 1.2}$$

where:

M_t = *stock of mineral C at time interval t*

M_0 = *stock of mineral C at time 0*

$\Delta t \cdot S_t$ = *sorption flux* S_t *at time interval* Δt

where:

$S_t = S_{t1} + S_{t2+} \ldots + S_{tx}$

S_{tx} = *sorption of C compound x*

$\Delta t \cdot D_t$ = *desorption flux* D_t *at time interval* Δt

where:

$D_t = D_{t1} + D_{t2+} \ldots + D_{tx}$

D_{tx} = *desorption of C compound x*

In our proposed equation, a modification of the classic mass-balance expression for net adsorption (See Eq. 8.8 (Sposito 2008)), $\boldsymbol{\Delta t \cdot S_t}$, is the aggregate of the sorption for each C compound that associates with the mineral, $\boldsymbol{S_{tx}}$. Then $\boldsymbol{\Delta t \cdot D_t}$, is the aggregate of the desorption for each C compound that associates with the mineral, $\boldsymbol{D_{tx}}$. The $\boldsymbol{S_{tx}}$ of a particular compound - for example, lipids - may not be the same as the $\boldsymbol{D_{tx}}$ for that same compound; indeed, we believe they often are different. Thus, it is not only the rate at which compounds are sorbed and desorbed from the mineral, but also the composition of those compounds that matters, as we discuss further in section 3.4. Additional factors we believe influence sorption and desorption fluxes include: pH, water potential, temperature, and mineral surface chemistry.

The rhizosphere is a hotspot of C exudation and microbial activity (Kuzyakov and Blagodatskaya 2015). Thus, we expected higher sorption in our rhizosphere treatment relative to our bulk soil treatment. We found that the total mineral-associated C was equal between the rhizosphere and bulk treatments. If C sorption to minerals was higher in the rhizosphere, as we expected, then C desorption from minerals must have also been higher in the rhizosphere.

Prior studies support the idea that in the rhizosphere, both C sorption and desorption might be higher than in the bulk soil. Higher microbial biomass and activity in the rhizosphere may lead to more mineral-associated microbes, microbial products (*e.g.* EPS) (Hong et al. 2013, Liu et al. 2013, Lin et al. 2016), and necromass (Miltner et al. 2012, Kallenbach et al. 2015, Creamer et al. 2019), but also higher rates of microbial decomposition and thus C loss. Rhizodeposition that supplies C, and particular rhizosphere-derived compounds such as oxalic acid, can also cause disassociation of mineral-bound C (Keiluweit et al. 2015).

We hypothesize that in the rhizosphere, there is a larger supply of C but also a faster turnover rate of mineral-associated C. The null hypothesis is that C source (and the unique rhizosphere environment, with its distinct microbial community and physical properties) has no impact on the total C that associates with a mineral surface. However, we see evidence for our alternative hypothesis. While Kaolinite does not accumulate more total C after 1 month, and Quartz has a slight decline in total C (**Fig 1.2a**), we see that the atom% ^{13}C of that C continues to increase (**Fig 1.2b**). The chemistry of SOM associated with minerals incubated in the rhizosphere provides evidence in support of our hypothesis. A second line of evidence supporting the dynamic nature of mineral associated C is discussed in section 1.4.2.

1.4.2 Mineral-associated SOM chemistry depends on mineral type and treatment

We used ^{13}C-NMR to assess the molecular composition of mineral associated C. In contrast to the trends observed in total C accumulation on minerals, in ^{13}C-NMR spectra we see a marked difference between rhizosphere and bulk soil treatments (**Figure 1.3**). While the ^{13}C-NMR spectra for minerals in the rhizosphere treatment show peaks in every major carbon functional group (carbonyls, aromatics, carbohydrates, and lipids), the bulk soil treatment is defined by a single prominent lipid/aliphatic peak. There are small peaks in the bulk soil treatment of the Native Minerals carbonyls and the Kaolinite carbohydrates but they are smaller than the lipid/aliphatic peak. Thus, while the rhizosphere treatment is characterized by a diverse array of carbon functional groups, the bulk soil treatment is distinct in its homogeneity.

The chemistry of mineral-associated SOM is one important predictor of C persistence (Torn et al. 1997, Mikutta et al. 2006, Schmidt et al. 2011, Torn et al. 2013). The striking contrast in chemistry between the Native Minerals in the rhizosphere treatment versus the bulk soil treatment suggests that the rhizosphere dramatically altered the chemistry of mineral-associated SOM. This is a particularly interesting finding because only 6% of the C on the Native Minerals was derived from the rhizosphere, based on our mixing model. Carbon sources in soils that are not proximal to roots, generally termed bulk soil, include C from plant litter, microbial products (*e.g.* EPS and necromass), dissolved organic C (DOC), and soil fauna. In the rhizosphere, root exudates release a wide array of small molecular weight compounds (Zhalnina et al. 2018), promoting the growth of a phylogenetically (Shi et al. 2015a), and potentially chemically distinct microbial community. The distinct ^{13}C-NMR chemical signature of the rhizosphere for the Native Minerals compared to the bulk soil suggests mineral-associated C is rapidly exchanging. In a single plant growing season, the Native Minerals acquired a unique rhizosphere chemical signature, providing another line of support for our hypothesis that in the rhizosphere, mineral-associated C has a faster turnover.

We used FTICR-MS to look at the molecular composition of compounds that were water-extractable from the minerals. These water-extracted compounds can be considered a "transient fraction" of mineral associated SOM: loosely associated compounds that are likely more easily released back into the soil. We found water-extracted samples analyzed by FTICR-MS were significantly different by mineral type ($p>0.001$), but not treatment (rhizosphere versus bulk) ($p>0.115$) (**SI Figure 1.8**). The absence of a treatment effect when we did see a treatment effect in the ^{13}C-NMR spectra suggests that what comes off the minerals in this transient water extractable fraction may depend more on mineral surface chemistry.

Van Krevlen diagrams of the O:C by H:C ratio for these compounds (**SI Figure 1.9)** group the distribution of compounds identified by FTICR-MS roughly by compositional class (Van Krevelen 1950, Kim et al. 2003) (Fenn et al. 1989). For each mineral type and treatment, we mapped the center of mass of the Van Krevlen diagram to observe overall shifts in O:C and H:C composition. The center of mass of compounds extracted from the Native Minerals had a lower H:C and higher O:C ratio than compounds extracted from the specimen minerals (Ferrihydrite, Quartz, and Kaolinite). The shift in the location of the center of mass for the Native Minerals is likely primarily due to the presence of more lignin-like compounds, which we observed in both the bulk and rhizosphere treatments. All the specimen minerals, particularly Kaolinite, had more condensed aromatic compounds and more carbohydrates than the Native Minerals.

In contrast to ^{13}C-NMR results, which show the full profile of mineral-associated SOM compounds, FTICR-MS was conducted on the water extracted compounds, and thus did not access many higher H:C compounds such as lipids and aliphatics, which are not easily released from the mineral surface with a simple water extraction. The compounds detected by FTICR-MS differ compositionally from those detected in the ^{13}C-NMR, suggesting that the transient, water-extractable fraction represented only a subset of the total range of compounds present on the minerals. The extractability of these compounds appeared to depend on mineral type. The carbon functional group that was highly abundant in the ^{13}C-NMR spectra and nearly absent from the FTICR-MS analysis was lipids, suggesting that lipids may be more strongly bound to the minerals.

Given the apparent importance of mineral associated lipids, we mapped lipid identity and distribution. We identified a total of 113 unique lipids across all four mineral types and two treatments (rhizosphere and bulk soil). The distribution of unique lipids class by mineral type was highly significantly different ($p>0.001$) (**SI Figure 1.7**). The interaction of mineral type and rhizosphere versus bulk soil treatment was significant ($p>0.025$) with a small effect by rhizosphere versus bulk soil treatment ($p>0.063$).

While different ionization potential prevents us from comparing between lipid categories, within a sub-class we were able to compare between mineral types and treatments (**Figure 1.4**). The Native Minerals had the highest lipid intensities for the majority of lipids observed in both rhizosphere and bulk soil treatments. Overall, Kaolinite had the second highest lipid intensities, with some triacylglyceride (TG) intensities higher than those on the Native Minerals. Overall, intensities of lipid classes associated with the specimen minerals types (Ferrihydrite, Kaolinite, and Quartz) were higher in the bulk soil treatment than the rhizosphere. This was particularly true of Ferrihydrite.

1.4.3 Microbial signature in mineral-associated SOM chemistry

The largest class of lipids observed across mineral type and treatment was Triradylglcerolipids (TG), with 59 total unique lipids. These storage lipids, which are highly abundant in fungi (Harwood and Russell 1984), and are also found in plant and the bacterial genus *Actinomyces* (Alvarez and Steinbuchel 2002). *Actinobacteria* were the second most abundant phyla associated with the incubated minerals(Whitman et al. 2018), so it is possible some of the observed TGs are bacterial. The distribution of unique lipids within the TG class by mineral type was highly significantly different ($p>0.001$). Comparing lipid intensities, for many of the TG, Kaolinite had almost as high a lipid intensity as the Native Minerals, and for a few of the TGs, a higher intensity (**Figure 1.4**). Ferrihydrite also had high TG intensities in the bulk soil treatment.

We observed many Glycerophospholipids [GP], primarily of the classes Diacylglycerophosphocholines (PC) and Diacylglycerophophoethanolamines (PE). Highly abundant in bacteria (Sohlenkamp and Geiger 2016), phospholipids are commonly structural components of cell membranes (Siliakus et al. 2017). Many of the GP lipids we observed had odd numbers of C atoms (15, 17, or 19 C long fatty acids). Many microorganisms have saturated branched-chained fatty acids (BCFAs) and cyclopropane fatty acids, but branched monounsaturated fatty acids are typically not bacterial (Frostegard et al. 1993, Zelles 1997, Chang and Cronan 1999, Poger and Mark 2015). Based on the structure of the Glycerophospholipids we identified, we believe that many were bacterial membrane lipids.

Unlike most of the putatively microbe-derived lipid classes we observed, most Sphingolipids are plant-derived (Harwood and Russell 1984), but they are also present in a few microbial species, including many found in the *Sphingomonadaceae* family (Glaeser and Kämpfer 2014). Only 9 Sphingolipids were observed, all of them in the Ceramides and Dihydroceramides sub-class. Ceramides are typically found in plants, but are also present in most fungi and in a few anaerobic bacteria, such as *Bacteroides* spp (Harwood and Russell 1984, Sohlenkamp and Geiger 2016), which are from one of the top ten bacterial phyla associated with incubated minerals (Whitman et al. 2018). Interestingly, we observed more unique Sphingolipids in the minerals from the bulk soil treatment than the rhizosphere treatment, perhaps suggesting these lipids are microbial rather than plant-derived (**Figure 1.4**).

We observed a distinct lipid signature on different mineral types. Prior work on this experimental system showed that mineral type shaped microbial association and assembly on mineral surfaces (Whitman et al. 2018). We expect the distinct lipid signature on different mineral types may have been driven in part by the phylogenetically distinct microbial communities on these minerals. Chemical sorption may play a role in determining which lipids end up on which mineral types. The microbial signature of mineral-associated lipids suggests that, if we know the soil mineral type, studying the microbial community composition and functional capacity may help in predictive modeling of mineral-associated SOM. New research efforts examining the role of microbial ecophysiology on the fate of SOM may provide key insights into the mechanisms through which soil microbes drive SOM persistence.

1.4.4 Towards predicting mineral-associated SOM persistence

Comparing the specimen minerals to Native Minerals allows for prediction of OM association over time. If we were to assume OM accumulates at a constant linear rate, in approximately 40

years, our specimen minerals, which were free of detectable OM, would be coated in as much OM as our Native Minerals. In reality, we expect it would take longer for a specimen mineral with no OM to accumulate the ~ 16 mg C per g mineral we observe in our Native Minerals extracted from the native soil. This is because accumulation is not likely a linear, constant process. We appear to be observing signals of a system in flux, as proposed in our **Eq. 1.2**. Given this view, how do we predict residence time, or persistence, of a particular compound on a particular mineral type?

In the rhizosphere, the actively growing plant releases a diverse array of carbon substrates (Pett-Ridge and Firestone 2017, Zhalnina et al. 2018). Our ^{13}C-NMR results suggest that the rhizosphere leaves a distinct chemical fingerprint on mineral-associated OM. While some of these unique rhizosphere compounds may be sorbed directly from the root, likely most root-derived compounds undergo some degree of transformation prior to mineral association. Rhizodeposits such as root exudates are generally lower molecular weight compounds, easily metabolized by soil microbes. We expect a large fraction of mineral-associated OM derived from the rhizosphere is chemically altered by microbes. In fact, the location of peaks in the ^{13}C-NMR spectra do resemble those of *E. coli* cells, as analyzed by Wang *et al*. (Wang et al. 2013), possibly suggesting that many of these SOM compounds unique to the rhizosphere treatment may be microbial. Rhizosphere compounds could also be altered by abiotic processes prior to sorption. However, despite likely transformation of a portion of the rhizosphere-derived compounds, the rhizosphere treatment maintains a unique chemical signature that distinguishes it from the bulk soil treatment.

We see evidence that the unique chemical fingerprint of the rhizosphere may not persist when we compare the Native Minerals to Kaolinite. In the past, the Native Minerals were likely periodically rhizosphere influenced. However, the chemistry of Native Minerals incubated in the bulk soil closely resembles that of the Kaolinite mineral that was incubated for only two months in bulk soil. The similarity between the broad ^{13}C-NMR chemistry of the Native Minerals and Kaolinite minerals in the bulk soil treatment suggest that, over time, many mineral-associated carbonyls and carbohydrates are either desorbed from the mineral surface or transformed, leaving behind mostly lipids.

The hydrophobic nature of lipids may lead to association with certain types of surfaces. In our system, lipids seemed to associate strongly with Kaolinite, which, of our three specimen mineral types, had the highest intensities of most lipid classes (**Figure 1.4**). The hydrophobic nature of lipids may mean that they are more difficult to desorb from the mineral surface. Microbial assimilation of C compounds may result in transformation of those compounds to lipids as microbes synthesize membranes and storage lipids. Our prior work (Whitman et al. 2018) reveals a diverse mineralosphere microbial community. We expect that over time, a larger portion of the mineral surface is occupied by microbial necromass, including microbial lipid residue. Returning to our proposed **Eq. 1.2**, we might expect that the sorption of lipids is larger than the desorption of lipids.

While lipids may persist, our sequential extractions showed that a large portion of mineral-associated C was water extractable, and thus may readily exchange with the soil DOC pool. The fraction of extractable total C was strongly dependent on mineral type, with some influence of

rhizosphere versus bulk soil treatment (**SI Figure 1.10**). Nearly all C was removed from Quartz through the water extraction, highlighting the importance of stronger chemical associations between SOM and the mineral (*e.g.* ligand exchange) for C persistence(Sposito 2008). The atom% ^{13}C enrichment of minerals from the bulk soil treatment was the same across all mineral types and extractions, and equal to natural abundance, as expected (**SI Figure 1.10**). Interestingly, in the rhizosphere treatment, we saw that atom% ^{13}C increased with each extraction for Kaolinite. The source of atom% ^{13}C on Kaolinite is from the actively growing *Avena barbata*. Therefore, an increase in atom% ^{13}C of Kaolinite-associated C following an extraction indicates preferential persistence of *A. barbata*-derived C compounds. This suggests that chemistry of both the mineral surface and also the carbon substrate are important in controlling mineral-associated C persistence.

Mineral type may be predictive of SOM persistence. Prior work reveals that short range order minerals, such as ferrihydrite, often have the oldest associated carbon (Torn et al. 1997, Kleber et al. 2005, Mikutta et al. 2006, Porras et al. 2018). While we did observe higher total C concentrations on Ferrihydrite than Quartz or Kaolinite, by the final harvest (2.5 months), we emphasize that our study spanned a single plant growing season - too short a time to support more than hypothesis generation. Kleber *et al.* (Kleber et al. 2007) propose a model for complex SOM association with mineral surfaces in which there are multiple zones of SOM association, moving out from the mineral surface: the contact zone, the zone of hydrophobic interactions, and the kinetic zone, or outer region. Interactions at the contact zone are strongly influenced by mineral type. Thus, mineral type may be particularly important in shaping the initial association of C with minerals. Once these contact zone interactions are established, it is possible that mineral type matters less in the zone of hydrophobic interactions and the kinetic zone. These outer zone compounds are also less strongly associated with the mineral surface, and thus more likely to be part of what we call the "transient fraction". On the Native Minerals, with an order of magnitude more total C than the specimen minerals, we expect more C compounds are in the outer zone. This is consistent with out finding that while we had an increase in total C on the specimen minerals over time, there was no significant change in total C on the Native Minerals from the start of the experiment.

In our study, mineral type was the most important determinant of the total quantity of mineral-associated C. However, we also suggest that the rate of C exchange - that is, C sorption minus C desorption from the mineral surface - accelerates in the rhizosphere. This may have important implications for C persistence in the whole soil system. In a natural grassland ecosystem, particularly one with annual grasses where root systems re-establish annually, it is likely that most minerals will be proximal to roots periodically. We found that while C association with minerals in the rhizosphere may be more dynamic, the rhizosphere left a distinct chemical fingerprint on the mineral-associated C.

1.5 FIGURES

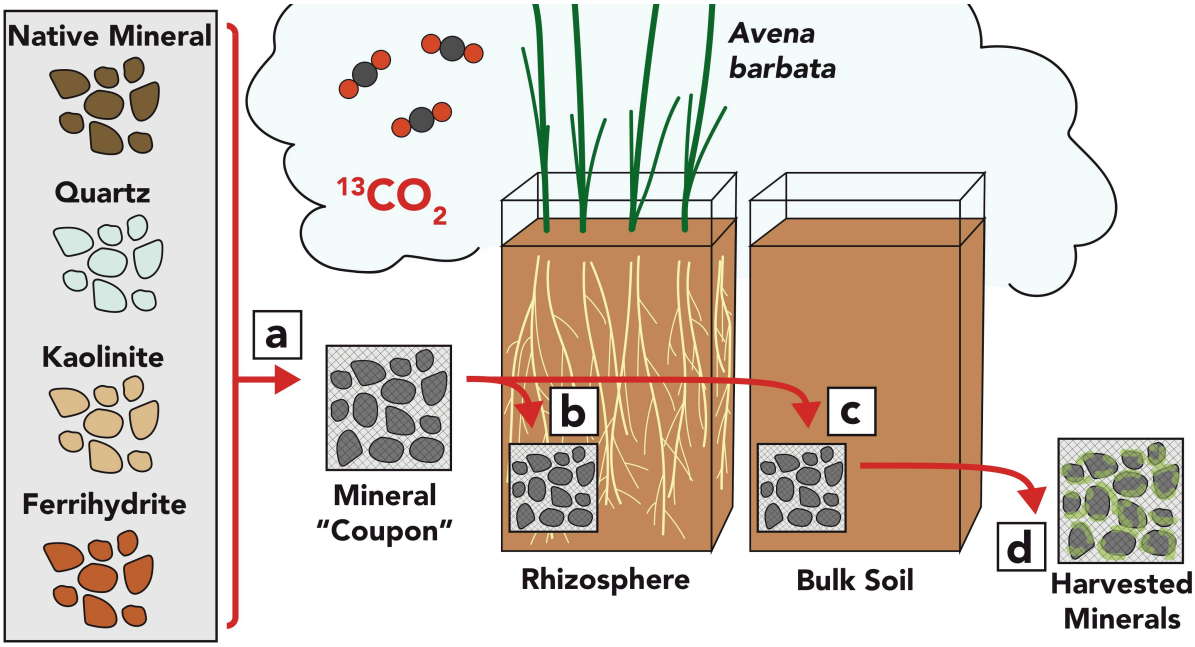

Figure 1.1. Experimental design for a rhizosphere mineral incubation in a Mediterranean-climate grassland soil from Hopland CA. Four mineral types, (1) "Native Minerals" (density fractionated from the soil), (2) "Quartz" (quartz sand), (3) "Kaolinite" (50:50 mix by volume of kaolinite and quartz sand), and (4) "Ferrihydrite" (ferrihydrite coated quartz sand), were placed in nylon mesh bags and placed in soil microcosms with growing *Avena barbata* plants (rhizosphere treatment) or no plants (bulk treatment). All microcosm were incubated in a 99 atom% $^{13}CO_2$ labeling chamber. Microcosms were destructively harvested and mineral "coupons" collected at 1, 2, and 2.5 months of incubation.

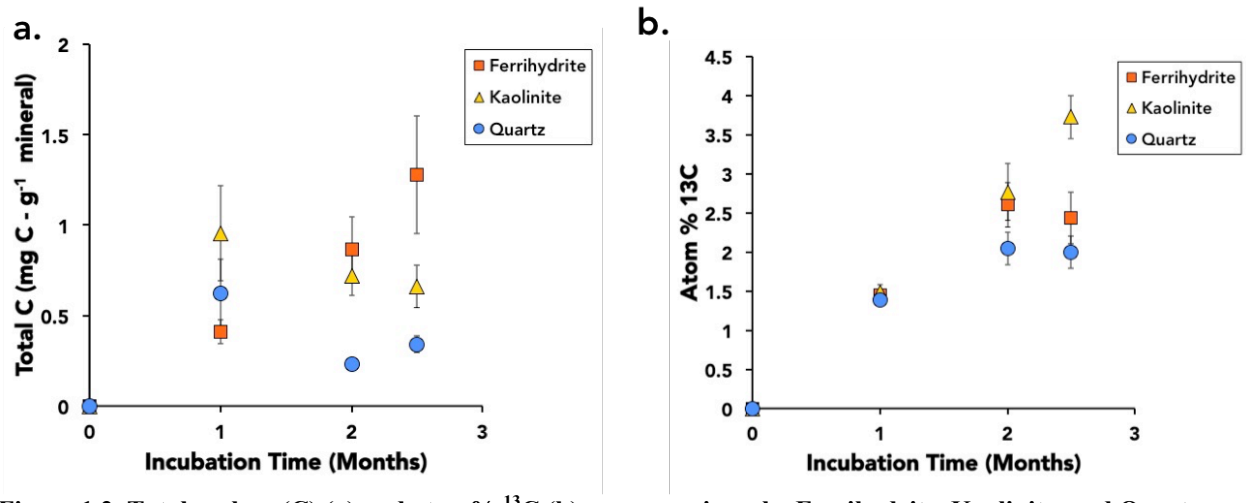

Figure 1.2. Total carbon (C) (a) and atom% ^{13}C (b) on pure minerals: Ferrihydrite, Kaolinite, and Quartz. Panel (a) shows accumulation over time for the rhizosphere treatment. Atom% ^{13}C (b) reveals how much C is derived from the *Avena barbata* plant, grown under $^{13}CO_2$.

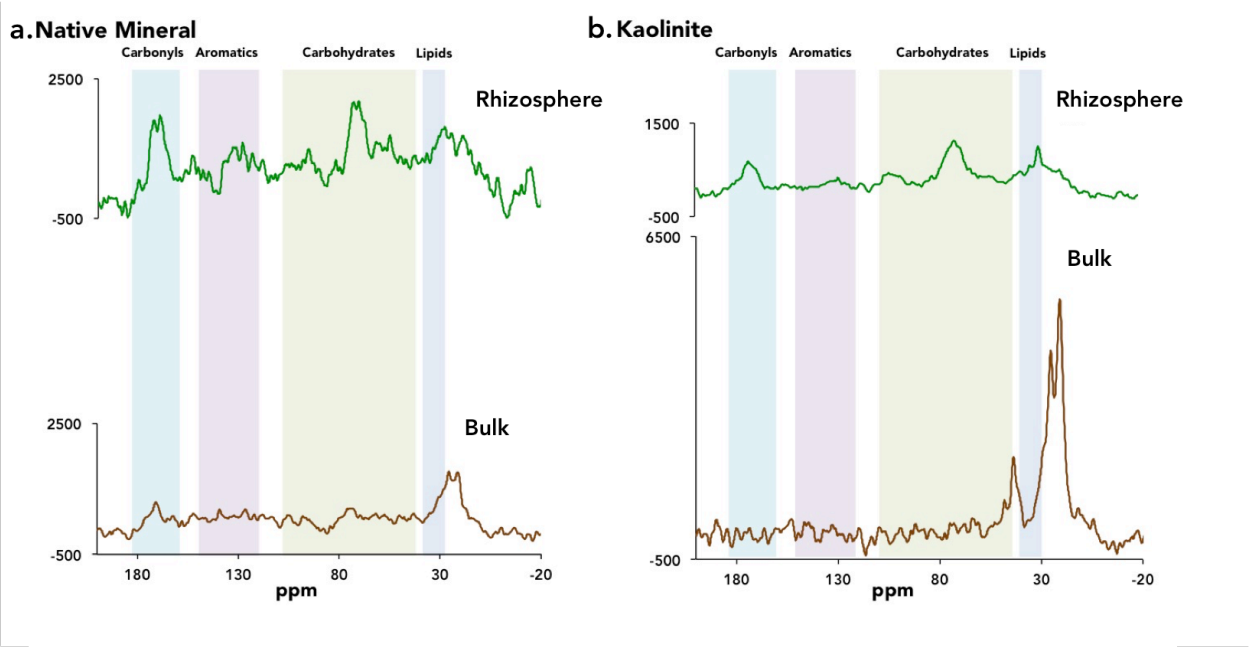

Figure 1.3. Solid-state ^{13}C-NMR spectra for Native Minerals (a) and Kaolinite (b), incubated in soil microcosms with rhizosphere and bulk treatments. Peaks are clustered into broad carbon functional group categories: carbonyls, aromatics, carbohydrates, and lipids.

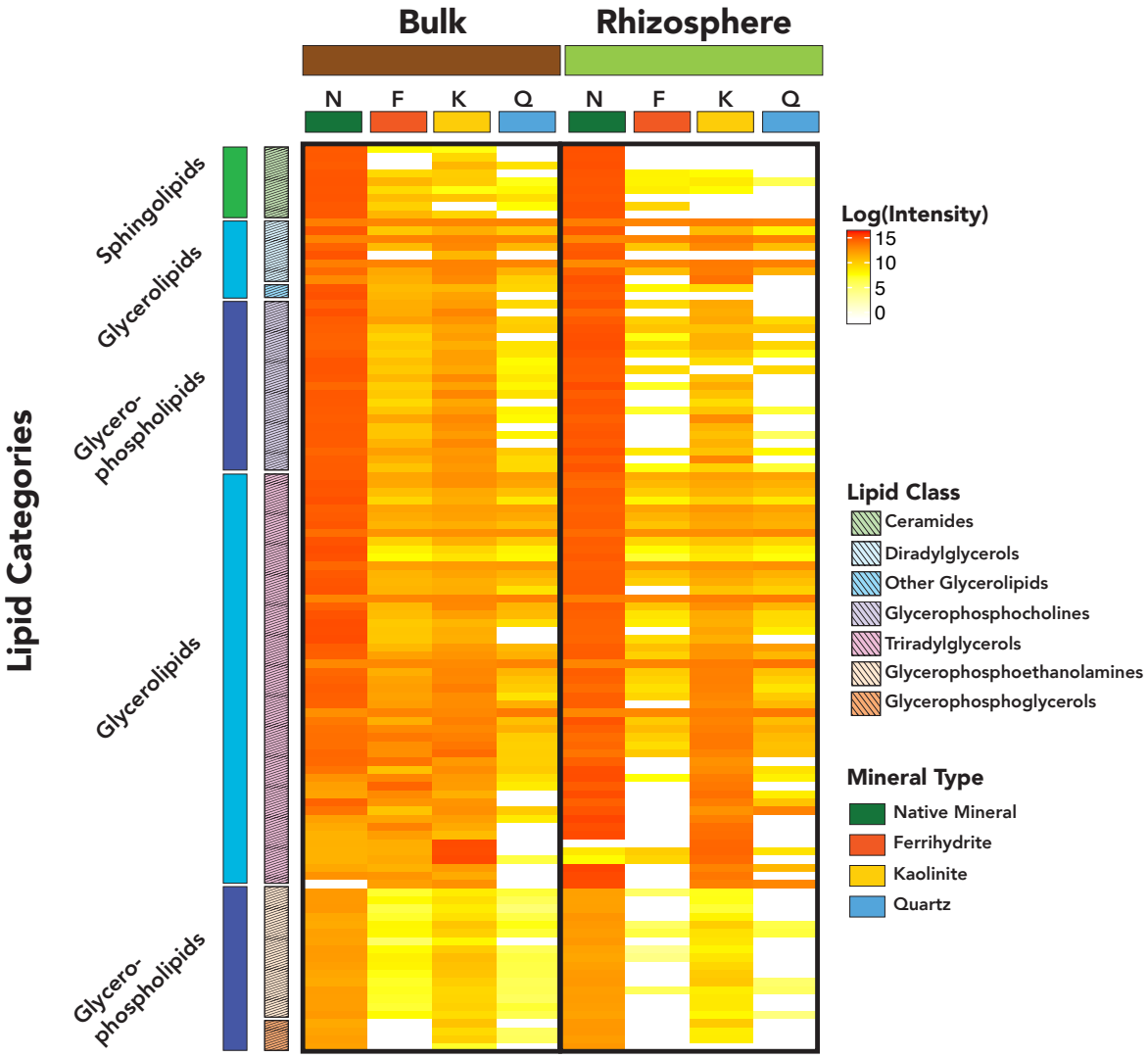

Figure 1.4. A heatmap comparison of log_{10} transformed lipid intensities for lipids identified in lipidomic analysis across treatment (bulk and rhizosphere) and mineral type (Native Mineral, Ferrihydrite, Kaolinite, and Quartz). Due to differences in ionization potential, comparisons should only be made within lipid sub-class, rather than across broad lipid categories. Overall, Native Minerals, which also had an order of magnitude more total C, had the highest lipid intensities. However, for a few of the glycerolipids, the pure minerals had higher lipid intensities. Of the pure minerals, kaolinite overall had the highest lipid intensities.

1.6 SUPPORTING INFORMATION

1.6.1 Supporting Methods

1.6.1.1 X-Ray Diffraction

To select minerals for the experiment that reflected the dominant mineral types found at Little Buck Field at HREC, we conducted X-Ray Diffraction (XRD) on the field soil (Panalytical X'Pert Pro diffractometer, Earth and Planetary Sciences Department, University of California, Berkeley). We analyzed finely ground bulk soil and then separated the clay fraction by suspension in dionized water and filtration. To resolve the clay mineralogy, we first analyzed the air-dried clay fraction. Next, we treated the clay fraction with ethylene glycol, air dried, and reanalyzed. Finally, we heated the clay fraction to 400°C, which allowed us to resolve the clay mineralogy. We also validated our lab-synthesized ferrihydrite-coated quartz using XRD. Peaks were analyzed using X'Pert Highscore Plus software and matched to reference peaks. We found that in the field soil, the dominant clay mineralogy was kaolinite. The dominant metal-oxide in the field soil was ferrihydrite, and we were also able to validate that our lab-synthesized ferrihydrite-coated quartz was ferrihydrite, and had not crystallized to goethite. The soil was also dominated by quartz. We also found feldspar, primarily albite, and mica, but these were not as dominant and so were not selected for the experiment.

1.6.1.2 Mineral Preparation

We prepared three pure mineral types for incubation in the soil microcosms, informed by the dominant mineralogy of Little Buck Field bulk soil (See **SI X-Ray Diffration**). For simplicity, we refer to the four mineral types as: "Quartz" (quartz sand), "Kaolinite" (50:50 mix of kaolinite and quartz sand), "Ferrihydrite" (ferrihydrite-coated quartz sand), and "Native Minerals" (heavy fraction of density fractionated Hopland field soil). Quartz sand (Sigma-Aldrich, 50-70 mesh particle size, CAS 14808-60-7) was acid washed with 10% HCl, then rinsed with deionized water until reaching a neutral pH. Kaolinite was purchased from the Clay Minerals Society (KGa-2 Kaolin) and combined in a 50:50 by mass mixture with a subset of the acid-washed quartz sand. To synthesize the ferrihydrite-coated quartz, we used a modified method from Hansel *et al.* (Hansel et al. 2003, Hansel et al. 2004). A solution of 34.4 mM $FeCl_3$, 6.87 mM $AlCl_3$, and 100 μm Na_2SiO_3 was mixed vigorously and the pH adjusted to 7.2-7.5 with the additional of 0.4 N NaOH, causing precipitation of the ferrihydrite. The supernatant was decanted and the ferrihydrite slurry was centrifuged at 3000 rpm. This process was repeated four times, with the centrifuge increased each time up to 8000 rpm. Centrifuge tubes with ferrihydrite slurry were sealed and left in a fume hood to age for one month. A subset of the acid-washed quartz sand was coated in the aged ferrihydrite slurry and mixed until homogenous, then dried. The ferrihydrite-coated quartz sand was washed with deionized water until it rinsed clear, then dried.

In addition to the three "pure" minerals prepared in the laboratory, we simulated "native" soil minerals by separating the heavy density fraction of soil collected at Little Buck Field (0-10cm). To separate the Native Minerals, we density fractionated air-dried soil samples. Following the density-fractionation method used in Pett-Ridge *et al.* (Pett-Ridge and Firestone 2017), modified from Sollins *et al*. (Sollins et al. 2006)we first separated the free light fraction (<1.75 g-cm^3). The remaining soil was sonicated to remove the occluded light fraction (<1.75 g-cm^3). We

washed the remaining heavy fraction (>1.75 g-cm^{-3}) with deionized water three times and lyophilized.

1.6.1.2 Lipidomics Analysis

Total lipid extracts (TLE) were analyzed as outlined in Kyle *et al.* (2017). Briefly, a Waters Acquity UPLC H class system interfaced with a Velos-ETD Orbitrap mass spectrometer was used for LC-MS/MS analyses. 10 µl of reconstituted sample was injected onto a Waters CSH column (3.0 mm x 150 mm x 1.7 µm particle size) and separated over a 34-minute gradient (mobile phase A: ACN/H2O (40:60) containing 10 mM ammonium acetate; mobile phase B: ACN/IPA (10:90) containing 10 mM ammonium acetate) at a flow rate of 250 µl minute^{-1}. TLEs were analyzed in both positive and negative modes, and lipids were fragmented using higher-energy collision dissociation and collision-induced dissociation.

1.6.2 Supporting Tables and Figures

SI Table 1.1. Mineral Properties

Property	**Quartz**	**Kaolinite**[a]	**Ferrihydrite**	**Native Mineral**[b]
Chemical Formula	SiO_4	$Al_2Si_2O_5(OH)_4$	$Fe(OH)_3$	NA
Source of Mineral	Purchased from Sigma-Aldrich[c]	Purchased from Clay Minerals Society[c]	Synthesized in Lab[c]	Density Fractionated from Soil[c]
Initial C%	Negligible	Negligible	Negligible	1.6
BET Surface Area[d] (m^2g^{-1})	0.01-0.05[e]	20.48	4.8	2.68
Particle Size Range (µm)	297-210	Mostly < 2	297-210	Not Determined
pH (1:1 m:v in 0.01 M $CaCl_2$)	4.12	3.03	6.23	Not Determined
Predicted Relative Charge Density	Very low	Low	High	Intermediate
Primary or Secondary Mineral?	Primary	Secondary	Secondary	NA
Hydroxyamine-Extractable Fe (mean ± SE, µg-1)	8 ± 2	8.4 ± 0.4	4563 ± 1535	Not Determined
Hydroxyamine-Extractable Al (mean ± SE, µg-1)	1.5 ± 0.1	77 ± 14	587 ± 268	Not Determined

a. Kaolinite was used in a 50:50 mixture with quartz

b. Numerous parameters were not determined due to low quantities

c. See Supplemental Methods for detailed description of preparation

d. N_2 analysis gas

e. Quartz surface area was too low to measure using BET with N_2 gas. Estimated from the literature (Xu *et al*., 2009, Mekonen *et al.*, 2013) and mesh size

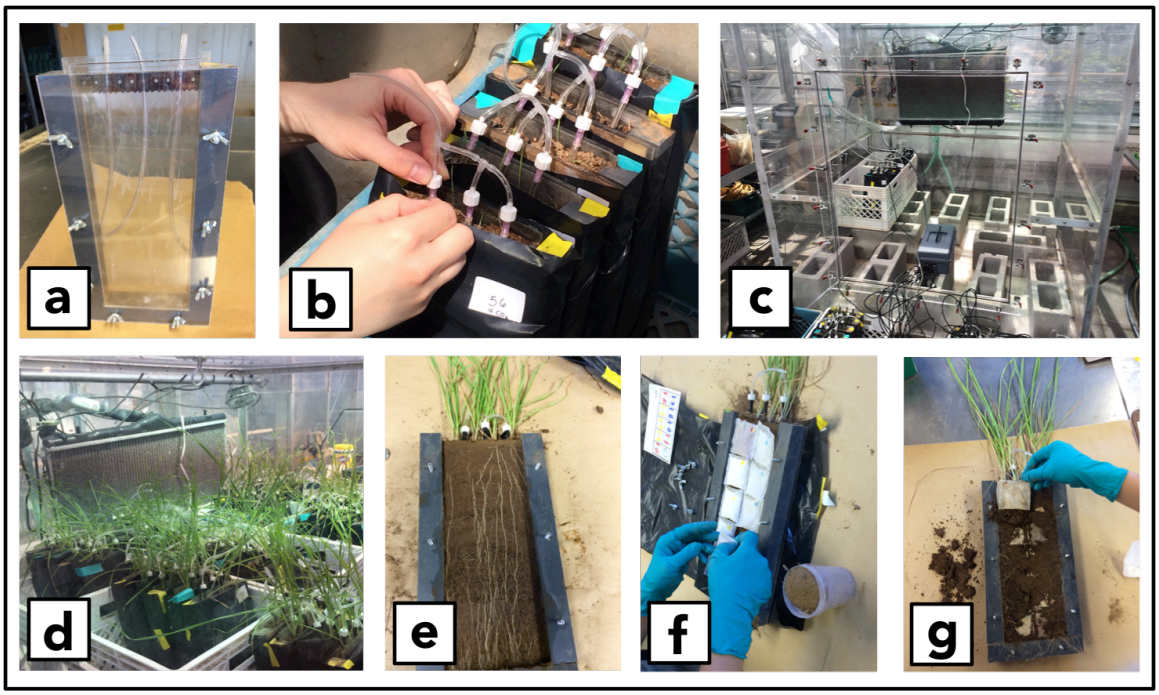

SI Figure 1.1. Experimental design for mineral "coupon" incubation in soil microcosms. Soil microcosms (a) were fitted with perforated tubing for automated watering and filled with soil (b). Soil microcoms were placed in an isotope labeling chamber (c) and *Avena barbata* seedlings were added to the rhizosphere treatment microcosms. Soil microcosms were tilted to 45° for 1 month (d), encouraging the *A. barbata* roots to grow along one face of the soil microcosm (e). Soil microcosms were opened and mineral coupons were placed along the rhizosphere face for the rhizosphere treatment microcosms (f), or, for the bulk treatment with no plants, they were placed along the soil. Soil microcosms were placed back in the isotope labeling chamber (c), now sealed with added 99 atom% $^{13}CO_2$ maintained at 400 ppm with an atmospheric $^{13}CO_2$ concentration of ~ 10 atm% ^{13}C. Soil microcosms were destructively harvested and mineral coupons were recovered after 1, 2, and 2.5 months.

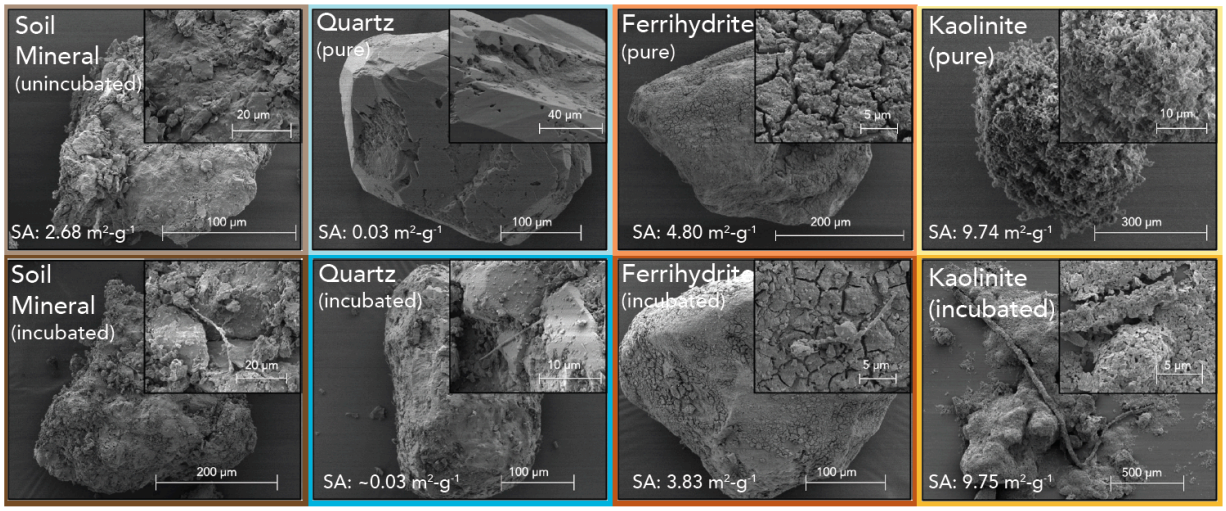

SI Figure 1.2. SEM images (5 eV) of minerals before and after incubation in rhizosphere treatment soil microcosms. Pure minerals, shown in the top panels, are of minerals prior to incubation in soil microcosms. Minerals after incubation in the rhizosphere treatment soil microcosms are shown in the bottom panels. Each panel shows an overview of the mineral with an inset panel in the upper right hand corner showing a higher resolution image of the same mineral. Scale bars are in the bottom right of each panel and inset. SA stands for BET surface area, measured with N_2 gas.

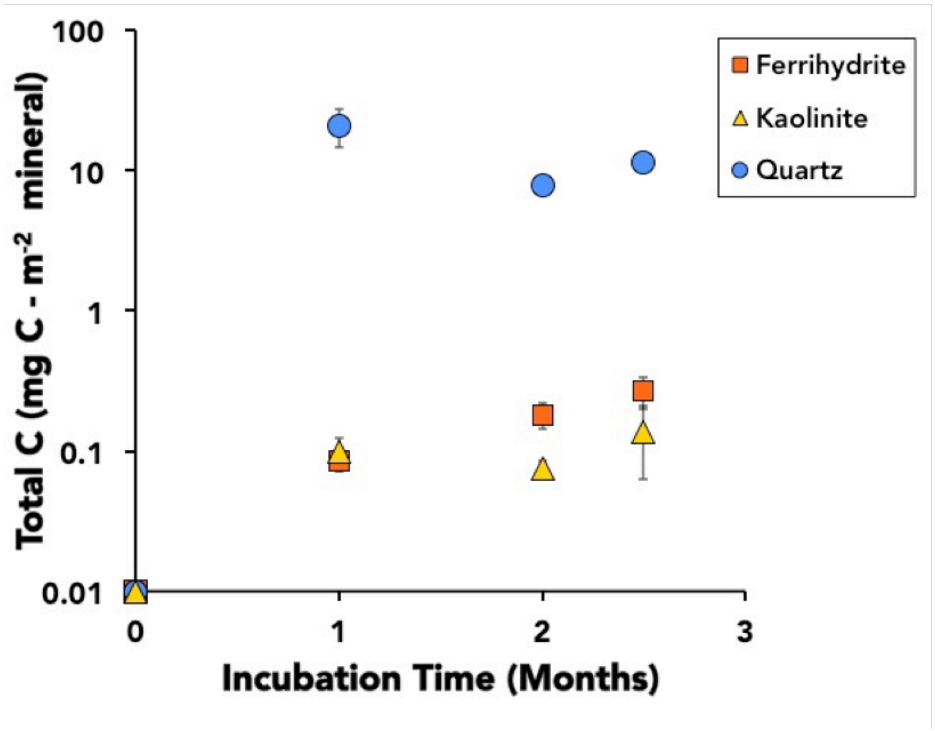

SI Figure 1.3. Total C accumulation on pure minerals in rhizosphere treatment incubations, normalized to BET surface area. Quartz had the highest surface-area-normalized total C. All minerals began with no measurable C. Most total C accumulation occurred in the first month of mineral incubation. Only Ferrihydrite accumulated total C after 1 month.

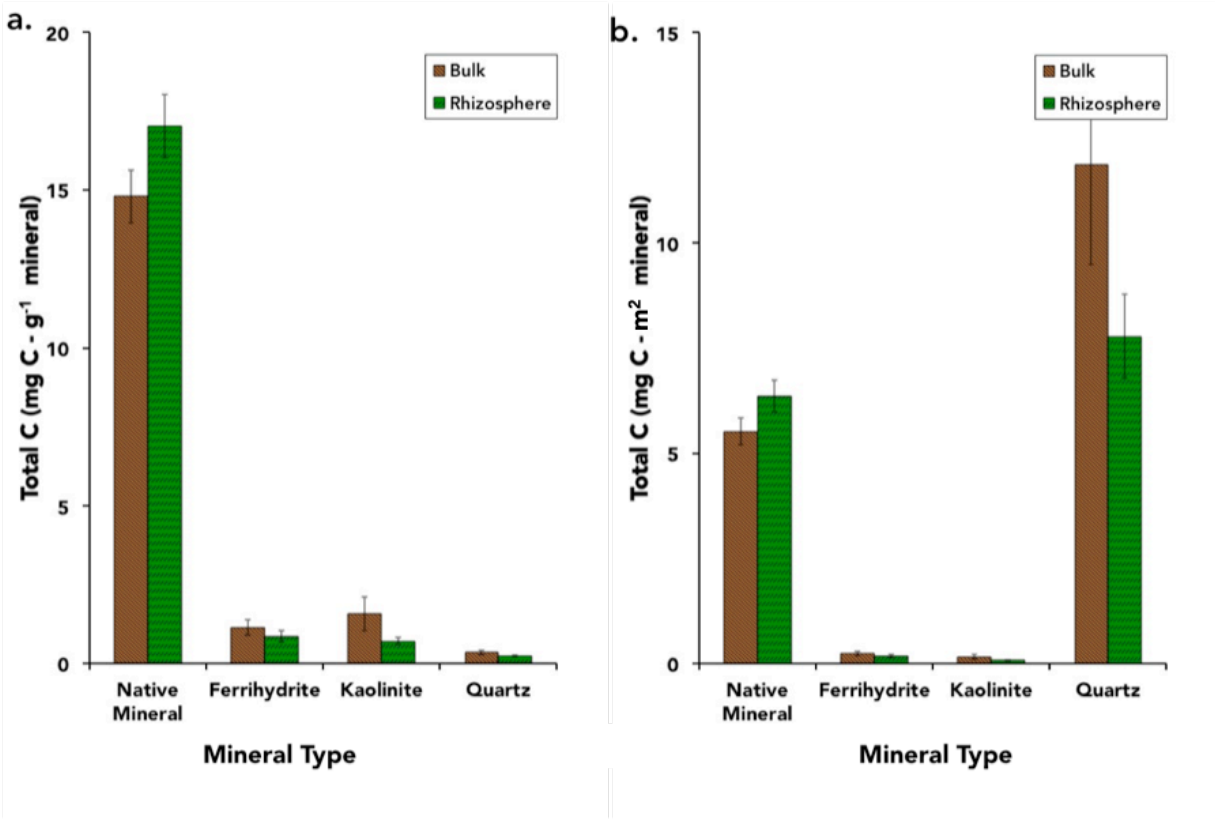

SI Figure 1.4. Comparison of total C on minerals incubated in the rhizosphere and bulk treatments by mass (a) and normalized to surface area (b). The bulk soil treatment is shown in brown and the rhizosphere treatment in green. The native mineral had the highest total C content by mass, but normalized to surface area, quartz had more total C. There was not a significant treatment effect on total C.

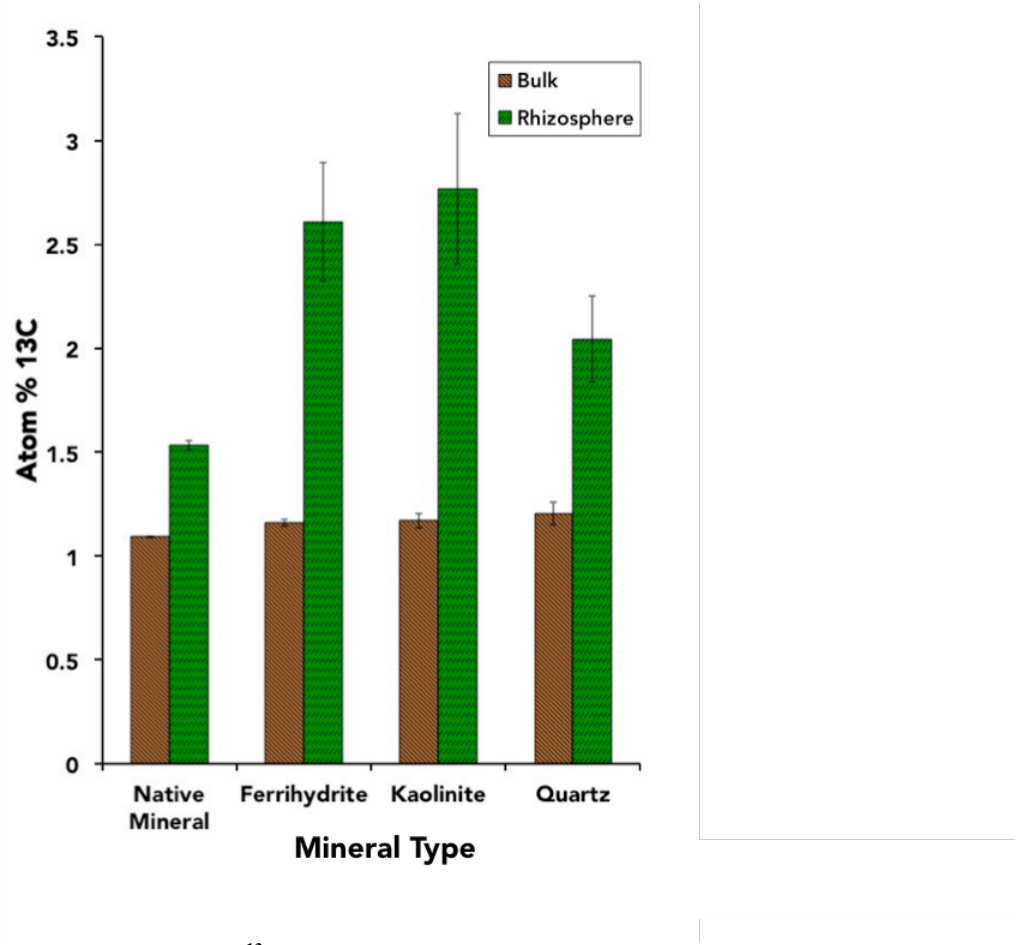

SI Figure 1.5. Atom% ^{13}C of each mineral type at 2 months after incubation in soil microcosms. Minerals incubated in the bulk treatment had no significant change in atom% ^{13}C compared with the native soil, as was expected in the absence of a plant. Minerals incubated in the rhizosphere had atom% ^{13}C values elevated above natural abundance, with the highest atom% ^{13}C - at this 2 month time point - associated with ferrihydrite and kaolinite. As shown in Figure 2, at 2.5 months incubation, kaolinite had a higher atom% ^{13}C. While atom% ^{13}C association with the native mineral incubated in the rhizosphere was lower than any of the pure minerals, this change in atom% ^{13}C actually represents a significant replacement of mineral associated C with new, plant-derived C, compared with the pure minerals which had no measurable C associated prior to incubation.

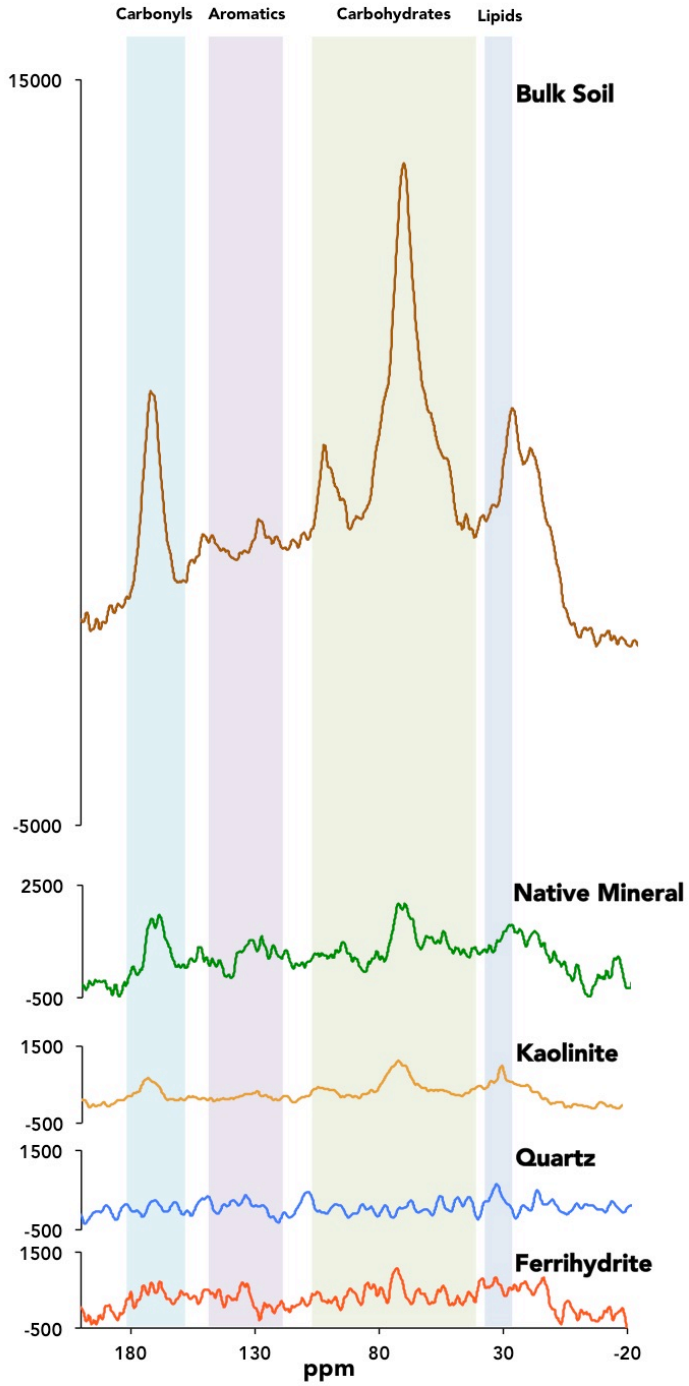

SI Figure 1.6. ^{13}C-NMR of all mineral types from the rhizosphere treatment compared with the bulk soil. The high iron content in the ferrihydrite caused interference, such that no clear spectra were obtained. Quartz, with a lower total C content by mass, also did not have well-resolved spectra.

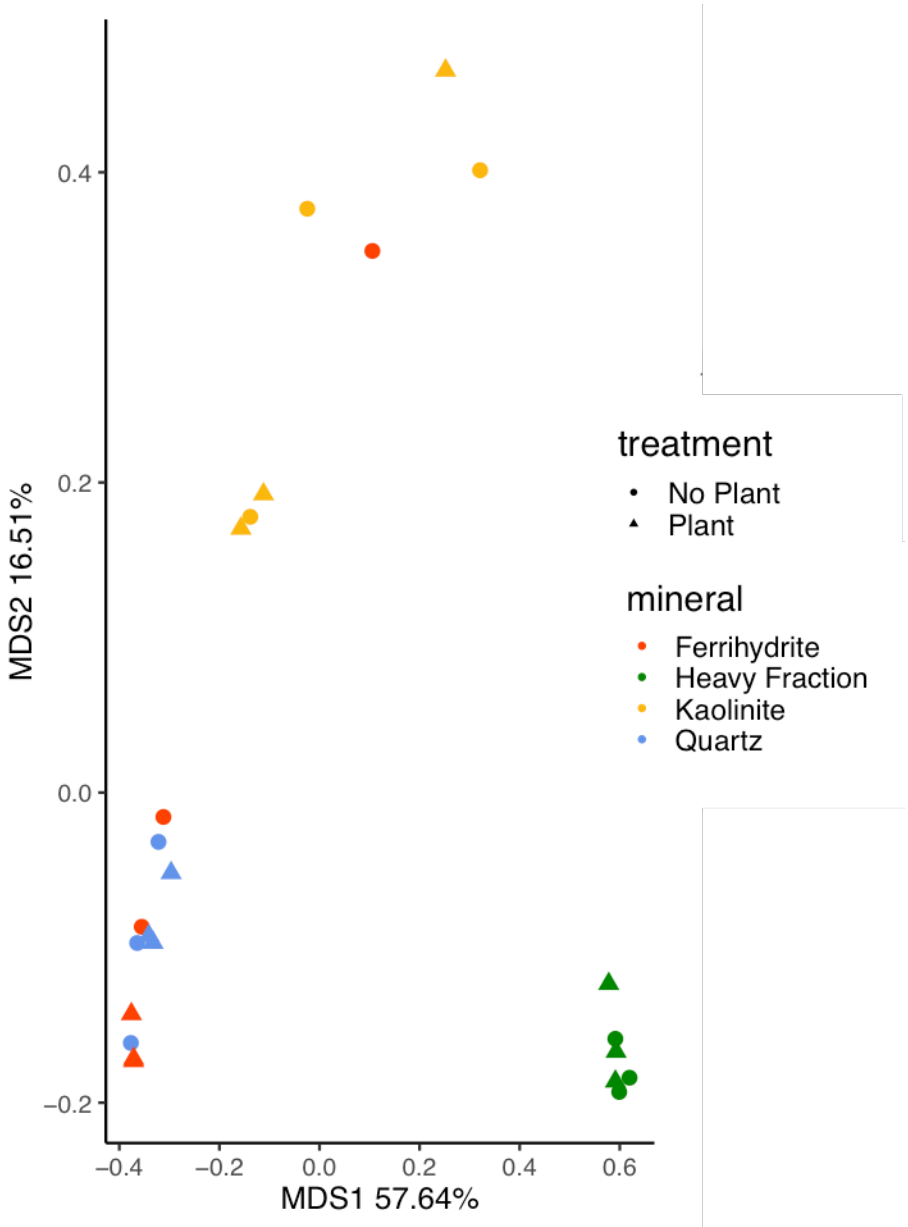

SI Figure 1.7. PCoA of lipidomic data with Bray-Curtis shows clear clustering by mineral type, with the heavy fraction and the kaolinite in distinct clusters.

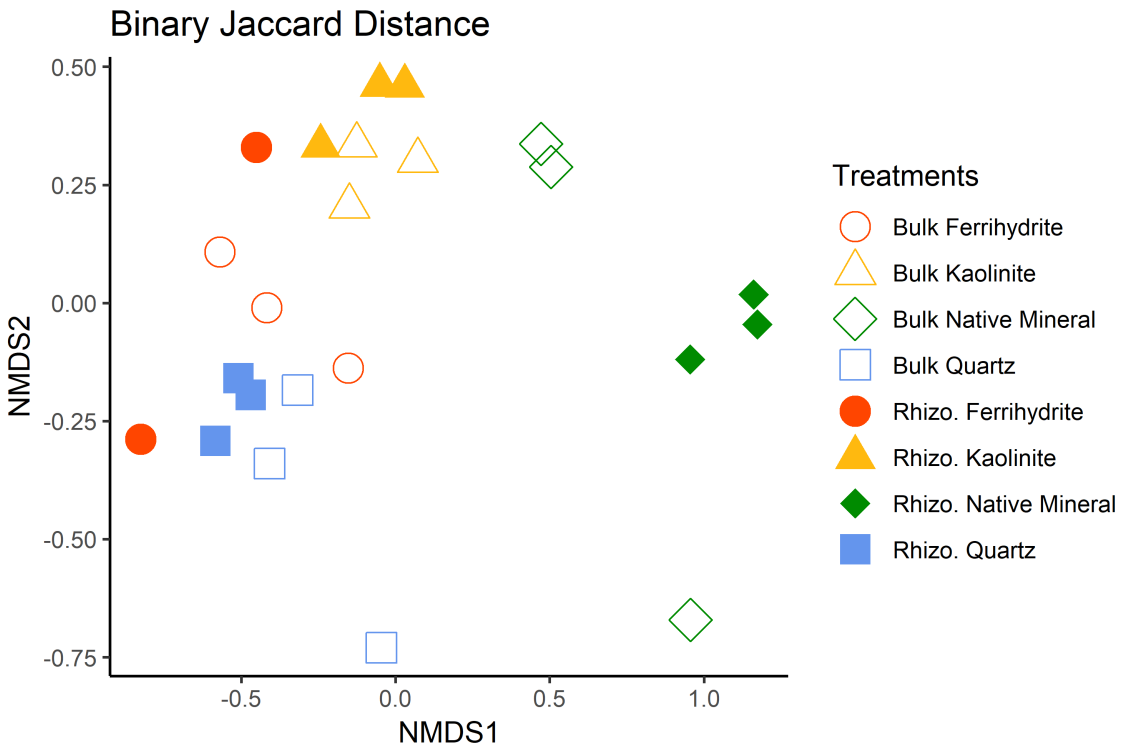

SI Figure 1.8. NMDS of FTICR-MS data with Jaccard distance shows clustering by mineral type.

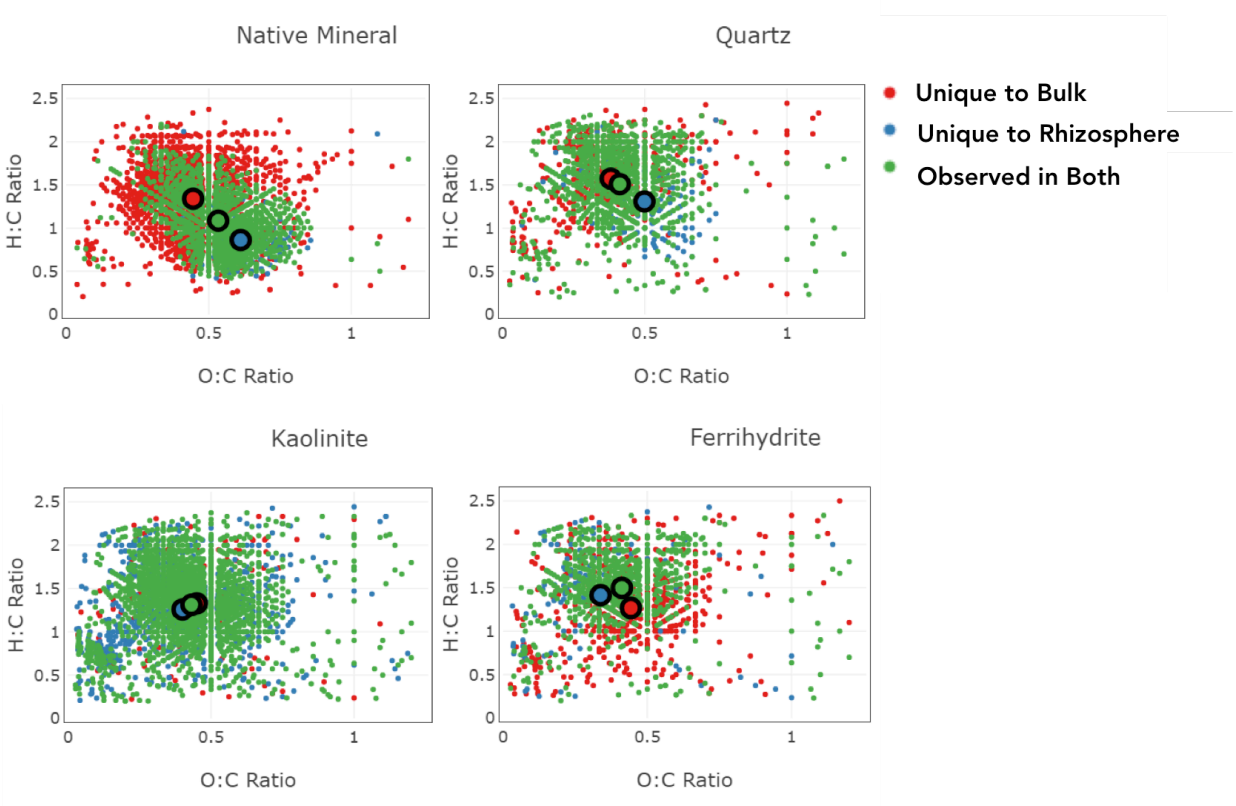

SI Figure 1.9. Van Krevlen diagrams of FTICR-MS data, with a graph for each mineral type. Compounds unique to the bulk are in red, unique to the rhizosphere in blue, and observed in both are green. The center of mass is shown for each.

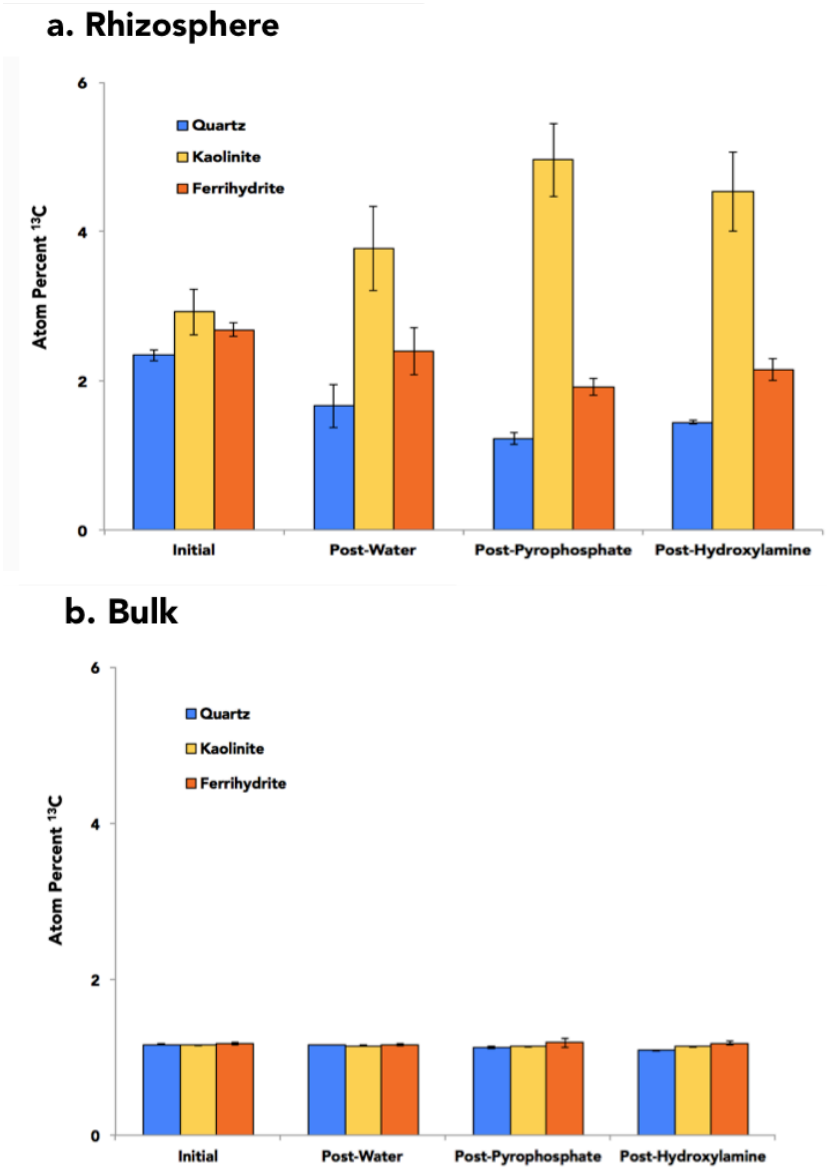

SI Figure 1.10. Atom% ^{13}C of sequential extractions of mineral-associated soil organic matter (SOM) from the rhizosphere (a) and bulk (b) treatments, showing the atom% ^{13}C before extractions, after a water extraction, after a sodium pyrophosphate extraction, and after a hydroxylamine extraction. We saw no change in the bulk treatment (b), where there was no ^{13}C enrichment, confirming that our sequential extraction procedure did not cause significant ^{13}C fractionation. We saw an increase in atom% ^{13}C of kaolinite from initial to post-water to post-pyrophosphate, while overall we observed a loss of total C with each subsequent extraction step. This indicates that relatively more ^{13}C-labeled plant-derived C persisted on kaolinite through these extractions.

2

Rapid carbon association with soil minerals in the detritosphere following a simulated wet-up

2.1 ABSTRACT

While minerals bind the oldest, most persistent carbon (C) in soils, recent work suggests that C association with minerals may be a dynamic process. It is also clear that soil microbial activity and C transformation are highly heterogeneous in both space and time, as evidenced by the popularity of the "hot spots" and "hot moments" paradigm. In our prior work, we saw evidence for dynamic OM association with minerals in soil near plant roots, the rhizosphere. Here, as a complement to our rhizosphere work, we examined the period of intense microbial activity following a simulated wet-up event, when a dry soil experiences the first rainfall of the growing season. We traced the fate of ^{13}C labeled root litter in soil microcosms with "native soil minerals" and three pure minerals: ferrihydrite, kaolinite, and quartz. Mineral-associated C and microbial communities were characterized with 16S and ITS rRNA Illumina sequencing, total C, ^{13}C, ^{13}C-NMR, FTICR-MS, and lipidomics. As in the rhizosphere, C accumulation was rapid and mineral-dependent, but, overall significantly less C became mineral associated than in the rhizosphere, and we observed different patterns of mineral C accumulation. In the detritosphere, high surface area minerals such as kaolinite accumulated more C during the wet-up period of intense microbial decomposer activity, whereas in rhizosphere, C accumulation was correlated with minerals such as ferrihydrite that have a high surface reactivity and form strong mineral-OM associations. In the detritosphere, mineral associated lipids were primarily microbially-derived, though some plant-derived lipids were also present. Lipids indicative of the lipid-rich fungal order *Mucorales* and bacterial order *Streptomyces* were prominent, suggesting these taxa may play an important role in mineral-associated lipid formation, which could have important implications for the persistence of mineral-associated OM. We propose that in Mediterranean-type climates with a distinct growing season followed by a dry season with little plant growth or microbial activity, we need an integrated understanding of how rhizosphere and detritosphere dynamics interact to control soil C persistence

2.2 INTRODUCTION

Soils are critical carbon (C) reservoirs, storing more C than the atmosphere and biosphere combined, and the mechanisms that regulate soil C persistence are a topic of intense recent interest (Sulman et al. 2018, Bailey et al. 2019, Creamer et al. 2019, Dwivedi et al. 2019, Sokol et al. 2019b, Lehmann et al. 2020). As climate change accelerates, recent work acknowledges that curbing anthropogenic CO_2 emissions may be insufficient without coupled sequestration of atmospheric CO_2 (Lehmann 2007, Chapman 2010, Lal 2010, Garcia et al. 2018). Management of soils to increase C storage may require both increased C inputs and increased C sequestration. Adding C substrates to soil that are rapidly released back to the atmosphere is far less effective than adding C that persists in soil. Mineral-associated C is the oldest, most persistent C in soil (Torn et al. 1997, Kogel-Knabner et al. 2008, Schmidt et al. 2011, Kleber et al. 2015b), but even C association with minerals is dynamic (Bailey et al. 2019, Shi et al. 2020).

In soils, there are "*hot spots*" and "*hot moments*" of microbial activity (Kuzyakov and Blagodatskaya 2015); it is also likely that there are areas and times in soil that carbon association with and loss from mineral surfaces is dynamic (Keiluweit et al. 2015, Bailey et al. 2019, Lehmann et al. 2020). In ecosystems with distinct wet and dry seasons, including grasslands in Mediterranean-type climates, the first rainfall, or wet-up, after the dry summer stimulates intense microbial activity and C transformation (Birch 1958, Kieft et al. 1987, Unger et al. 2010, Placella et al. 2012, Barnard et al. 2013, 2015, Blazewicz et al. 2020). After wet-up, there is a large pulse of CO_2 release from soil (Birch 1958, Unger et al. 2010). This large pulse of CO_2 may be derived from microbial degradation of several different substrate pools (Barnard et al. 2020). This period of rapid microbial growth and C transformation following wet-up, may have important implications for C storage and persistence in soils.

The rhizosphere is a zone of enhanced microbial activity and C transformation (Jones et al. 2009, Philippot et al. 2013, Pett-Ridge et al. 2020 (in press)). In Mediterranean-type climate annual grasslands, when plants senesce each spring, their root litter becomes and active detritosphere. Throughout the summer dry season, there is little microbial activity, and thus little C transformation and turnover (Barnard et al. 2013, Schimel 2018). Then, a switch is flipped at wet-up, and the detritosphere begins to develop rapid microbial activity and C transformation. In most surface soils, particularly grassland and agricultural soils, minerals likely periodically experience a rhizosphere-dominated system when a root is growing past, or a detritosphere-dominated system as that root dies and begins to decompose. We propose that we need an integrated view of both rhizosphere and detritosphere processes to understand soil C dynamics in Mediterranean-type ecosystems.

The C transformations and microbial community dynamics that occur after a wet-up may set the stage for the remainder of the growing season. Just as growth of a root can "reset" microbial communities at the microscale (DeAngelis et al. 2008, DeAngelis et al. 2009), microbial colonization of minerals after resuscitation from wet-up may have priority effects that influence the types of microbe-mineral interactions that drive mineral-OM associations. Both mineral type, and the presence of root litter may influence microbial colonization of minerals and mineral-OM associations. However, the interaction of mineral type and litter amendment, and implications for C persistence, is largely unknown. Recent interest in enhancing soil C storage often involves managing soils to increase soil C inputs. Here we focus on root litter because in uncultivated systems, most C stabilized is root C (Rasse et al. 2005). To control for the impact of our litter addition, we used a soil collected from the same site with no litter addition.

In soil microcosms, we incubated four mineral types that represent a spectrum of surface area and reactivity in microcosms with and without added ^{13}C *Avena barabata* root litter. We simulated a wet-up of dried soil from a California Mediterranean-type grassland and traced C association with minerals and microbial community dynamics. We hypothesized that, as in the rhizosphere, mineral type would control the quantity of C on mineral, but that mineral-OM C would look compositionally distinct from the rhizosphere. We expected a distinct mineral-associated microbial community in the detritosphere as compared to bulk soil or the rhizosphere, and hypothesized that, as in the rhizosphere, mineral-OM chemistry would largely be a reflection of microbial activity and assemblage composition. After wet-up, we saw a large pulse of $^{13}CO_2$

in the litter treatment, with only a small fraction of added litter associating with soil minerals. We suggest that in our system, due to rapid mineralization of added litter, there was not a large impact on C persistence. We found that while mineral type drove the total quantity of mineral-associated SOM, in the detritosphere total C was primarily impacted by mineral surface area and not surface reactivity, as we saw in the rhizosphere. As in the rhizosphere, most mineral-associated C, particularly lipids, appeared to be of microbial origin. We see evidence that the lipid-rich fungal order *Mucorales* and bacterial order *Streptomyces* may play an important role in mineral association of lipids.

2.3 MATERIALS AND METHODS

2.3.1 Experimental Design

The soil used in the soil microcosms were collected from 0-10 cm at Little Buck Field (38.992938° N, 123.067714° W) at the Hopland Research and Extension Center (HREC), in Hopland, CA, in March, 2017, just before the start of the California summer dry season. The soil, a fine-loamy, mixed, active, mesic Typic Haploxeralf (Sudderth et al. 2012), was sieved to <2 mm in the field, dried, and stored at 4°C. Six microcosms (37.0 x 26.5 x 2.8 cm) were filled halfway with Hopland soil to field bulk density (1.2 g-cm^{-3}) (**Figure 2.1**). Mineral coupons were placed on the soil, then the microcosms were filled the rest of the way with soil at the same bulk density.

As in the rhizosphere (**Section 1.3.1**), nylon mesh bags (18 μm mesh, 5 x 5 x 0.2 cm dimensions) were filled with one of four mineral types: quartz sand ("Quartz"), ferrihydrite-coated quartz sand ("Ferrihydrite"), 50:50 mixture kaolinite and quartz sand ("Kaolinite"), or the heavy density fraction (>1.75 g-cm^{-1}) ("Native Minerals") of the field soil from HREC (**Figure 2.1**). Mineral preparation is described in the **Chapter 1 SI Methods**. The minerals added reflect the dominant components of our field site (determined by XRD, see **Chapter 1 SI Methods)**, and a range of surface area and reactivity: quartz (low surface area, low reactivity), kaolinite (high surface area, moderate surface reactivity), ferrihydrite (moderate surface area, high surface reactivity) (**Chapter 1 SI Table 1.1**). Microcosm soil and mineral bag bulk density were equal to the field bulk density at Little Buck Field (1.2 g-cm^{-3}).

In 3 microcosms, dried, ^{13}C labeled *Avena barbata* root litter (7.19 ± 0.40 SE atom% ^{13}C), produced in the rhizosphere experiment (**Section 1.3.1**), was ground to a coarse powder and added to a total concentration of 320 g root litter per m^2 soil, which is typical for a grassland surface (0-10 cm) soil. To simulate a detritosphere in which roots die and decay *in situ*, the 2 mm above and below the minerals had a higher fraction of ^{13}C *A. barbata* root litter. In the other 3 microcosms, we did not add any root litter.

As soil microcosms acclimated for three days prior to the simulated wet-up, they underwent a large temperature change from 4°C to ~ 27°C. A volumetric water content (VWC) sensor (Decagon, EC5) was buried in each soil microscom. At the start of the experiment, we simulated a wet-up event, which is the first rainfall of the growing season in a Mediterranean climate. Soil was ~ 4% VWC prior to the simulated wet-up. We watered microcosms with a spray mister to replicate rainfall until we reached 14% VWC. We maintained 14% VWC for the remainder of the experiment, watering with the spray mister.

Microcosms were destructively harvested after 1 week, 1 month, and 3 months. A subset of minerals were immediately placed on dry ice and then stored at -80°C for DNA extraction. At harvest, both minerals and soil were weighed, dried (65°C), and weighed again to obtain soil moisture content. The dried minerals and soil were stored at 4°C until analysis.

2.3.2 CO_2, $^{13}CO_2$, Total C, and Isotope Ratio Mass Spectrometry

We followed CO_2 release for 5 days following wet-up. To measure CO_2 and $^{13}CO_2$, microcosms were sealed so they were airtight. The ^{13}C litter addition microcosms were connected to a Picarro G2131-I Analyzer (Santa Clara, CA). The control microcosms with no litter addition were connected to a Infrared Gas Analyzer, (IRGA, Campbell Scientific, Logan, UT). Both gas analyzers were combined with a CR1000 Datalogger (Campbell Scientific, Logan, UT) to enable real-time assessment of [$^{12}CO_2$] and [$^{13}CO_2$].

To measure total C accumulation on mineral surfaces, in bulk soil and near roots, we used Elemental Analysis (EA) coupled to an IsoPrime 100 Isotope Ratio Mass Spectrometer (IRMS) (Isoprime Ltd, Cheadle Hulme, UK), to measure total C simultaneously with ^{13}C. Peach leaf standards (NIST SRM 1547) were run to ensure accuracy and duplicates for precision. Samples were then analyzed for ^{13}C enrichment through IRMS. *Avena fatua* roots, labeled with a range of ^{13}C atom%, were ground and used as additional IRMS standards.

2.3.3 Mixing Model

To calculate the relative contribution of total C on mineral surfaces from the added ^{13}C root litter, we used a mixing model (**Eq. 2.1**). In our mixing model, the two pools of C were the root litter and the bulk soil:

$$E_M = E_L \cdot f_L + E_B \cdot f_B \qquad \textbf{Eq. 2.1}$$

Where E_M is the atom% enrichment of the mineral, E_L is the atom% enrichment derived from the root litter, f_L is the fraction of C from the root, E_B is the atom% enrichment derived from the bulk soil, and f_B is the fraction of C from the bulk soil. In our equation, $f_L + f_B = 1$. Bulk soil had a natural abundance^{13}C (1.074 ± 0.001 SE atom% ^{13}C). Root litter was pooled, ground, and analyzed by IRMS to calculate an average enrichment of 7.191 ± 0.398 SE atom% ^{13}C.

2.3.4 ^{13}C-Nuclear Magnetic Resonance Mass Spectrometry

Major chemical classes of mineral-associated organic matter were identified by ^{13}C-Nuclear Magnetic Resonance Mass Spectrometry. Finely ground samples were packed in a 5 mm optical density ceramic rotor and analyzed on 500 MHz solid-state ^{13}C-NMR (Oxford) at the Environmental Molecular Sciences Laboratory (EMSL) at the Pacific Northwest National Laboratory (PNNL). Standards of potassium bromide and Adamantine were run at 5,000 Hz. The soil standard was "Pahokee Peat" (IHSS, Standard Sample), collected from Florida and sieved to <53 μm. The low C concentrations in our samples required long ^{13}C-NMR runs, thus we ran pooled samples (n=3) for each minerals type rather than replicates.

2.3.5 Fourier Transform Ion Cyclotron Resonance Mass Spectrometry and Lipidomics

FTICR-MS and lipidomics analysis of mineral samples extracted with water (FTICR-MS) and then chloroform/methanol (lipidomics (Tfaily et al. 2019)) was conducted at the Environmental Molecular Sciences Laboratory (EMSL). Analyses were conducted on dried mineral samples from the 2-month sampling. We ran 3 biological replicates of each sample. Total lipid extracts were analyzed in both positive and negative modes, and lipids were fragmented using higher-energy collision dissociation and collision-induced dissociation. Confident lipid identifications were made using LIQUID (Lipid Quantitation and Identification) (Kyle et al. 2017). Aligned features were manually verified and peak apex intensity values were exported for statistical analysis. Identified lipids were selected by manually evaluating the MS/MS spectra for diagnostic and corresponding acyl chain fragment ions. In addition, the precursor isotopic profile, extracted ion chromatogram, and mass measurement error along with the elution time were evaluated. All LC-MS/MS runs were aligned and gap-filled using the identified lipid name, observed m/z, and the retention time using MZmine 2 (Pluskal et al. 2010). Each ionization type was aligned and gap-filled separately. Aligned features were manually verified and peak apex intensity values were exported for statistical analysis. Additional information on lipidomic analysis is in **Chapter 1 SI Methods.**

2.3.6 16S and ITS MiSeq

2.3.6.1 DNA Extraction

We extracted DNA for 16S and ITS4 sequencing using a modified protocol from Hurt *et al.* (Hurt et al. 2014). We selected and modified the Hurt *et al*. protocol to optimize DNA yield. Details of our modified protocol are in the **SI**. Briefly, we extracted DNA from 0.25g aliquots of soil or mineral in lysing matrix E (LME) tubes using a two-part protocol. Our protocol used a clay lysis buffer with beta mercaptoethanol and urea extraction buffer to improve DNA release from Kaolinite and Ferrihydrite. LME tubes were beat in a FastPrep and centrifuged before transferring the aqueous phase to a new tube. To the aqueous phase, we added a detergent solution, 5M potassium acetate, and Chloroform:IAA. After vortexing and centrifuging, we transferred the supernatant to a new tube and added isopropanol and glycoblue. While this incubated at room temperature, we added 1M $NaPO_4$ to the LME tube from the initial setup, still with soil or mineral inside. This was vortexed, centrifuged, and the aqueous phase was transferred. After repeating this step, we diluted the aqueous phase 1:10 in 1xTE. To this solution, we added Chloroform:IAA, centrifuged, and transferred the supernatant to a new tube. To this tube, we added 0.6 volumes isopropanol and glycoblue, then incubated at room temperature. We then centrifuged, washed the pellet with ice-cold ethanol, centrifuged again, and pipet off ethanol. After the pellets were dry, we resuspended the pellet in nuclease-free water. Next, we purified the DNA with 7.5M nuclease-free LiCl. Purified DNA was dissolved in nuclease-free water at -80°C. DNA yields from mineral samples were low so we used Zymo Genomic DNA Clean & Concentrator (D4064) to concentrate a subset of our DNA prior to PCR and sequencing.

2.3.6.2 Sequencing

We used a two-step PCR to prepare amplicon libraries as described previously (Wu et al. 2015). In addition to our samples, we ran negative controls (DEPC water), 2 ITS synthetic mock communities (Nguyen et al. 2015, Palmer et al. 2018), and a positive 16S control. For the first step, primer sets used for amplification of the ITS4 and 16S rRNA genes were 5.8S-Fun/ITS4-

FUN (fungal ITS4) (Taylor et al. 2016) and 515F/808R (bacterial and archaeal 16S rRNA gene v4 region). For the second step, primers with different-length (phased) spacers (to increase base diversity in sample library sequences), barcodes, Illumina sequencing region and Illumina adapters were used. Procedures differed from Wu and colleagues (2015) in amplification cycles (10 cycles in the first step and 20 cycles in the second step for 16S rRNA gene; 12 cycles in the first step and 22 cycles in the second step for ITS4). Sample libraries were sequenced on a MiSeq system (Illumina, San Diego, CA) (2 Å~ 250 bp paired ends) at the Institute for Environmental Genomics, University of Oklahoma.

2.3.6.3 Analysis

For processing and analyzing the 16S rRNA gene data, we drew on methods from McMurdie and Holmes and Woolet and Whitman (McMurdie and Holmes 2013, Woolet and Whitman 2020). From input paired-end reads (mean 90,580 reads per sample, minimum 23,109, maximum 171,894), we first trimmed primers using cutadapt (Martin 2011) as implemented in QIIME 2 (Caporaso et al. 2010) (v. 2019.7). We then created a table of exact sequence variants using DADA2 (Callahan et al. 2016) as implemented in QIIME 2, and truncating trimmed reads (225 bp forward, 180 bp reverse). After filtering, denoising, merging, and removing chimeras, we were left with a mean of 70,053 reads per sample (minimum 19,094 and maximum 148,496). We assigned taxonomy using the QIIME 2 feature-classifier classify-sklearn (a naïve Bayes classifier (Pedregosa et al. 2011)) with the SILVA 132 Ref NR 99 database (Quast et al. 2012, Yilmaz et al. 2013, Glöckner et al. 2017), trained on the regions specific to our primers. Herein, we refer to exact sequence variants as "taxa", while acknowledging the two are not precisely synonymous. We used phyloseq (McMurdie and Holmes 2013) to remove mitochondria and chloroplasts and transform counts to relative abundance. We analyzed the ITS4 rRNA gene data using a similar approach to the 16S rRNA gene data, with the addition of ITSxpress (Rivers et al. 2018) to extract only the fungal ITS4 regions of the reads (omitting the primer trimming step, and thus starting with a mean of 159,819 sequences per sample (minimum 1,505, maximum 352,647 sequences)). For DADA2, we truncated reads only at 300 bp, leaving a mean of 136,523 sequences per sample (minimum 1,091 and maximum 303,215), and used the UNITE database (v. 8.2, dynamic) to assign taxonomy. Because the ITS4 region has variable length across taxa and because the trimming from ITSexpress may have trimmed individual reads at slightly different locations, we merged all taxa that had identical sequences except for length using DECIPHER (Wright 2016) to cluster by exact sequence variants, or "taxa". We assigned AMF status to any taxa within the Glomeromycota phylum according to Glassman *et al.* (Glassman et al. 2015).

2.3.7 Statistics

Carbon concentrations are reported with standard error (n=3). We used a partially-nested mixed effects model according to Doncaster and Davey (Doncaster and Davey 2007) to analyze the total C results and IRMS results. To do an analysis of variance (ANOVA) on these data, we used the nlme package(Pinheiro et al. 2019) in R v.3.5.1 (R Core Team, 2018) on log-transformed data to maintain assumptions of normality. To conduct pairwise comparisons, we used the emmeans package (Lenth 2019) in R. We performed non-metric multidimensional scaling (NMDS) analysis using presence/absence data and Jaccard distances on FTICR-MS data to determine group differences in R using the package ftmsRanalysis (Bramer and White 2018). To determine whether the differences illustrated in the NMDS plot were significant, we ran a

permutational multivariate ANOVA (PERMANOVA) analysis in R using the adonis function in the vegan package(Oksanen et al. 2019). We performed principal coordinate analysis (PCoA) with a Bray-Curtis dissimilarity matrix on the lipidomic data to determine sub-class differences in R using the vegan package (Oksanen et al. 2019). To determine whether the differences in the PCoA plot were significant, we ran a permutational multivariate ANOVA (PERMANOVA) analysis in R using the adonis function in the vegan package (Oksanen et al. 2019). To characterize differences in community composition between samples based on 16S rRNA and ITS4 rRNA, we performed a NMDS analysis on Bray-Curtis dissimilarities (Bray and Curtis 1957) between samples with k = 3 (Oksanen et al. 2019). To determine whether mineral type and litter additions had significant effects on microbial community composition, we performed a PERMANOVA on Bray-Curtis dissimilarities using the vegan package in R (Oksanen et al. 2019). To determine which taxa had significantly higher or lower relative abundance on the minerals compared to soil, we conducted a differential test using corncob (Martin et al. 2020) with a false discovery rate cutoff of 0.05, controlling for differential variance and filtering any taxa with <0.01% relative abundance. We reported differences in relative abundances between the minerals and soil as log_2-fold changes.

2.3 RESULTS

2.4.1 Tracing the Fate of ^{13}C Root Litter

2.4.1.1 $^{13}CO_2$ Release Following Wet-Up

We traced CO_2 release from microcosms before simulating wet-up. At the start of the experiment, ^{13}C-litter microcosm was 79.5 ± 2.4 SE ppm CO_2/min and control microcosms was 36.4 ± 3.3 SE ppm CO_2/min (**Figure 2.2**). This indicates that we did have some decomposition and microbial activity prior to wet-up. Initial CO_2 release from the ^{13}C-litter microcosms was significantly higher ($p > 0.001$) and was enriched in ^{13}C, with 2.6 atm% ^{13}C.

Following our simulated wet-up at the start of the experiment, we observed a large pulse of CO_2 from the ^{13}C litter amended microcosms following our simulated wet-up (**Figure 2.2**). In the control microcosms, CO_2 accumulation increased to 247.2 ± 70 ppm CO_2/min 11 hours after wet-up and then held steady near 267.6 ± 166 ppm CO_2/min for the following 4.5 days. In contrast, CO_2 accumulation was actually lower in the ^{13}C-litter microcosms for the first 11 hours following wet-up, at 116.9 ± 9.7 SE ppm CO_2/min. By 31 hours following wet-up, however, ^{13}C-litter microcosms had such a large increase in CO_2 release that it saturated the detector on the Piccaro analyzer (>1,510 ppm CO_2/min). After 24 hours, the CO_2 was 5.8 atm% ^{13}C and after 72 hours it was 6.2 atm% ^{13}C. Added root litter was 7.20 ± 0.40 SE atom% ^{13}C, so the high CO_2 enrichment levels in the ^{13}C litter microcosms suggest that most of this large CO_2 pulse after wet-up is derived from decomposing root litter.

2.4.1.2 ^{13}C Association with Soil Minerals

Despite ^{13}C root litter addition, there was low ^{13}C enrichment of mineral-associated OM (**SI Figure 2.1**). The Native Minerals were the least enriched, at 1.10 ± 0.003 atom%^{13}C at 3 months, though the enrichment compared to Native Minerals in the control microcosms was significantly higher ($p=0.008$). Kaolinite was the most enriched, with 1.28 ± 0.10 SE atom% ^{13}C at the final 3-month harvest. However, Kaolinite actually lost ^{13}C between the 1-week and 1-month harvests. At 1-week, Kaolinite had 1.55 ± 0.14 SE atom%^{13}C. ^{13}C enrichment on Ferrihydrite, Quartz, and

the Native Mineral did not significantly change from 1-week to the final harvest at 3-months. This suggests that most ^{13}C-labeled root litter derived C associated with the minerals in the first week of incubation in soil microcosms. Using a mixing model (**Eq. 2.**1), we calculated the percent root-derived C on each mineral type. Root litter-derived C contributed only a small portion of the C on mineral surfaces (1.16% ± 0.38% for Ferrihydrite, 3.41% ± 1.6% for Kaolinite, 1.81% ± 0.80% for Quartz, and 0.36% ± 0.05% for the Native Minerals) (**Figure 2.3d**).

2.4.2 Total Carbon Accumulation on Minerals

Ferrihydrite, Kaolinite, and Quartz had no associated C before incubation in soil microcosms. At the final 3-month harvest, these specimen minerals accumulated a modest quantity of mineral-associated OM, ~ 98% less total C than the bulk soil and ~78% less total C than the Native Minerals (**Figure 2.3a**). At 3-months, there was no significant effect of ^{13}C litter addition on total C in any of the minerals as compared to the soil incubation without litter (Native Mineral: $p = 0.849$, Ferrihydrite: $p = 0.382$, Kaolinite: $p = 0.976$, Quartz: $p= 0.361$) (**Figure 2.3a**).

Carbon association with specimen minerals was rapid and varied significantly by mineral type ($p<0.001$), with the most total C accumulation on Kaolinite and the least on Quartz (**Figure 2.3b**). After the initial rapid C accumulation in the first week, there was no significant change in total C across any of the specimen minerals (Ferrihydrite: $p = 0.392$, Kaolinite: $p = 0.583$, Quartz: $p= 0.439$). The only significant change over time was in the Native Minerals in the control treatment, which actually lost C from 1-week to 3-months ($p = 0.043$) (**Figure 2.3c**). Native minerals incubated in the ^{13}C litter treatment had a trend of C loss but, due to high variability between biological replicates, this change was not significant ($p = 0.146$).

2.4.3 Carbon Chemistry

2.4.3.1 Solid-State ^{13}C-NMR

As with total C accumulation on minerals, we do not see a clear treatment effect in our ^{13}C-NMR spectra (**Figure 2.4**). Solid-state ^{13}C-NMR shows bulk chemistry, but it does not detect C associated with paramagnetics, such as iron (Fe). We know that our bulk soil and Native Mineral fraction contain ferrihydrite, and that there is some inclusion of Fe in our Kaolinite, so **Figure 2.4** shows the major chemical functional groups present that are not associated with Fe. Some peaks in the ^{13}C litter treatment are marginally better defined than those from the no litter, which could be due to improved signal to noise resulting from more ^{13}C compounds in the labeled samples. The actual peak locations are identical. We do see a shift from bulk soil to Native Mineral to Kaolinite, where the detected C compounds become less diverse and more aliphatic in character. In the bulk soil, the largest peak is characteristic of carbohydrates. There are also aromatic and aliphatic peaks. In the Native Mineral fraction, peak locations resemble those in the bulk soil, indicating that Native Minerals have the same range of broad C functional groups. However, in the Native Minerals, the aliphatic peak was higher than in the bulk soil, with a peak intensity similar to carbohydrates, suggesting a shift to more aliphatic material. In the Kaolinite, the only clearly defined peak is aliphatic. While the aliphatic peaks in the ^{13}C-NMR spectra have a lower ppm than classically interpreted lipids, C detected in this region could also include lipids.

2.4.3.2 FTICR-MS

We found a mineral effect in the water-extracted samples analyzed by FTICR-MS, with a compositional profile that was significantly different by mineral type ($p<0.001$). Unlike the results of ^{13}C-NMR, we found that the water-extracted FTICR-MS metabolites were significantly different in the ^{13}C-litter and no litter treatments ($p=0.002$). We interpret the water-extractable compounds detected by FTICR-MS as the "transient fraction" of mineral-associated SOM. These are compounds that are loosely associated with the mineral surface and more readily released back into the soil. Van Krevlen diagrams of O:C by H:C ratio (**SI Figure 2.2)** group the distribution of metabolites identified by FTICR-MS roughly by compositional class. For each mineral type and treatment, we mapped the centers of mass of the Van Krevlen diagram to observe overall shifts in O:C and H:C composition. We found that all mineral types and treatments shared a similar center of mass, with an O:C ratio of ~ 0.5 and a H:C ratio of ~ 1.5. Higher counts of total metabolites were detected in the bulk soil and Native Mineral than the specimen minerals, consistent with higher C concentrations (**SI Figure 2.3)**. Ferrihydrite had a lower diversity and lower total counts of metabolites than the other mineral types. None of the mineral types had many lipid-like compounds or protein-like compounds. In contrast to ^{13}C-NMR results, which show a relatively broad profile of mineral-associated SOM compounds, FTICR-MS was conducted on the water extracted compounds, and thus did not access many higher H:C compounds such as lipids and aliphatics, which are not easily released from the mineral surface with a simple water extraction.

2.4.4 Lipidomics

We identified a total of 219 unique lipids across all four mineral types and two treatments (litter and no litter). While different ionization potentials prevent us from comparing quantities between lipid categories, within a sub-class we were able to compare between mineral types and treatments (**Figure 2.5**). The distribution of unique lipid classes by mineral type was highly significantly different ($p<0.001$).

With a total of 115 unique lipids identified, Glycerophospholipids [GP] were the largest lipid category observed across samples. Most of these lipids belonged to the classes Glycerophosphocholines (PC) and Glycerophosphoethanolamines (PE), but we also observed Glycerophosphoglycerophosphoglycerols (CL), Glycerophospohoglycerols (PG), and Glycerophosphoinositols (PI). Highly abundant in bacteria (Sohlenkamp and Geiger 2016), phospholipids are commonly structural components of cell membranes (Siliakus et al. 2017). Many of the GP lipids we observed have odd numbers of C atoms (15, 17, or 19 C long fatty acids) with some saturated but mostly unsaturated. Many microorganisms have saturated branched-chained fatty acids (BCFAs) and cyclopropane fatty acids (Frostegard et al. 1993, Zelles 1997, Chang and Cronan 1999, Poger and Mark 2015).

The second largest class of lipids observed across mineral type and treatment was Triradylglycerols (TG), of the Glycerolipid category, with 75 total unique lipids. These storage lipids are highly abundant in fungi (Harwood and Russell 1984). TGs are also found in plants and the bacterial genus *Actinomyces* (Alvarez and Steinbuchel 2002). *Actinobacteria* were the second most abundant phyla associated with the incubated minerals (Whitman et al. 2018), so it is possible some of the observed TGs are bacterial. The distribution of unique lipids within the

TG class by mineral type was highly significantly different ($p<0.001$). The other two classes of Glycerolipids observed were Diradylglycerols (DG) and other Glycerolipids (DGTSA).

Unlike most of the putatively microbe-derived lipid classes observed, most Sphingolipids are plant-derived (Harwood and Russell 1984), but theyare also present in a few microbiak species, including many found in the *Sphingomonadaceae* family (Glaeser and Kämpfer 2014). A total of 17 Sphingolipids were observed, with 16 in the Ceramides (Cer) class and a single neutral Glycosphingolipid (HexCer). Ceramides are typically found in plants, but are also present in most fungi and in a few anaerobic bacteria, such as *Bacteroides* spp (Harwood and Russell 1984, Sohlenkamp and Geiger 2016), one of the top ten bacterial phyla associated with incubated minerals (Whitman et al. 2018).

Comparing lipid intensities across lipid classes and sub-classes, we see that, as expected given the higher total C, the Native Minerals had much higher lipid intensities than the specimen minerals (**Figure 2.5**). Overall, lipid intensities in the Native Minerals were higher in some classes in the litter-amended microcosms than the no litter control. In the Triradylglycerols lipid class, there are some lipids that are completely absent from the control Native Minerals, but present at a relatively high intensity in the litter amendment treatment. Of the specimen minerals, overall, Quartz had the highest lipid intensities. Kaolinite had the lowest lipid intensities of the specimen minerals, with many lipids completely absent, particularly in the Glycosphingolipids. Ferrihydrite has higher lipid intensities in the no litter control treatment, but nearly as low lipid intensities overall as Kaolinite in the litter amendment treatment.

2.4.5 Mineral-Associated Microbial Community

Community composition Bray-Curtis dissimilarities show significant correlation with mineral type for bacteria/archaea and fungi ($p<0.001$) (**SI Figure 2.4**). However, litter treatment was not significant for bacteria/archaea ($p=0.217$) or fungi ($p=0.143$). All minerals, including the Native Minerals, had lower 16S and ITS richness estimates by WLRM (Willis 2016) than the bulk soil (**SI Figure 2.5**). ITS richness estimates for all the specimen minerals were in the same range as those for the Native Mineral. 16S richness estimates for Ferrihydrite and Quartz were in the same range as those for the Native Mineral, but Kaolinite had a lower 16S richness estimate.

At the phyla level, the bacteria and archaea with the highest relative abundance overall were *Proteobacteria* and *Actinobacteria* (**Figure 2.6**). *Ascomycota* had the highest fungal relative abundance across all mineral types (**Figure 2.7**). Most fungal phyla were present at very low relative abundance on the specimen minerals. *Ascomycota* was the major exception. Also, on Quartz, *Mucoromycota* had a much higher relative abundance than any other mineral type.

To identify taxa that were significantly enriched or depleted on minerals relative to the bulk soil, we compared $\log_2$-fold change compared to bulk soil (e.g. 4x or greater – $\log_2$-fold change = 2) (**Figures 2.6-7**). We see a high degree of variability within phyla. In bacteria, *Proteobacteria*, for example, has both highly enriched and highly depleted taxa on the Native Mineral relative to bulk soil (**Figure 2.6b**). Kaolinite had very few taxa enriched or depleted in both bacterial/archaeal and in fungal analysis. However, of the three 16S taxa enriched in Kaolinite compared with bulk soil, all belonged to the family *Burkholderiaceae*. The family *Burkholderiaceae* is also enriched on the Native Mineral (n=4), Ferrihydrite (n=3), and Quartz

(n=1). *Burkholderiaceae* is a very diverse family, but many are beneficial plant partners (Compant et al. 2008). All the minerals but Kaolinite had taxa of the genus *Streptomyces* enriched relative to bulk soil (Native Mineral: n=4, Ferrihydrite: n=4, Quartz: n=4). Member of the genus *Streptomyces* are saprotrophs, known to grow in particular on cellulose and lignin, can be beneficial to plant growth (Schlatter et al. 2009). On the Native Mineral, two taxa from the genus *Luteibacter* (from the phyla *Proteobacteria*) are highly enriched (log_2-fold 10.0 and 6.8, respectively). Member of the genus *Luteibacter* can produce lipases, chelate ferric ions, and promote plant growth (Guglielmetti et al. 2013, Bresciani et al. 2014, Aamot et al. 2016).

In fungi, there was no clear trend in log_2-fold change compared to bulk soil at the phyla-level (**Figure 2.7**). Nearly all enriched and depleted fungal taxa belong to the *Ascomycota* phylum. An interesting outlier was the phylum *Mucoromycota*, with one enriched taxon in the Native Minerals and one enriched taxon in the Quartz. The *Mucoromycota* in Quartz was the well-studied *Rhizopus arrhizus* species (Dolatabadi et al. 2014), which was highly enriched (log_2-fold 5.7) and had a high relative abundance (0.0018). Kaolinite only had a single enriched taxon, of the genus *Talaromyces,* which we also detected on Ferrihydrite (n=1) and the Native Mineral (n=2). The genus *Talaromyces,* which not well studied in soil, is primarily known for its role as a human pathogen (Pitt 2014, Kauffman 2017). Taxa from the genus *Penicillium* were enriched on Ferrihydrite (n=2), the Native Mineral (n=1) and Quartz (n=2). The genus *Penicillium* is common in soils and members of the genus can promote plant growth, particularly through helping plants with abiotic stress (Chaudhary et al. 2018). One taxa from the species *Metacordyceps chlamydosporia* was found on Ferrihydrite, the Native Mineral, and Quartz. The genus *Metacordyceps* can be a pathogens of arthropods and *Elaphomyces*, though *Metacordyceps chlamydosporia* are more closely related to grass symbionts (Sung et al. 2007).

2.5 DISCUSSION

2.5.1 Wet-up Propels Rapid Carbon Association with Minerals

Prior to our simulated wet-up, we observed higher CO_2 release in our ^{13}C litter amended microcosms. The ^{13}C enrichment of 2.6 atom% $^{13}CO_2$ suggests that a significant portion of the higher CO_2 release from the litter addition microcosms before wet-up originated from decomposition of the ^{13}C litter. After wet-up, the release of CO_2 from both treatments increased, but the CO_2 accumulation rate in the litter amended microcosms eclipsed that of the control microcosms, with more than 3 times as much CO_2 released. As CO_2 accumulation increased in the litter amended microcosms, so, too, did the ^{13}C enrichment of that CO_2. Thus, most of the large CO_2 pulse must have been derived from the added litter. This observed large pulse of CO_2 after wet-up of the soil containing root litter may be due to the cumulative effect of added litter and a Birch effect (Birch 1958, Unger et al. 2010), a wet-up driven CO2 pulse.

It is interesting that we see a small lag (~10 hrs) in CO_2 accumulation after wet-up in the litter amended treatment. Placella *et al.* (2012) found a three-step resuscitation of soil microbes after wet-up (based on 16S rRNA), with *Actinobacteria* responding within the first hour and *Proteobacteria* at 24-72 hours (Placella et al. 2012). *Actinobacteria* and *Proteobacteria* were the most abundant phyla in our soils, but these time frames do not quite match the CO_2 pulse we observe occurring after 11 hours. While this could be due to different soil edaphic conditions in our experiment, it is possible that fungi in our system are responsible for a greater fraction of

CO_2 release (Allen 1965) as the primary C source for the CO_2 pulse appears to be litter. Blazewicz *et al*. found that fungi recover more slowly from a wet-up than bacteria, with a timeframe consistent with our findings (Blazewicz et al. 2014).

Given the large pulse of litter-derived CO_2 following wet-up, it is interesting that we did not observe a significant difference in total C associated with minerals in the litter amended treatment compared with the no litter treatment. This implies that the primary fate of added litter C was CO_2. As we see in our mixing model **(Eq. 2.1**), only a very small percent of C that became associated with soil minerals (1 – 3%) originated from the added ^{13}C litter. Most of the C associated with minerals came from other native soil C pools.

The initial carbon association with specimen minerals was rapid and apparently occurred within 1 week. We also saw rapid C association with minerals in a parallel experiment we conducted in microcosms designed to explore rhizosphere C association with the same specimen mineral types (**Chapter 1**). After the 1-week harvest of this detritosphere experiment, we saw no significant change in total C in any of the mineral types except the Native Mineral incubated in the no-litter control microcosms, which lost total C. The Native Mineral incubated in the litter treatment also showed a trend of C loss, but it was not significant due to high variability between samples. The ^{13}C enrichment (**SI Figure 2.1**), of C associated with Kaolinite was higher at 1 week and declined from 1.55 ± 0.14 SE to 1.28 ± 0.10 SE atom%^{13}C by the final harvest at 3 months. Given that there was no significant change in total C, the decline in ^{13}C indicates turnover, with some of the initial litter-derived ^{13}C replaced by natural abundance C from the surrounding soil over time.

The wet-up event likely initiated a period of rapid organic C transformation and mineralization, with rapid turnover of added root litter and C association with minerals. However, even though the soil remained moist throughout the experiment, there was no significant change in total C on minerals after the initial pulse of C accrual on the minerals. The litter amendment did not impact total C on minerals. In other studies, litter additions have not always increased the quantity of total C in soil (Lajtha et al. 2014, Lajtha et al. 2018). In our study, the large pulse of $^{13}CO_2$ after wet-up suggests the primary fate of the added root litter was mineralization. However, a small amount of litter-derived ^{13}C did associate with minerals. While we did not observe a difference in the chemistry of mineral-associated C at the bulk scale with ^{13}C-NMR, FTICR-MS analyses revealed significant effects of the litter amendment treatment, and we observed some differences in lipid intensities between the two treatments. Thus, even though litter addition did not significantly impact total C associated with minerals, the resulting small differences in chemistry may influence the long-term persistence of that C. Overall, in our system, litter addition did not appear to be an effective method for increasing mineral-associated C stocks in soil.

2.5.2 Comparison to the Rhizosphere

2.5.2.1 Carbon Dynamics in the Detritosphere and Rhizosphere

In our prior work (**Chapter 1**), we traced ^{13}C flow from the rhizodeposits of growing *Avena barbata* using the same mineral types, mineral bags, and source soil as in this experiment. Both the rhizosphere and detritosphere are zones of enhanced microbial activity and increased C availability (Jones et al. 2009, Finzi et al. 2015, Kuzyakov and Blagodatskaya 2015). We found striking differences, as well as some similarities, between our model two systems.

In both the detritosphere and rhizosphere, we found that mineral type was highly significant in determining the total C associated with the minerals. However, while the magnitude of total C association was similar between specimen minerals in the rhizosphere and detritosphere experiments, in the rhizosphere, Ferrihydrite accumulated the most total C, while in the detritosphere, Kaolinite accumulated the most total C. In the rhizosphere, Ferrihydrite, with higher *surface reactivity,* accumulated more total C. In the detritosphere, Kaolinite, with higher *surface area,* accumulated more total C (**Figure 2.8)**.

Here, we calculated the relative contribution of labeled root litter on the different mineral types using a mixing model (**Eq. 2.1**). In our prior work on the rhizosphere, we made the same calculation for the relative contribution of labeled rhizodeposits (**Chapter 1**). The percent C from litter in the detritosphere was significantly smaller (average 1.7%) than that in the rhizosphere (average 21.0%). In the detritosphere, a larger fraction of mineral-associated C was from the surrounding soil. In both the rhizosphere and detritosphere, certain minerals may "select" a higher proportion of plant-derived compounds compared to soil-derived compounds. In both systems, Kaolinite had the largest fraction of plant-derived C. In **Chapter 3**, we examine C association with minerals at the microscale, and we found that Kaolinite, which has small, platy minerals, formed microaggregates when incubated in soil. These microaggregates may be capable of encapsulating larger plant-derived C compounds and fragments. In the rhizosphere, Kaolinite preferentially retained ^{13}C-labeled C through a series of sequential extractions, further suggesting that Kaolinite may be particularly well-suited to accumulating plant-derived C.

We explored the C dynamics of the detritosphere in an annual grassland from a Mediterranean-type climate characterized by a very dry summer with reduced microbial activity. In these systems the dry period commonly ends with a rainfall mediated wet-up event, mobilizing litter C and revitalizing the soil microbial community. We found that in our system, mineral surface area may be the most important factor in determining total C association. Following wet-up, there is a pulse of C available for mineral association. The detritosphere after wet-up is both a "hot spot" and "hot moment" of microbial activity and C transformation. In contrast, the rhizosphere is a "hot spot" but C release is more continuous, though there is variability in rhizodeposit chemistry as the root ages (Schweinsberg-Mickan et al. 2012). In the rhizosphere, there is also more sustained high microbial activity (Philippot et al. 2013), as well as the release of organic acids such as oxalic acid that can liberate mineral-associated C (Keiluweit et al. 2015). In **Chapter 1**, we concluded that C association with minerals is more dynamic in rhizosphere soil than in bulk soil. Thus, in the rhizosphere, higher surface reactivity, which more strongly binds mineral-associated OM, may be a stronger determinant of total C accumulation.

2.5.2.2 Microbial Community Composition in the Detritosphere and Rhizosphere

As we saw in the rhizosphere, minerals in the detritosphere are colonized and inhabited by bacteria, archaea, and fungi (Whitman et al. 2018). As we might expect, many of the abundant bacterial and fungal taxa in the detritosphere were saprotrophs. At the phyla level, the community composition of mineral-associated bacteria and archaea was similar to that of the rhizosphere, but as we focus in with higher phylogenetic resolution, we uncover differences.

One of the biggest contrasts between the rhizosphere and detritosphere microbial communities is the presence of plant symbiotic fungi in the rhizosphere. Most of these symbiotic fungi were

arbuscular mycorrhizal fungi (AMF), but we also detected some ectomycorrhizal fungi (EM) (Whitman et al. 2018). In the rhizosphere, the order *Glomerales*, to which AMF belong, was particularly enriched on Ferrihydrite (Whitman et al. 2018), and we found fungal hyphae that were morphologically consistent with AMF associating with Kaolinite, Ferrihydrite, and the Native Mineral by SEM and NanoSIMS. In **Chapter 3**, we discuss how at the microscale fungal hyphae acted as a "shunt" for plant-derived C from *Avena barbata* to the mineral surface in the rhizosphere. In the detritosphere, in the absence of a growing root, we expect that the few *Glomerales* taxa associated with minerals are from fungal spores and do not play a large role in transferring C to the mineral.

2.5.3 Microbial Lipids and the Potential for Carbon Persistence

Lipidomics showed that many of the identified lipids on all mineral types are likely microbially-derived. While in the rhizosphere, many of the lipids identified and patterns of lipid intensity across mineral types differed from the detritosphere, we made similar overall interpretations based on lipid structures (**Chapter 1**). Our prior work using this experimental system showed that mineral type shaped microbial association and assembly on mineral surfaces (Whitman et al. 2018). We expect the distinct lipid signature on different mineral types may be driven in part by the phylogenetically distinct microbial communities associated with these minerals. In our prior work on the rhizosphere, we found that overall, Kaolinite had higher lipid intensities than the other specimen minerals and Quartz had the lowest lipid intensities overall. However, in the detritosphere, Kaolinte had the lowest lipid intensities overall, despite having a higher total C content than in the rhizosphere (**Figure 2.5**). Quartz, which had a comparable total C content to that in the rhizosphere and the lowest total C content in both systems, had the highest lipid intensities overall in the detritosphere (**Figure 2.5**). The clear microbial signature on mineral-associated SOM suggests that, if we know the soil mineral type, studying the microbial community composition and functional capacity may help in predictive modeling of mineral-associated SOM.

The high lipid intensities on Quartz in the detritosphere could be explained by high relative abundance of the genus *Mucorales*. On Quartz, the *Mucorales* species *Rhizopus arrhizus* was $\log_2$-fold 5.7 higher than bulk soil. Members of the *Mucorales* genus are considered "oleaginous fungi", and *Rhizopus arrhizus* is particularly rich in lipids, with a lipid content of 57% dry weight(Yang et al. 2019). The lipid composition of *Rhizopus arrhizus* is ~ 44% polar lipids and ~ 22.1% triglycerides (Weete et al. 1970).

Triacylglycerols (TG) were one of the most common lipid categories across all samples. While most of the TGs are likely from fungal storage lipids, the bacterial genus *Streptomyces* is unique for a bacteria in its ability to store *triacylglycerols* (Olukoshi and Packter 1994). Members of the genus *Streptomyces* were highly enriched relative to bulk soil on Ferrihydrite, Quartz, and the Native Mineral. Miltner *et al.* (Miltner et al. 2012) found that microbial cell envelope fragments are important components of soil OM. We found a high diversity of Glycerophospholipids, many of which appeared to be bacterial membrane lipids, associated with all mineral types.

The potential of particular fungal and bacterial species with high lipid contents to influence the overall lipid profile of mineral-associated OM could have important implications for C persistence in soil. In the past, the primary paradigm explaining the persistence of soil OM was

that chemical composition, particularly chemical "recalcitrance", dictated the fate of the OM. The newer and now well-accepted paradigm is that the soil physical environment is far more important to controlling the persistence of soil OM (Torn et al. 1997, Schmidt et al. 2011). Both our prior rhizosphere experiment and this detritosphere experiment show total C was significantly influenced by mineral type – but not the same minerals. In the rhizosphere experiment, Ferrihydrite accumulated the most total C, while in the detritosphere experiment, Kaolinite accumulated the most total C. We suggest that while mineralogy is important, the factors controlling the persistence of soil OM are more complex. Other recent studies propose that microbial dynamics, particularly microbial efficiency, influence the persistence of soil OM(Kallenbach et al. 2016, Sokol et al. 2019b). Kallenbach *et al*. (2016) also found that soils with higher SOC had higher lipid abundances (Kallenbach et al. 2016). Based on our work, we suggest mineral type, microbial community dynamics, and chemistry may all interact to control the persistence of soil OM. We posit that managing soils to promote growth of lipid-rich microbial communities may be one approach to increasing C storage. However, doing so may require a tailored approach that considers mineral type. For example, in a quartz-rich soil, promoting the growth of members of the *Mucorales* fungal genus, such as *Rhizopus arrhizus,* may increase total C. However, in a soil rich in Fe-oxides, such as ferrihydrite, promotion of *Streptomyces* bacterial genus may increase total C associated with minerals.

2.6 FIGURES

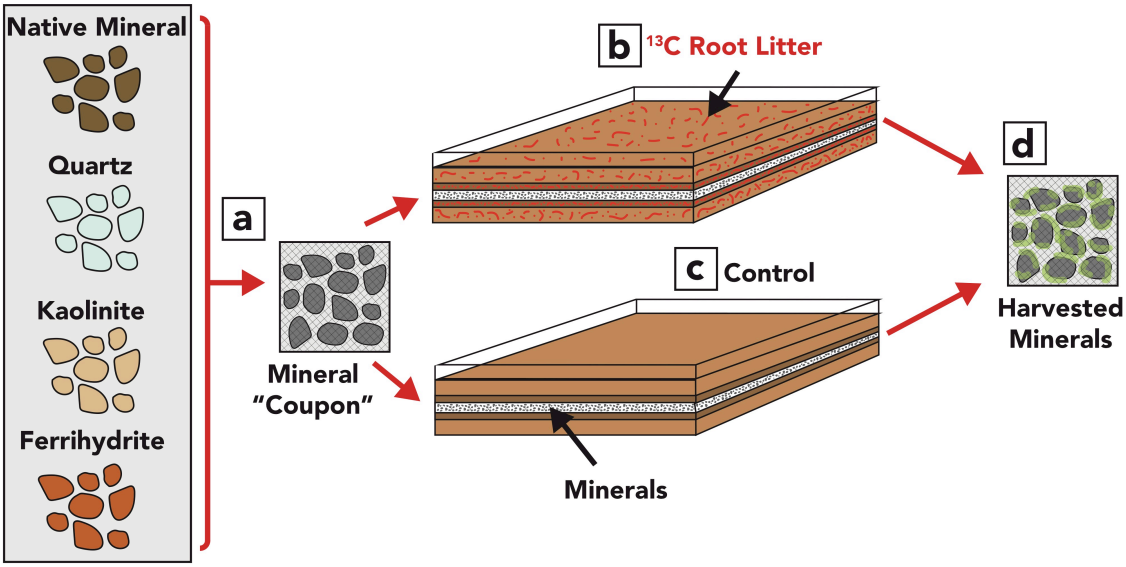

Figure 2.1. Experimental setup, with four mineral types (a) placed into mineral bags, or "coupons". Quartz, Kaolinite, and Ferrihydrite were specimen minerals with no detectable initial carbon. The Native Minerals were density fractionated from soil, and thus were already associated with unlabeled C. Mineral coupons were place in soil microcosms with added ^{13}C root litter (b) or a no-litter control (c). ^{13}C root litter was added to simulate field density for surface soil, and was added at higher density 2 mm above and below the mineral coupons. Mineral coupons were destructively harvested at 1 week, 1 month, and 3 months.

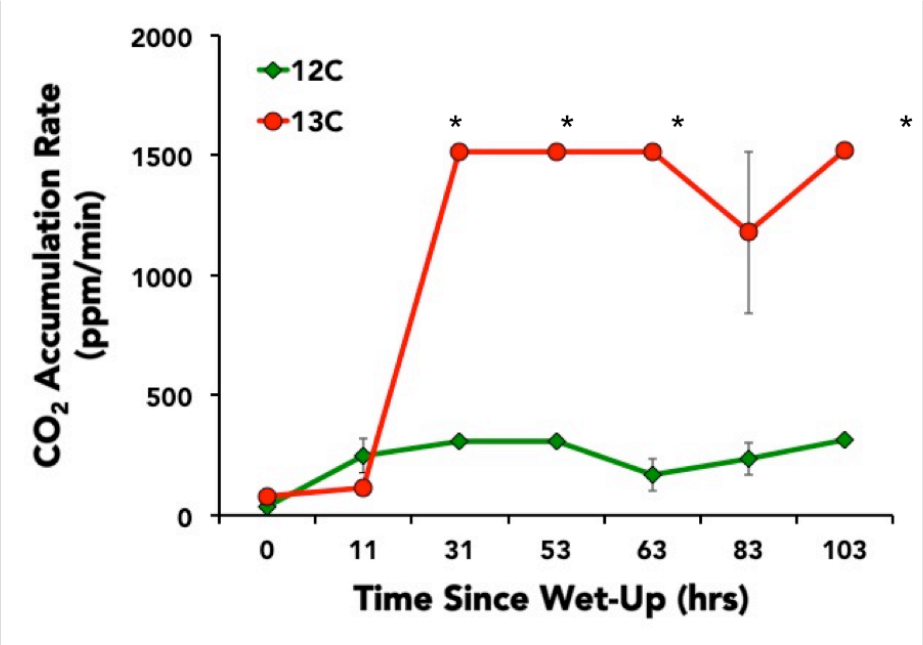

Figure 2.2: CO_2 accumulation rate (ppm/min) after simulated wet up. $^{13}CO_2$ derived from decomposition of soil amended *Avena barbata* root litter was measured with a Picarro, while CO_2 fluxes in the control microcosms were measured with an IRGA. Each point is the average of three microcosms ± standard error. Stars above the points for the ^{13}C litter microcosms indicate times when the instrument saturated, and thus provide a minimum CO_2 accumulation rate.

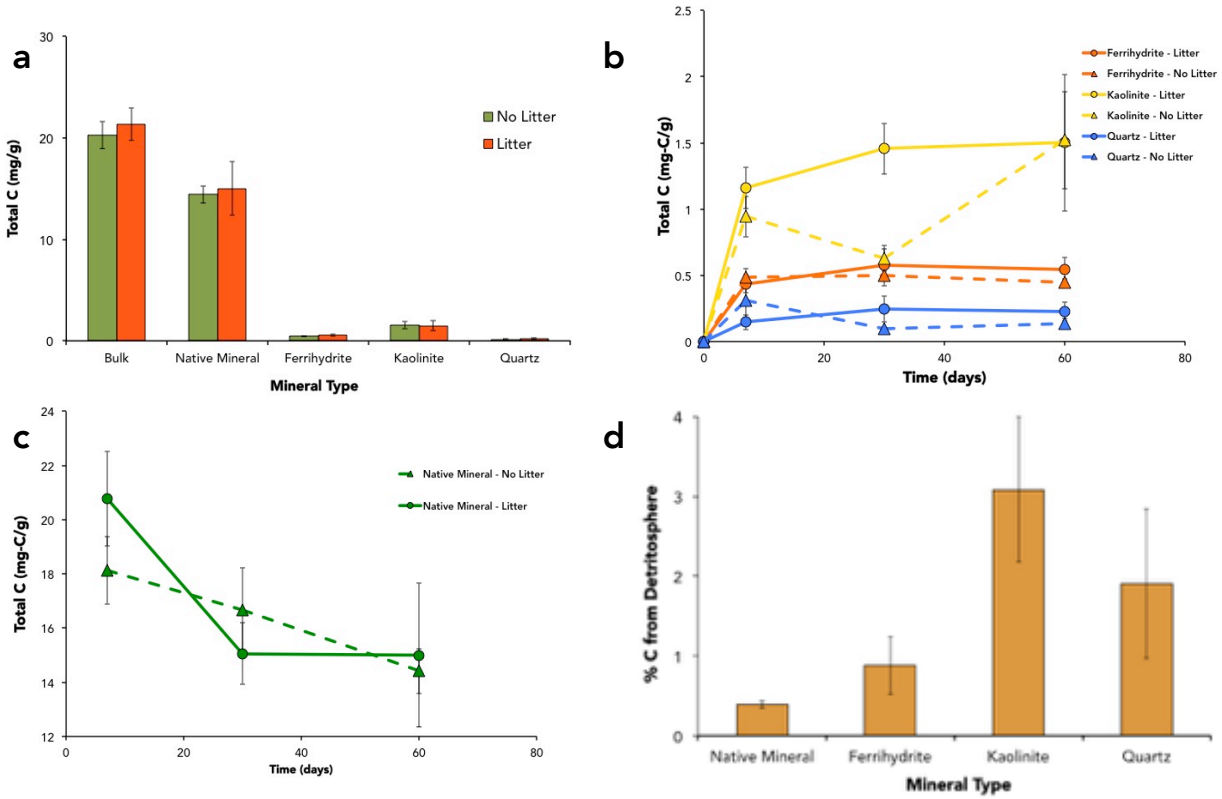

Figure 2.3. Total carbon and ^{13}C root-litter association with minerals revealed rapid, mineral-dependent dynamics. At the final sampling after 3 months of mineral incubation, total C was not significantly different between litter and no litter treatments for any of the mineral types (a). Most total C association with specimen minerals occurred in the first week (b). Kaolinite accumulated the most total C of the specimen minerals (a, b). However, the Native Mineral lost total C over time in both treatments, with a more rapid total C loss in the ^{13}C litter treatment. Using a mixing model (Eq. 1), the percent carbon from root litter was calculated from the ^{13}C content of the litter, bulk soil, and minerals (d). Kaolinite and quartz had the highest percentages of litter-derived carbon.

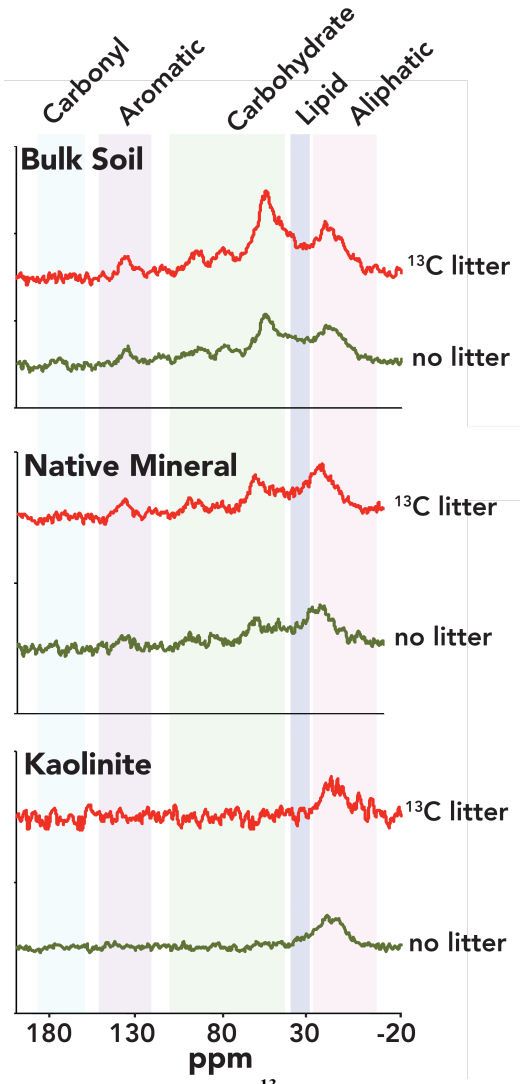

Figure 2.4. Solid-state ^{13}C-NMR analysis of bulk soil (a), native mineral (b), and kaolinite (c) from the ^{13}C litter treatment (red) and the no litter control treatment (green).

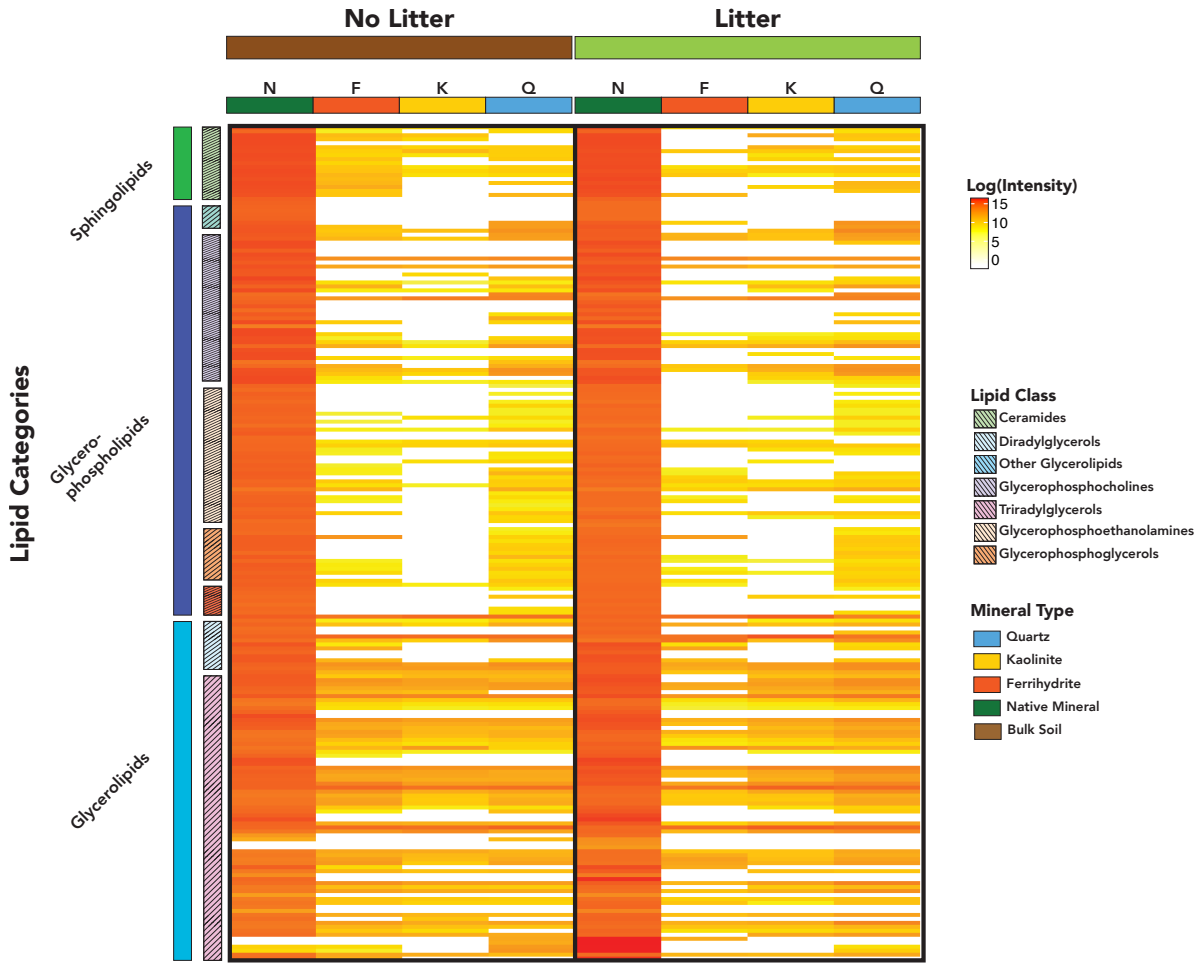

Figure 2.5. Heat map of lipid intensities from lipidomic analysis of mineral extracts from native minerals, ferrihydrite, kaolinite, and quartz incubated in soil with no litter addition or a ^{13}C labeled litter addition.

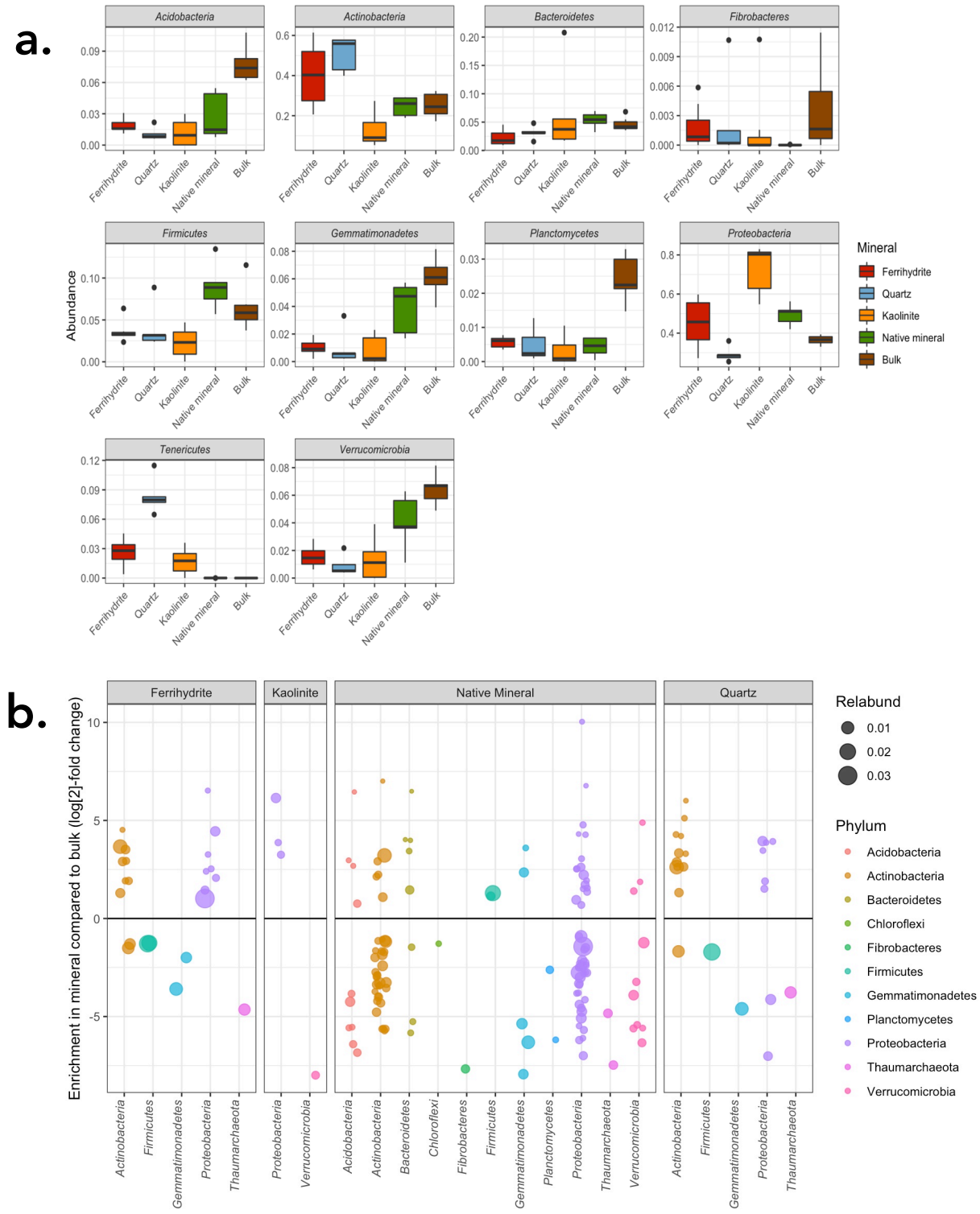

Figure 2.6. Relative abundance of the top 10 bacterial/archaeal phyla on minerals and bulk soil (a), shows differential relative abundance by mineral type within several phyla. Bacterial and archaeal OTUs, colored by phyla, significantly enriched or depleted on minerals compared to bulk soil (b) was calculated as log(2)-fold change. Positive values indicate enrichment compared with bulk soil and negative values indicate depletion.

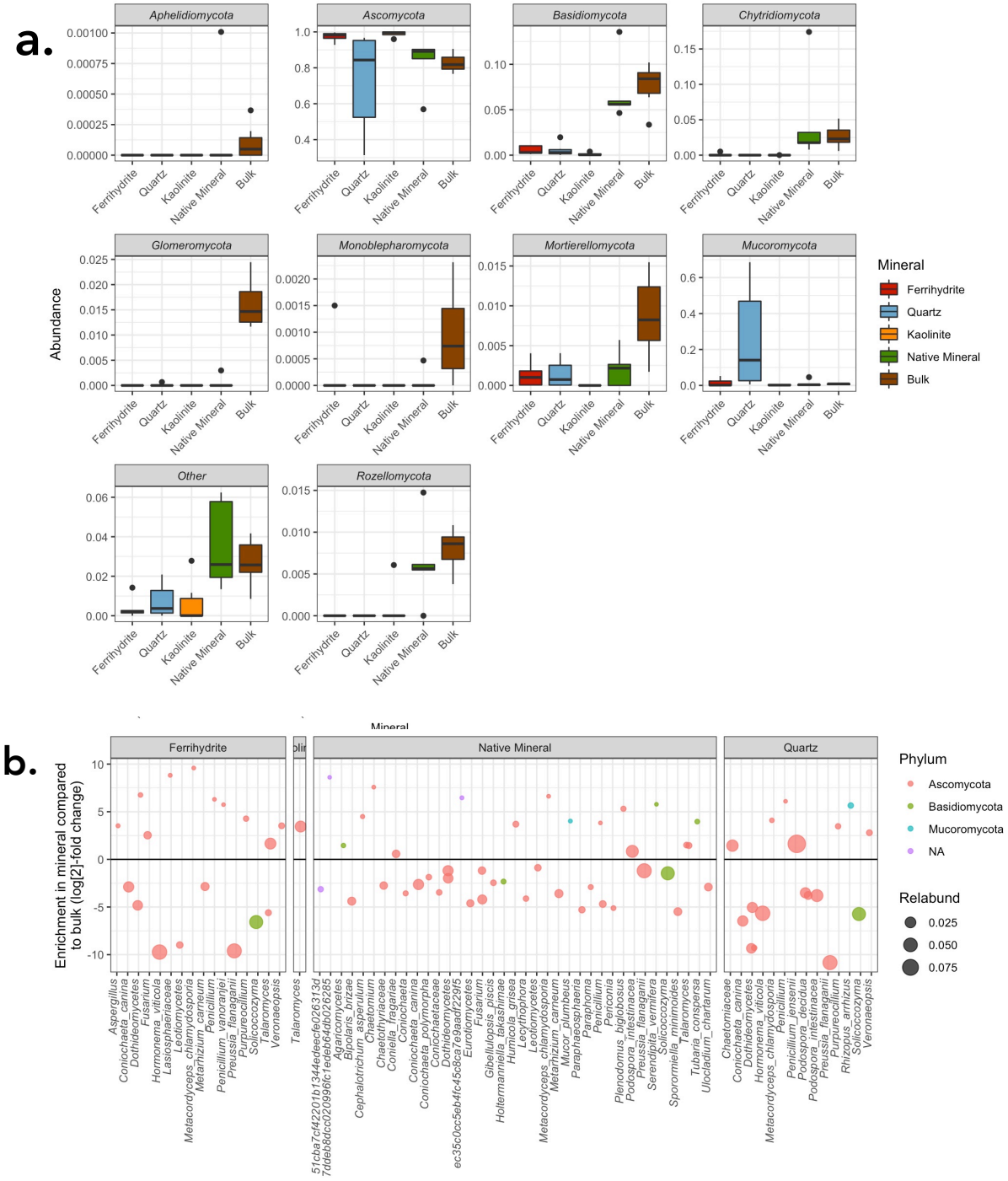

Figure 2.7. Relative abundance of the top 10 fungal phyla on minerals and bulk soil (a), shows differential relative abundance by mineral type within several phyla. Fungal OTUs, colored by phyla, significantly enriched or depleted on minerals compared to bulk soil (b) was calculated as log(2)-fold change. Positive values indicate enrichment compared with bulk soil and negative values indicate depletion.

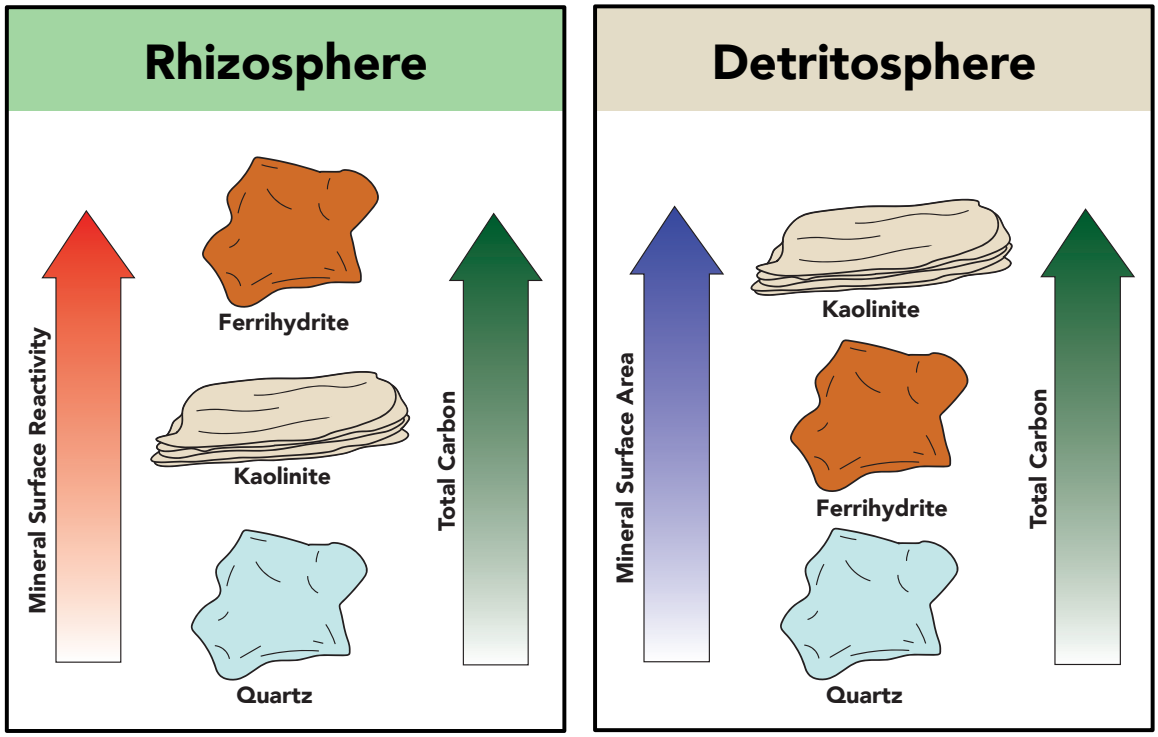

Figure 2.8. Conceptual models comparing total C association with quartz, kaolinite, and ferrihydrite in the rhizosphere and detritosphere. In a prior complementary study of C association with minerals in the rhizosphere (Neurath *et al.*, *in prep*), minerals with higher surface reactivity had more total C. In contrast, in the detritosphere, minerals with higher surface area had more total C.

2.7 SUPPORTING INFORMATION

2.7.1 Supporting Tables and Figures

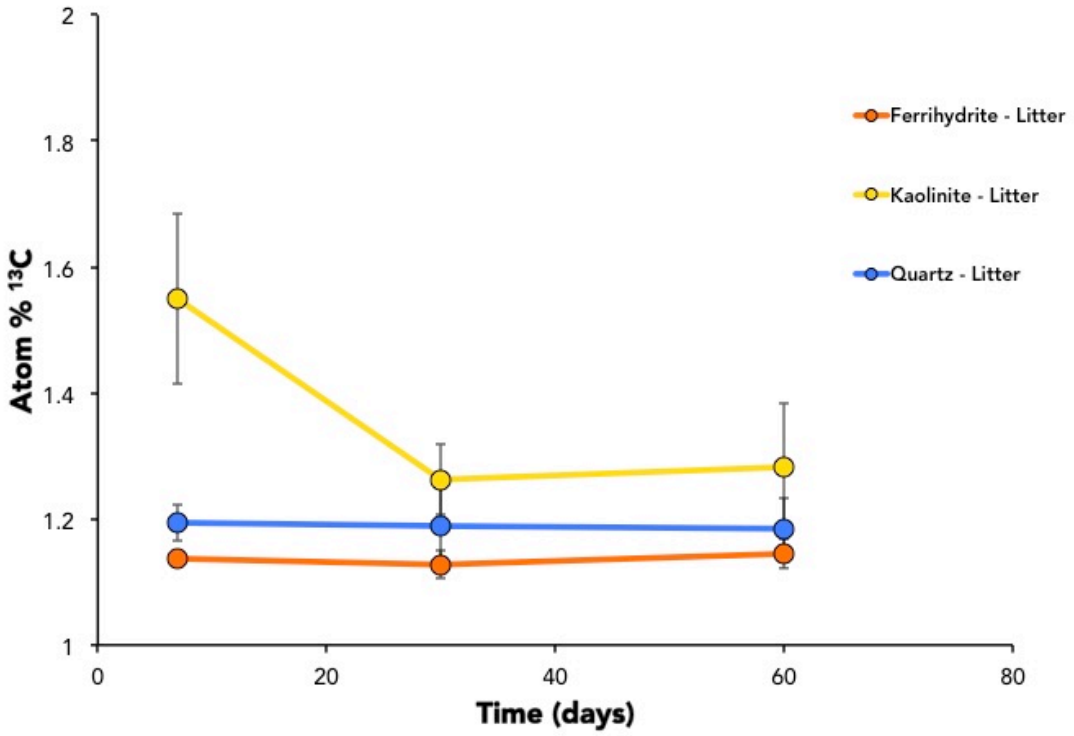

SI Figure 2.1: Atom% ^{13}C over time of Ferrihydrite, Kaolinite, and Quartz minerals incubated in microcosms with added ^{13}C *Avena barbata* root litter.

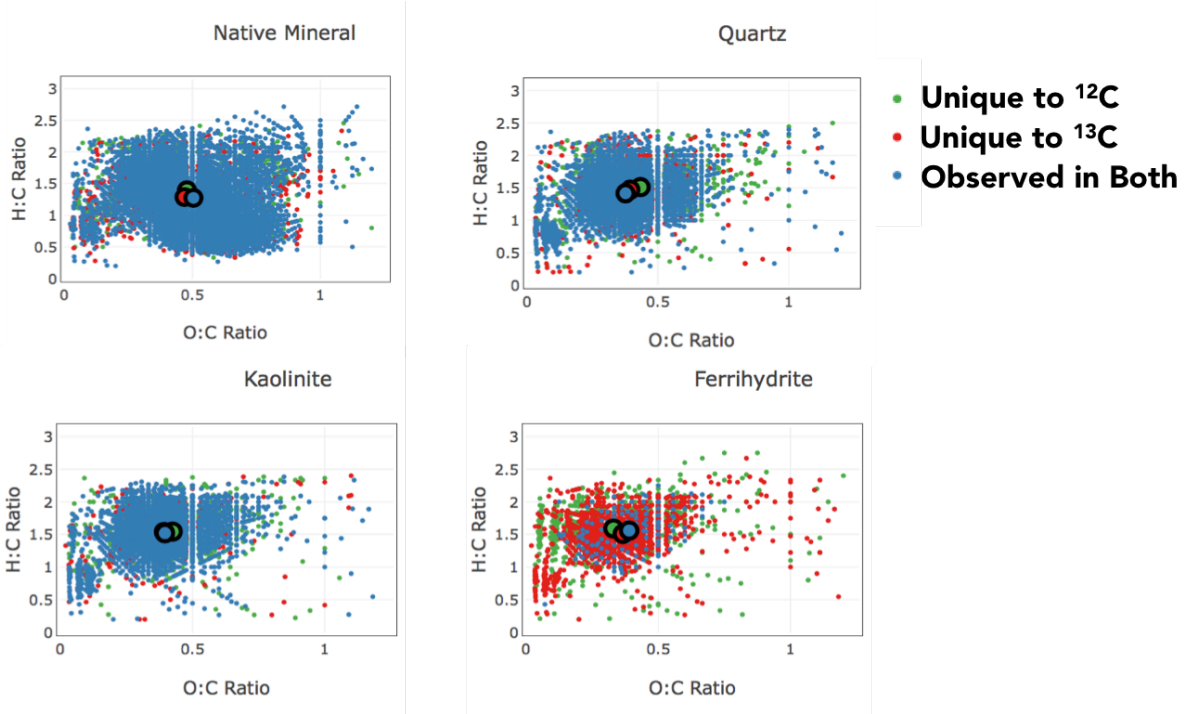

SI Figure 2.2: Van Krevlen diagrams of FTICR-MS data, with a graph for each mineral type. Compounds unique to the ^{13}C litter are in red, unique to the un-enriched control are in green, and observed in both are blue. The center of mass is shown for each.

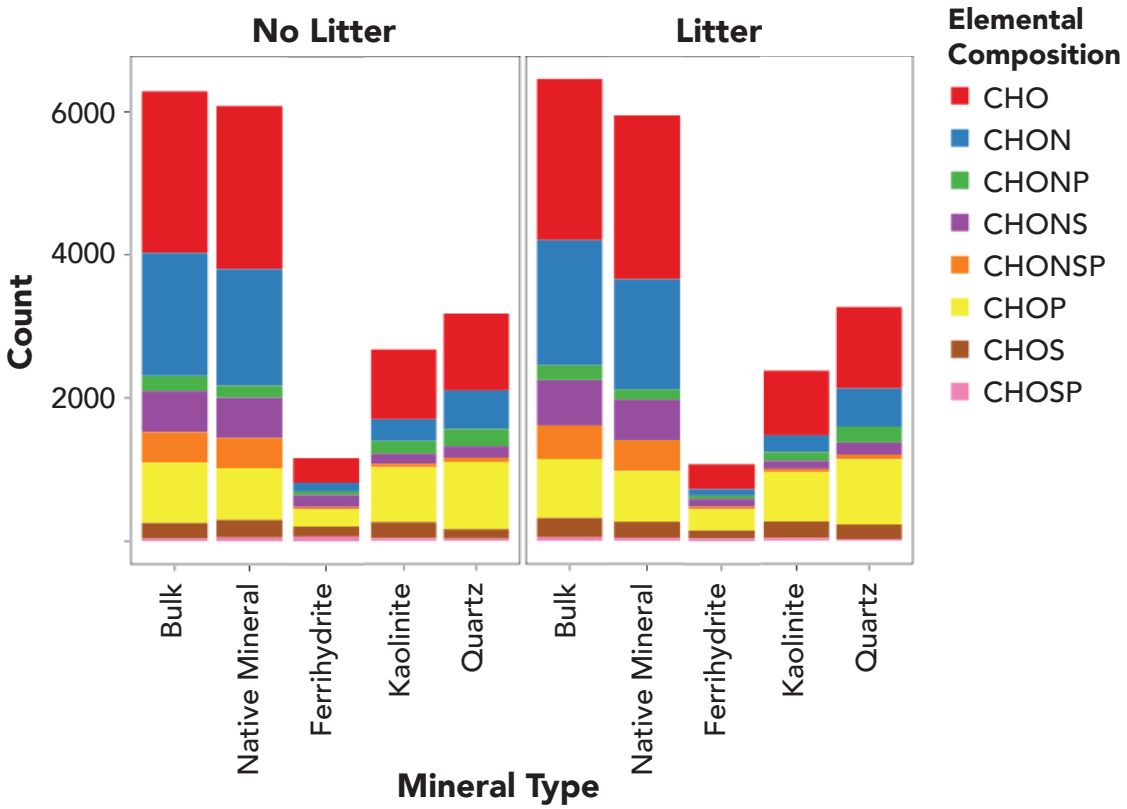

SI Figure 2.3: Counts of metabolites detected by FTICR-MS and sorted by elemental composition of C, H, O, N, P, and S.

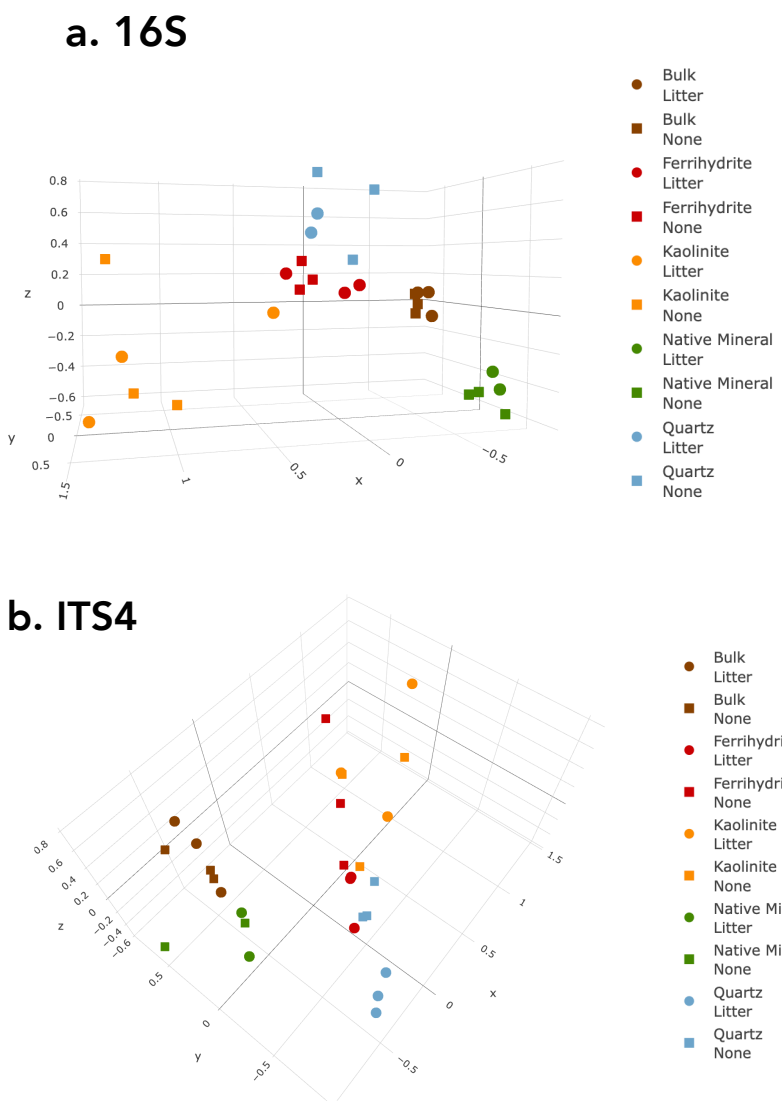

SI Figure 2.4. Three-dimensional NMDS plots of Bray Curtis distances for (a) bacterial/archaeal 16S (k=3, stress=0.05) and (b) fungal ITS4 (k=3, stress=0.09). Both plots show clustering by mineral type but not treatment.

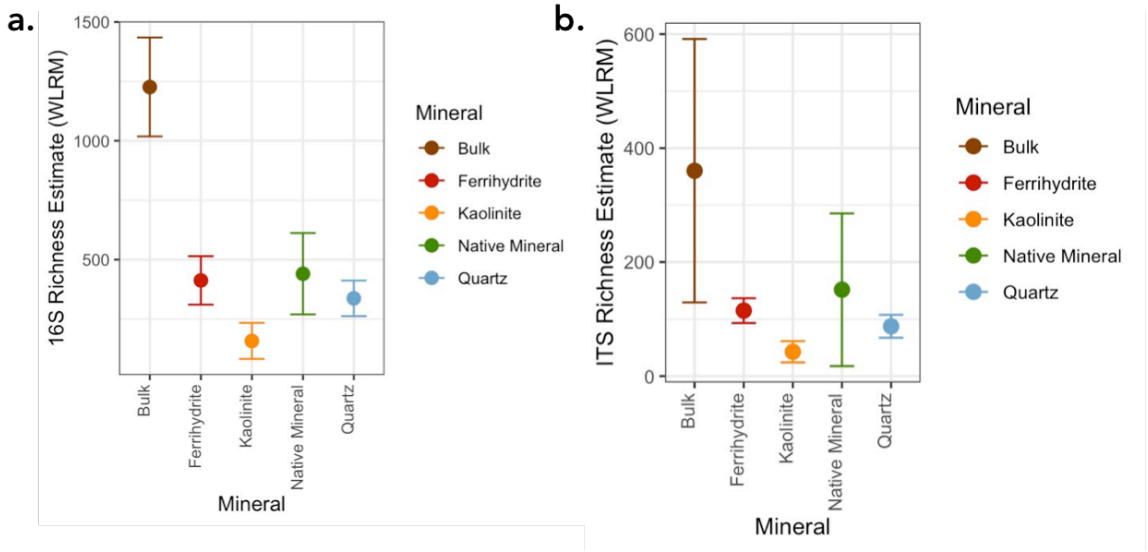

SI Figure 2.5: Richness estimates (WLRM) for 16S bacteria/archaea (a) and ITS fungi (b).

2.7.2 Supplemental Protocol

Adapted OakRidge Protocol for Mineral Samples

Make Clay Lysis Buffer (CLB): Make enough for 1 week of extractions and remake every week

- For each sample, need **82.5µL/sample** (approx. **0.6mL for 6 samples**; **2.4mL for 24 samples**)
- Pre-make BSA/PBS solution and GIT/Sark/PBS solution and mix BSA:GIT/Sark at **1:3 ratio**
  - For 0.6ml total = mix 150µL BSA with 450µL GIT/Sark.
  - For 2.4ml total = mix 600µL BSA with 1,800µL GIT/Sark.
- Mix enough BSA+GIT/Sark for one week, vortex 20 sec, fast spin down 5 sec
- Aliquot into amount needed for each day.
- Day of: Add 0.001% BME to CLB (6µL / 0.6mL CLB; 24µL / 2.4mL CLB); vortex 20 sec, spin down 5 sec.

Prep: Before each extraction

- Pre-labeling, for each sample:
  - Part 1: **1**-15mL tube, **2**-2mL tubes
  - Part 2: **2**-15mL tubes, **2**-2mL tubes
- Make sure isopropanol and 1xTE are aliquoted
- Put glycoblue in chiller rack to thaw

Part 1

1. Wipe down all surfaces, pipets, centrifuge, FastPrep, etc with Eliminase.
2. [Weigh **0.25g** soil into LME tubes] – can do in advance
3. In fume hood, add BME to CLB: **10µL BME/ 1mL CLB (6µL/0.6mL)**; vortex 20 sec, fast 5 sec
4. Add **1.168mL** (4.67mL/g) **urea extraction buffer** and **82.5µL** (.33mL/g) **clay lysis buffer** (**CAUTION**: contains BME! Work in fume hood).
5. Beat in FastPrep **for 30 sec at 5.5 m/s**.
6. Centrifuge for **2 min at 16KxG at 21°C**.
7. Transfer **aqueous phase** to a new **15mL tube**. Record volume transferred. Put aside LME tubes with soil and non-aqueous phase for steps 14-20.
8. Add **325µL** of **detergent solution** (5% sarkosyl and 5% CTAB) (to tube containing aqueous phase).
9. Add **168µL** of **5M potassium acetate**. Vortex 10 sec to mix.
10. Add **equal volume** (volume transferred + 493) of **Chloroform:IAA**. Vortex 10 sec to mix.
11. Centrifuge at **16KxG for 5 min at 21°C**.
12. Transfer supernatant to new tube and add **0.6** volumes of **isopropanol** and **2µl glycoblue**. Vortex 10 sec to mix. Fast spin down 5 sec
13. Incubate at RT for **1.5 - 2 hours**. Move on to step 14 with LME tubes, then spin down all precipitations at the same time at step 21.

Part 2

14. Add **250µL** (1ml/g) of **1M Na_PO_4 (pH 7.2)** to the LME tube saved from step 6. Vortex 10 sec, centrifuge at **10KxG for 1 min at 21°C**, and transfer aqueous phase to new **15ml tube**. Record volume transferred.
15. Repeat step 14.
16. Dilute aqueous phase **1:10** in **1xTE**.
    - (i.e. volume transferred 401µl → V_2= 4.010ml)
17. Add equal volume of **Chloroform:IAA**. Vortex 10 sec to mix.
18. Centrifuge at **16KxG for 5 min at 21°C**.
19. Transfer supernatant to new tube and add **0.6** volumes of **isopropanol** and **2µL glycoblue**. Vortex 10 sec to mix.
20. Incubate at RT for **1 – 1.5 hours**.
    - FastTemp centrifuge to **4°C** while waiting.

Adapted OakRidge Protocol for Mineral Samples

21. Centrifuge for **30 min at 16KxG at 4°C**. Pipet off supernatant.
22. Wash pellet by vortexing with **1mL/5ml** of **70% ice-cold ethanol**. Centrifuge for **10 min** at **16KxG at 4°C**. Pipet off ethanol and let pellets dry for 2 min.
23. Resuspend pellet in **90µl nuclease-free water** for LiCl DNA Purification.

LiCl DNA Purification Protocol

Wipe down all surfaces, pipets and centrifuge with Eliminase
All spins are max speed (16.1KxG) and at 4ºC

1. Make **5 mL** 70% molecular grade EtOH (for 8-sample set), store at -20 ºC or on dry ice
2. Dilute DNA/RNA solution to **90 µL (optimal for DNA yield)**
3. Add **30 µL** 7.5M nuclease-free LiCl
4. Vortex 5 sec at speed 6, spin-down 5 sec
5. Store **30 min** at **4 ºC** (Max incubation time: 1 hour 15 minutes)

6. Spin **20 min** at max speed (**16.1KxG**) at **4° C**
7. Pipette off supernatant (DNA) into new labeled 2 mL tube
    a. Discard old tube containing RNA and protein precipitate
8. Add **80 µL** isopropanol to tube with DNA supernatant
9. Store for **30 min** at **-20 ºC** (Max incubation time: overnight).

10. Spin DNA tube for **10 min** at max speed
11. Remove and discard supernatant.
12. Wash **DNA pellet** with **200 µL** EtOH (vortex at speed **6**, briefly spin-down)
13. Spin **5 min** at **16.1KxG.**
14. Pipette off EtOH supernatant; air-dry pellet in UV hood for **2-3 min**
15. Dissolve the DNA pellet in **20 µL water**
16. Aliquot **4ul** of DNA solution for Picogreen. Store remaining DNA solution at **-80 ºC.**

DNA extraction protocol adapted by Ilexis Chu-Jacoby and Rachel Neurath (2019 Firestone Lab, UCB) from protocol by Jess Wollard (LLNL) based on original protocol from ORNL.

DNA purification protocol adapted by Ilexis Chu-Jacoby (2019 Firestone Lab, UCB) from 2018 Nameer Baker + Christina Fossum protocol, adapted from Untergasser A. “Separate RNA and DNA.”

3

Tracing microscale patterns of carbon association with soil minerals in the rhizosphere and detritosphere

3.1 ABSTRACT

Mineral surfaces provide key sites for C stabilization in soils, protecting soil OM from microbial degradation. Our work takes a microbe-centric view, examining how microbial transformation of soil organic matter (OM) and microbial cells as a component of OM are important factors in the persistence of OM on mineral surfaces. Plant roots are a dominant source of soil C, via exudation by living roots, or, when they die, though decomposition. Here, we examine rapid transformation and association of root-derived C with surfaces of different mineral types, and compare two root C sources: ^{13}C labeled fresh rhizodeposits and ^{13}C root litter. We grew *Avena barbata*, a Mediterranean annual grass, with 99 atom% $^{13}CO_2$ and traced ^{13}C from roots into soil microcosms. In these soil microcosms, we incubated density-fractionated soil minerals and three pure minerals: ferrihydrite, kaolinite, and quartz. After plant senescence at 2.5 months, ^{13}C roots were collected and dried. In a second, complementary experiment, this dried ^{13}C litter was incubated in soil microcosms for 3 months with the same mineral types to simulate the detritosphere. Using a coupled STXM/NEXAFS-NanoSIMS approach, we imaged OM on minerals to determine both the molecular composition and isotopic enrichment. We found that ^{13}C root-derived OM from the growing root and root litter distribution on minerals was patchy and sparse. Minerals incubated in bulk soil, rhizosphere, and detritosphere had distinct C chemistries and their microenvironment (mineral size, morphology, and ability to form nano and microaggregates) not just mineral surface reactivity, influenced mineral-associated C chemistry. In the bulk soil and rhizosphere, we saw more variation between the OM composition associated with different mineral types, but the rhizosphere appeared to exert a homogenizing effect, with more similar OM molecular compositions across mineral types. While most mineral-associated OM generally resembled microbial and microbial-derived C, in the detritosphere, phenolic C, which may be derived from root litter, also associated with minerals. In the rhizosphere, arbuscular mycorrhizal fungi appear to play an important role in shuttling C from roots to minerals. In the detritosphere, microaggregate formation appears ro play a particularly important role in protecting less microbially-degraded, litter-derived C compounds.

3.2 INTRODUCTION

A multitude of microscale interactions between plants, microbes, and minerals govern the fate of soil carbon (C). Bacterial cells attach to clay mineral surfaces, encasing themselves in matrices of extrapolymeric substances (EPS) (Lunsdorf et al. 2000). Under osmotic stress, other bacterial cells lyse and the microbial necromass associates with a mineral, adding to a growing layer of mineral-organic matter (OM) (Creamer et al. 2019). Ferrihydrite coprecipitates with plant root exudates (Eusterhues et al. 2011). Soils are highly complex, and to uncover their complexity at the scale where C dynamics occur, the microscale, we must use tools to characterize nano- to microscale processes (Kinyangi et al. 2006, Solomon et al. 2012, Mueller et al. 2013). Here, we coupled nanoscale secondary ion mass spectrometry (NanoSIMS) with scanning transmission X-

ray microscopy/near edge X-ray adsorption fine structure spectroscopy (STXM/NEXAFS) to visualize microscale patterns of C association with different types of soil minerals. We compared the results of minerals incubated in the rhizosphere (zone of living root influence), versus in the detritosphere (soil amended with dead organic matter 'litter').

Coupled STXM-NanoSIMS analysis of soil samples allows for complementary mapping of mineral-associated OM chemistry and isotopic enrichment at the nanoscale. STXM can map organic C distribution, image associations of organics with specific mineral types, and has been used to trace organic matter of differing origins into the soil matrix (Lehmann et al. 2007, Wan et al. 2007). NanoSIMS and STXM analysis are synergistic, with a similar spatial resolution, and together yield data on both molecular class isotopic enrichment. STXM is based on transmission, while NanoSIMS can characterize either surfaces or a 3-dimensional volume depending on the method of preparation and analysis conditions. NanoSIMS may be preceded by synchrotron-based x-ray imaging techniques such as STXM/NEXAFS to determine mineral oxidation state or dominant organic constituents.

Plant roots are the primary mediators of C transfer into soil (Finzi et al. 2015, Paul 2016, Sokol et al. 2019a), allocating C captured from the atmosphere to the soil system (Kuzyakov and Domanski 2000). Traditionally, studies of soil OM association with minerals examine the transformation and association of plant litter (Heckman et al. 2013, Castellano et al. 2015, Tamura et al. 2017). More recently, the importance of the rhizosphere, or zone of root influence, has come into focus, with a growing body of work on rhizosphere-derived OM on minerals (Pett-Ridge and Firestone 2017, Jilling et al. 2018, Sokol et al. 2019a, Sokol et al. 2019b). In most surface soils, particularly grassland and agricultural soils, the environment experienced by an individual mineral periodically changes from a rhizosphere-dominated system when a root is growing past, to a detritosphere-dominated system as that root dies and root litter begins to decompose. This oscillation between rhizosphere-dominated and detritosphere-dominated may be particularly pronounced in ecosystems with distinct growing seasons, such as a grassland in a Mediterranean-type climate. In the growing season, a large fraction of surface soil may be in the rhizosphere, but in the summer, annual grasses senesce, and the soil becomes a dominantly detritosphere system with decomposing root litter. The impact of random and/or seasonal oscillation between a rhizosphere-dominated system and a detritosphere-dominated system on mineral-associated C chemistry and persistence is unknown.

In the rhizosphere, C is released primarily as root exudates composed of a broad array of small molecular weight compounds (Lynch and Whipps 1990, Bertin et al. 2003, Farrar et al. 2003, Jones et al. 2009, Finzi et al. 2015, Zhalnina et al. 2018). These C substrates may be oxidized, metabolized and transformed by microbes, or become associated with soil minerals. We expect that mineral-associated OM in the rhizosphere could be root fragments, root exudates, microbial cells, or microbially-derived compounds. In the detritosphere, the potential fate of the C is same, but the starting C substrate is decomposing root macromolecules. We expect that mineral-associated OM in the detritosphere could be root litter fragments, dissolved organic C leached from litter, microbial cells, or microbially-derived compounds.

To uncover the mechanisms of mineral-OM association and predict soil C persistence, we need to consider the importance of scale, both spatially and temporally. Microorganisms play an

important role in soil C transformation, and to understand basic processes in the rhizosphere and detritosphere, we need to look at a microbe-size scale. Temporal changes are also critically important, including the changes we might expect to occur as we shift from a detritosphere-dominated system to a rhizosphere-dominated system, and back again.

Using a coupled NanoSIMS-STXM/NEXAFS approach, we integrate two complementary experiments, one focusing on the rhizosphere (**Chapter 1**) and one on the detritosphere (**Chapter 2**), to build a comprehensive view of how C source shapes mineral-associated OM at the microscale. Stable isotopes, such as ^{13}C, provide key insights into complex plant-microbe-mineral interactions (Pett-Ridge and Firestone 2017). To simulate the rhizosphere in the first experiment, we labeled the slender oat grass, *Avena barbata*, with $^{13}CO_2$ while it grew in soil microcosms (**Chapter 1**). To simulate the detritosphere in the second experiment, we added dried ^{13}C root litter from the rhizosphere experiment to the soil microcosms (**Chapter 2**). We traced ^{13}C labeled root C onto different types of soil minerals representing a spectrum of surface area and reactivity: quartz, kaolinite, and ferrihydrite. We compare these simplified specimen minerals to density-fractionated native soil minerals. Both experiments were designed to capture C transformations and association with soil minerals that occur in a single season. Using NanoSIMS, we mapped the distribution and enrichment of ^{13}C on minerals incubated in a bulk soil control, the rhizosphere, and the detritosphere. STXM/NEXAFS allowed us to map C distribution and identify C chemistry with 50 nm resolution, the same resolution as in the NanoSIMS. Coupling NanoSIMS and STXM/NEXAFS, we identify the molecular composition of ^{13}C enriched mineral-associated OM. We hypothesized that both mineral type and C source (rhizodeposits or root litter) would influence the chemistry of mineral-associated OM. Specifically, we sought to answer (i) how a microscale view of mineral-OM heterogeneity differed from a bulk analysis of mineral-OM, (ii) whether ^{13}C root-derived C undergoes transformation prior to association with minerals, and (iii) how the composition of mineral-associated C varies between the rhizosphere and detritosphere.

3.3 MATERIALS AND METHODS

3.3.1 Experimental Design

3.3.1.1 Rhizosphere Experiment

We constructed soil microcosms to study the rhizosphere of *A. barbata* plants, as described in detail in **Chapter 1**. Briefly, we had two treatment types: (1) a *rhizosphere treatment* (n=50), with actively growing *A. barbata* planted in the soil microcosm, and (2) a *bulk soil treatment* (n = 10), which was left unplanted. Nylon mesh bags were filled with one of four mineral types: quartz sand ("Quartz"), ferrihydrite-coated quartz sand ("Ferrihydrite"), 50:50 mixture kaolinite and quartz sand ("Kaolinite"), or the heavy density fraction (>1.75 g-cm^{-1}) ("Native Minerals") of Hopland soil. Microcosms watered to 14% VWC and were continuously labeled in a sealed labeling chamber with added $^{13}CO_2$. Atmospheric CO_2 in the chamber was maintained at 400 ppm and ~ 10 atom% $^{13}CO_2$. Mineral bags were harvested after 2 months of rhizosphere incubation. At harvesting, both minerals and soil were weighed, dried (65°C), and weighed again to obtain soil moisture content. Plant roots and shoots were separated, weighed, and dried. The dried minerals and soil were stored at 4°C until analysis.

3.3.1.2 Detritosphere Experiment

We constructed soil microcosms to study the detritosphere of *A. barbata* root litter, as described in detail in **Chapter 2**. Briefly, we had two treatment types: (1) a *litter amended treatment* (n=3), with added ^{13}C labeled *A. barbata* root litter in the soil microcosm, and (2) a *bulk soil treatment* (n = 3), with no litter addition. As in the rhizosphere incubations (**Section 1.3.1**), nylon mesh bags were filled the same four mineral types. In the detritosphere experiment, soils were dry (~ 4% VWC) at the start of the experiment, when we simulated a wet-up and maintained a 14% VWC for the remainder of the experiment. Mineral bags were harvested after 3 months of detritosphere incubation. At harvesting, both minerals and soil were weighed, dried (65°C), and weighed again to obtain soil moisture content. The dried minerals and soil were stored at 4°C until analysis.

3.3.2 STXM/NEXAFS

We conducted STXM/NEXAFS analysis on beamline 5.3.2.2 (250-780 eV) and 11.0.2 (160-2000 eV) at the Advanced Light Source (ALS) at Lawrence Berkeley National Laboratory (Kilcoyne et al. 2003). Air dried minerals were from the same microcosm were combined by mineral type and ground to a powder. The ground minerals were suspended in MiliQ water and wet-spotted with a pipette onto silicon nitride STXM windows (0.5 x 0.5 mm membrane size, 200 nm membrane thickness, Silson Ltd.), and air-dried. For "rhizosphere soil" samples, we immersed dried roots with clinging soil in MiliQ water, lightly vortexed, and then wet-spotted with a pipette onto silicon nitride windows. "Root litter" samples from the detritosphere experiment, which had been ground, were lightly vortexed in MiliQ water and wet-spotted on silicon nitride windows.

Carbon maps were collected at the carbon K-edge by comparing changes from 280 – 295 eV. Once carbon-rich areas were identified, we collected image sequences, or carbon stacks, from 278 – 330 eV to extract NEXAFS spectra. We also mapped the iron (Fe) L-edge by comparing changes from 703-710 eV. We collected a minimum of three C stacks for every mineral type in each treatment (bulk, rhizosphere, and litter).

3.3.3 Scanning Electron Microscopy

Minerals on silicon nitride windows were imaged using Scanning Transmission Electron Microscopy (SEM) at Lawrence Livermore National Laboratory (FEI, Inspect F) before and after incubation in soil microcosms. SEM images were taken of both unground mineral samples and also the ground minerals on silicon nitride STXM windows. The unground minerals were wet mounted with MiliQ water on silicon wafers, air dried, and gold-coated before imaging. The ground minerals on STXM windows were gold coated after STXM/NEXAFS analysis was complete. Images were acquired at 5 kV and 15 kV energy.

3.3.4 NanoSIMS

We measured the isotopic composition of mineral-associated OM by NanoSIMS (CAMECA NanoSIMS 50, Physical and Life Sciences Directorate, Lawrence Livermore National Laboratory). After SEM imaging, gold-coated STXM windows were transferred to NanoSIMS analysis holders. Analysis regions (40 x 40μm) were chosen to match STXM analysis areas. We collected a total of 25 additional analysis regions (40 x 40μm) to gain a broader survey of the distribution of ^{13}C enrichment in samples. We also analyzed the bulk soil treatment, which had

no ^{13}C addition, as a control. A Cs^+ primary ion beam (2–4 pA) with a nominal spot size of 100–200 nm was used to raster over the minerals. After presputtering, we collected 20 – 200 scans per sample, depending on sample thickness. Four masses were collected: $^{12}C_2^-$, $^{12}C^{13}C^-$, $^{12}C^{14}N^-$, and $^{29}Si^-$ using electron multipliers and a mass resolving power ~7,000 (1.5× correction) (Pett-Ridge and Weber 2012). To minimize charging effects, we used an electron flood gun (Pett-Ridge and Weber 2012). Bacillus spores with known isotopic composition (previously analyzed by isotope-ratio mass spectrometry) were used as standards. We also analyzed our own control samples, Ferrihdyrite, Kaolinite, and Quartz incubated in bulk soil, which had no ^{13}C addition, to determine a threshold for region of interest definition in our data processing (**see 3.3.5.2**). Dried ^{13}C *Avena barbata* root provided a benchmark for ^{13}C enrichment from the plant.

3.3.5 Data Processing

3.3.5.1 STXM/NEXAFS Data

We used aXis 2000 to align stack images with Zimba and select regions of interest (ROIs) (Hitchcock 2009). For each stack image, we selected a mineral and C-free region for the incident photon flux, or I_0. We then selected transmission images at energies below and above the K-edge and converted them to optical density (OD) images, where $OD=\ln(I_0/I)$ and I is the transmitted flux. In most samples, we conducted a dark current subtraction such that I_0 was close to zero. While this improved resolution of the spectra overall, in some cases it caused a potential distortion around the transition of aromatic C (285.1 eV). Due to this potential distortion, we evaluated aromatic C as either present or absent, but did not interpret differences in relative size of peaks at 285.1 eV. ROIs were chosen at areas with a strong C signal based on a C map, or ratio image of 280 and 295 eV. We processed NEXAFS spectra from our ROIs with the program Athena (Ravel and Newville 2005) across the full analysis range (278-330) using an E_0 of 290. We normalized NEXAFS spectra in Athena by defining pre- and post-edges such that all ROIs were as consistent as possible from 278-284 eV and 290-330 eV.

3.3.5.2 NanoSIMS Data

Images were processed using L'Image software (developed by L Nittler, Carnegie Institution of Washington, Washington, DC, USA). Images were corrected for deadtime and drift. Regions of interest (ROIs) of OM on minerals, as defined below, were selected based on from ratio images of $^{12}C^{13}C^-$:$^{12}C_2^-$. Based on analysis of our unlabeled control samples, Ferrihydrite, Kaolinte, and Quartz incubated in bulk soil, we determined that some natural fractionation was present in our soils. We selected a lower threshold of $\delta^{13}C$ 300‰ to ensure that any spot we classified as enriched must have some portion of its C from our added ^{13}C label. Using our threshold, we identified four ROI types of ^{13}C-enriched regions: (1) *indistinct hotspots*, (2) *distinct hotspots*, (3) *fungal hyphae*, and (4) *hyphosphere*. These ROIs are described in further detail in **Section 3.4.2**. For each ROI type, we calculated the percent coverage and average ^{13}C enrichment for each mineral type. To calculate percent coverage, we divided the total ROI area by the total area analyzed for the mineral, including raster images with no detectable ^{13}C. We also developed ROIs for unenriched regions and ROIs for the entire raster area to determine average enrichment across the analysis area.

3.4 RESULTS AND DISCUSSION

3.4.1 Microscale View of Mineral-Organic Matter Interaction

Scanning electron microscope (SEM) images of minerals before and after incubation in the rhizosphere (**Figure 3.1**) and detritosphere illustrate the soil microenvironment where plant-microbe-mineral interactions occur. **Figure 3.1a-d** shows minerals prior to incubation in soil microcosms; **Figure 3.1e-h** shows minerals after 2 months of incubation adjacent (<2 mm) to actively growing *Avena barbata* roots.

We chose our specimen minerals based on the mineralogy of our field-extracted, density-fractionated Native Minerals, and also because they represent a range of surface area and surface reactivity. In the Native Minerals, large, mostly quartz particles (~200-500 μm diameter) are often coated by smaller mineral and OM particles. While the Native Minerals already had associated C from up to millennia *in situ* in soil at our field site at HREC (Hopland, CA), the specimen minerals (Quartz, Ferrihydrite, and Kaolinite) had no detectable C prior to incubation (**Chapter 1**). After incubation, SEM images showed OM association with all minerals types, including microbial cells, such as fungal hyphae (based on morphology and size), as seen in **Figure 3.1e-h** and **SI Figure 3.1-3**. From prior work on our model system, we know that after 2 months incubation adjacent to the rhizosphere, specimen minerals had an average total C of 0.6 ± 0.1 mg C- g^{-1}, while the Native Minerals had 17.0 ± 1.0 mg C- g^{-1} (**Chapter 1**).

Our SEM images help illustrate that size and morphology are key attributes governing mineral-OM interactions. Quartz minerals are hundreds of microns in diameter, while kaolinite is generally < 2 μm, with some larger size particles (Mackinnon et al. 1993) and natural ferrihydrite is poorly crystalline with particles typically 1-7 nm size (Cismasu et al. 2013, Wang et al. 2016). These size differences are particularly relevant to the interaction of microbial cells and mineral surfaces. Quartz is much larger than a bacterial cell (~ 2 μm), kaolinite is a similar size to a bacterial cell, and ferrihydrite is much smaller. The ferrihydrite in our study system coated quartz minerals, and was composed of nanometer-size poorly-crystalline minerals. We saw evidence of re-mineralization and nano-aggregate formation of ferrihydrite, including ferrihydrite coating of fungal hyphae (**SI Figure 3.1**). We also observed kaolinite coating fungal hyphae (**Figure 3.1h inset, SI Figures 3.3**). Prior work has shown the formation of "clay hutches"(Lunsdorf et al. 2000), and we see possible examples of bacteria encased in kaolinite in our samples (**SI Figure 3.2**).

The surface area of the different minerals varies widely, as measured by BET surface area (**Chapter 1**) (**Figure 3.1**), with the highest surface area for Kaolinite and the lowest for Quartz. Morphology is also important, as demonstrated by comparing **Figure 3.1d** and **Figure 3.1h** of Kaolinite before and after incubation. Prior to incubation, these platy kaolinite minerals were randomly assembled, but after exposure to water, dissolved organic C, and OM during incubation, kaolinite minerals were stacked in an organized arrangement of microaggregates. What SEM images do not show is the mineral surface chemistry, which is also very important (Eusterhues et al. 2005), in governing mineral-OM interactions. Quartz has the least reactive surface chemistry (Jones and Singh 2014), ferrihydrite has a high surface reactivity (Kaiser et al. 2007, Eusterhues et al. 2008, Eusterhues et al. 2011, Hiemstra 2013, Chen et al. 2014), and kaolinite is intermediate, with higher reactivity at edge locations (Schroth and Sposito 1997, Liu et al. 2014, Mbey et al. 2019).

3.4.2 Tracing the Fate of Plant-Derived Carbon with NanoSIMS

NanoSIMS analyses allowed us to map the distribution and enrichment of the added ^{13}C label. In the rhizosphere, regions enriched above our control samples (> $\delta^{13}C$ 300‰) indicate that some fraction of that C is derived from the ^{13}C-labeled *Avena barbata* root. These ^{13}C-enriched regions could be root fragments, root exudates, microbial cells that have incorporated root-derived substrate into their biomass, or microbially-derived compounds produced from the utilization of root-derived substrate. In the detritosphere, regions enriched above our control samples (> $\delta^{13}C$ 300‰) indicate that some fraction of that C is derived from the ^{13}C-labeled *Avena barbata* root litter. These ^{13}C-enriched regions could be root litter fragments, microbial cells that have incorporated litter-derived substrate into their biomass, or microbially-derived compounds produced from the utilization of litter-derived substrate.

We identified four major types of ^{13}C-enriched regions of interest in our samples incubated in the rhizosphere (**Table 3.1**). The first we term *indistinct hotspots*. These regions are ^{13}C enriched above our control threshold, but do not have a distinct morphology. We expect these regions could be mineral-associated root exudates, root or litter fragments, microbial products (e.g. EPS), or microbial necromass (Miltner et al. 2012). The second region of interest were *distinct hotspots*. These regions are the size (~ 2 μm) of a bacterial cell, with distinctly defined margins and a circular or oblong morphology, and may represent bacterial cells. The third type of region of interest were *fungal hyphae*. These areas have a size and morphology consistent with fungal hyphae in the SEM images. All but one hyphae was surrounded by a halo of ^{13}C enrichment that, referenced to the SEM image, was outside the putative fungal hyphae wall. We called this fourth region of interest the *hyphosphere*.

Only a small percent of the specimen minerals we imaged were significantly ^{13}C enriched above our control samples (**Table 3.1**). However, in the rhizosphere soil itself, 59% of the total area analyzed was ^{13}C enriched. The Native Mineral and Quartz minerals had the smallest total ^{13}C enriched area, at only 0.99% and 1.0%, respectively. On Ferrihydrite, 4.9% of the total area was enriched, on Kaolinite, 2.4% of the total area was enriched. In our prior work on the rhizosphere experiment (**Chapter 1**), we calculated IRMS-based estimates of the *A. barbata* root-derived C associated with each mineral type; 6.2 ± 0.4% of this C was associated with the Native Mineral, 21.2 ± 5.5% with Ferrihydrite, 42.6 ± 4.6% with Kaolinite, and 13.9 ± 3.4% with Quartz. If ~ 40% of the C associated with Kaolinite is ^{13}C enriched C from the rhizosphere, then ~ 60% must have come from the surrounding soil. Therefore, based on our NanoSIMS analysis where 2.4% of the total surface area was enriched, we can estimate that just over ~ 5% of Kaolinite is coated in OM. Similarly, we can estimate a sparse OM coating on Quartz (~ 7%) with more on Ferrihydrite (~25%). From these estimates, we surmise that OM distribution on minerals is patchy. This is not surprising, particularly with the specimen minerals, which have an order of magnitude less total C than their Native Mineral counterparts (**Chapter 1**). The patchy nature of OM on mineral surfaces is consistent with other studies, including prior NanoSIMS analysis of mineral-OM association (Heister et al. 2012, Mueller et al. 2012, Vogel et al. 2014).

Indistinct hotspots, or morphologically unidentifiable regions of ^{13}C enrichment, were found across mineral types. For every mineral type but Kaolinite, which was highly variable, the *indistinct hotspots* had the lowest ^{13}C enrichment when compared to distinct hotspots and hyphal associated locations (**Table 3.1**). The high degree of variability in Kaolinite *indistinct hotspots* (δ

^{13}C 1,207 ± 1,163) could be explained by the microaggregation we observe in SEM images (**Figure 3.1h**), which could potentially "trap" less degraded, and thus, more highly ^{13}C labeled, root litter-derived compounds.

Distinct hotspots, which may represent ^{13}C-labeled bacterial cells, only comprised a small fraction of total area analyzed, but had higher ^{13}C enrichment. This is consistent with Miltner *et al.* (Miltner et al. 2012), where they found that only a small portion of added ^{13}C labeled microbes were found intact on minerals, with most transformed to indistinguishable necromass. In the rhizosphere soil, *distinct hotspots* were very highly enriched, with an average enrichment in the same range as the actual root material and highly variable (δ ^{13}C 26,144 ± 9,728‰). If these distinct hotspots are indeed bacterial cells, this is consistent with what we know of rhizosphere bacteria, where some consume a high portion of root exudates, others consume a mix of exudates and other C substrates, and some do not consume root-derived C (Zhalnina et al. 2018, Nuccio et al. 2020).

Hyphae were highly enriched in ^{13}C, and also comprised a relatively high portion of total ^{13}C enriched area observed. The *hyphosphere* surrounding the hyphae in Ferrihydrite and in Kaolinite was less enriched than the hyphae itself, but in the Ferrihydrite, the percent coverage of the *hypohosphere* is larger than the actual hyphae. In the Kaolinite, the percent coverage is only slightly smaller for the *hyphosphere* than the actual hyphae.

We identified two fungal hyphae in the rhizosphere treatment that are likely arbuscular mycorrhizal fungi (AMF). The putative AMF were found inside our mineral bags, one in Ferrihydrite and one in Kaolinite (**Figure 3.2**). The morphology, particularly the branched morphology in **Figure 3.2c**, size, and highly enriched ^{13}C suggest these are likely AMF. From prior ITS2 rRNA fungal gene high throughput sequencing (MiSeq) of DNA extracted from these minerals, we know that the fungal order *Glomerales*, to which AMF belong, were present on all mineral types and were significantly enriched in the Ferrihydrite minerals compared with the bulk soil(Whitman et al. 2018). When we account for both percent coverage and degree of ^{13}C enrichment, we find that AMF and their associated hyphosphere C account for 77% of the total ^{13}C in our observed Ferrihydrite samples, and 95% of the total ^{13}C in our observed Kaolinite samples. We therefore suggest that in the rhizosphere, AMF are important carbon shunts from the rhizosphere to mineral surfaces. While we saw probable fungal hyphae in SEM images from the detritospshere, their size and morphology were suggestive of saprotrophic fungi. None of the detrituosphere putative saprotrophic hyphae we analyzed were ^{13}C enriched. We expect that if our proposed AMF C shunt phenomenon is correct, it is exclusive to the rhizosphere or soil accessible to hyphae. Our finding is consistent with prior work demonstrating C flow through hyphae with NanoSIMS (Nuccio et al. 2013, Vidal et al. 2018).

3.4.3 Carbon Chemistry Varies with Treatment and Mineral Type

To investigate dominant trends in the chemical composition of mineral-associated OM, we merged our NEXAFS spectra according to mineral type and treatment. Each spectra is merged from a minimum of 3 individual STXM/NEXAFS areas. In **Figure 3.3a**, we show the merged NEXAFS spectra of minerals incubated in bulk soil. In **Figure 3.3b**, we show the merged NEXAFS spectra of minerals incubated in *A. barbata* rhizosphere soil, and we also include a merged rhizosphere soil spectra. The rhizosphere soil was taken from directly along the root

face, whereas the minerals incubated in the rhizosphere soil were in mineral bags placed within 2 mm of the growing root. In **Figure 3.3c**, we show the merged NEXAFS spectra of minerals incubated in the detritosphere with added *A. barbata* litter. We describe spectral features by focusing on six energies that indicate a transition of C chemistry: (a) aromatic C at 285.1 eV, (b) phenolic C (ene-ketone) at 286.7 eV, (c) aliphatic C at 287.4 eV, (d) carboxylic and/or amide C at 288.3 eV, (e) carbohydrate C (alcohol C-OH) at 289.4 eV, and (f) carbonyl C at 290.3 eV (**Figures 3.3-6**).

3.4.3.1 Chemistry in the Bulk Soil

In the bulk soil (**Figure 3.3a**), the Native Mineral and Ferrihydrite shareed similar spectral features, while the Kaolinite and particularly the Quartz displayed different spectral features. The Native Mineral and Ferrihydrite both had a small peak at the transition of aromatic C (a), a very slight peak at the transition of phenolic (b), a pronounced peak at the transition of carboxylic and/or amide C (d), and then a dip at the transition of alcohol C-OH, which we interpret as likely carbohydrate C (e). With all our samples, we found that the aromatic location was highly variable based on sample thickness, and thus we focus on the presence or absence of a peak at the aromatic location, rather than interpreting the relative size of the peak. However, prior work suggests the ratio of carbohydrate-like compounds at carboxylic and/or amide C compared with carbohydrate C can indicate the degree of oxidation (Bhattacharyya and *al. in prep*). From this, based on other spectral characteristics, we can infer whether a C-rich region is likely microbially processed. Here, the high carboxylic and/or amide peak compared with carbohydrate C suggests that Native Mineral and Ferrihydrite associated OM is more oxidized, and based on overall spectral characteristics, these spectra resemble both the *Escherichia coli* bacterial cell standard and the iron (Fe) associated OM analyzed by Keiluweit *et al*. (Keiluweit et al. 2012). The Kaolinite has a very large aromatic peak (a), which we believe may reflect sample thickness more than true OM chemistry. Similar to the Native Mineral and Ferrihydrite, there is a peak at the transition of carboxylic and/or amide C (d), but it is a smaller peak. Kaolinite also appears to have a small but poorly defined peak at the transition of carbohydrate C (e). We interpret the Kaolinite spectra as less oxidized, perhaps with a larger fraction of less degraded plant-derived OM. The Quartz looks starkly different from the other spectra, with only a very slight aromatic peak (a), a small peak at the transition of carboxylic and/or amide C (d), and then a leveling off at the transition of carbohydrate C (e). This is characteristic of more carbohydrate-like C, which could be more plant-derived, although a microbial-origin, such as extracellular polymeric substance (EPS) is also possible. However, the small peak at the transition of carboxylic and/or amide C (d) does suggest there is some more oxidized, potentially microbially-derived C as well.

Overall, in the bulk soil, we saw that chemistry varied with mineral type (**Figure 3.3a**). The Native Mineral and Ferrihydrite appeared to have more oxidized, potentially microbial C, while the Kaolinite appeared to have a larger fraction of carbohydrate-like, potentially plant derived C, and Quartz an even higher portion of potentially plant-derived C. The similarity between the Ferrihydrite and Native Mineral spectra was interesting, and we asked whether there was a difference between the chemistry of C in the Native Mineral sample that was associated with iron (Fe) and C that was not associated with Fe. We mapped the distribution of Fe in Native Mineral samples with STXM across the L-edge and found that in our samples, everywhere that we had high C at the K-edge, we also had Fe. Examining our SEM images, a large portion of our Native Minerals does appeared to have what may be a ferrihydrite coating. The similarity

between the Native Mineral and Ferrihydrite spectra may be due to the prevalence of ferrihydrite coatings on the Native Minerals. It is interesting that in the short timeframe of our experiment, the chemistry of OM associated with ferrihydrite-coated quartz sand closely approximated that of the Native Minerals, even though there was an order of magnitude less total C (1.14 ± 0.24 mg C- g^{-1} on Ferrihydrite and 14.80 ± 0.84 mg C- g^{-1} on Native Minerals) (**SI Table 3.1**).

3.4.3.2 Chemistry in the Rhizosphere

We examined the effect of the rhizosphere on the molecular composition of mineral-associated OM across mineral types. In the rhizosphere soil (**Figure 3.3b**), all the minerals have more similar spectral features than in the bulk soil (**Figure 3.3a**). The Native Mineral and specimen minerals all have a peak at the transition of aromatic C (a), a pronounced peak at the transition of carboxylic and/or amide C (d), and then a dip at the transition of carbohydrate C (e). The Native Mineral does have a slight peak at the transition of phenolic (b) that is absent in the other minerals, and the Ferrihydrite has a slight peak at the transition of aliphatic C (c) that we do not see in the other minerals. We also examined the chemistry of rhizosphere soil taken from directly adjacent to the growing root, and in the rhizosphere soil the peak at the transition of carboxylic and/or amide C (d) is much smaller, as is the dip at the transition of carbohydrate C (e). This suggests that the C associated with rhizosphere soil is less oxidized than the C associated with the minerals. The relatively higher carboxylic and/or amide C of mineral-associated C indicates a relatively high degree of oxidized C that is likely more microbially processed. The more carbohydrate-like rhizosphere soil is consistent with more freshly released exudates and other plant-derived compounds. Overall, we see evidence that the rhizosphere exerts a "homogenizing effect" on the mineral-associated chemistry. We observed a similar trend in ^{13}C-NMR analysis of minerals that underwent the same treatment in our prior work (**Chapter 1**). Total C in the rhizosphere soil was similar to the bulk soil (**SI Table 3.1**). However, compared with the bulk soil, there is little difference in the chemistry of C associated with the Native Mineral in the rhizosphere based on NEXAFS spectra.

3.4.3.3 Chemistry in the Detritosphere

As in the bulk soil, in the detritosphere, spectra vary strongly by mineral type (**Figure 3.3c**). Overall, the Native Mineral, Ferrihydrite, and Kaolinite have similar spectral features to the bulk soil with a small peak at the transition of aromatic C (a), a pronounced peak at the transition of carboxylic and/or amide C (d), and then a dip at the transition of carbohydrate C (e). However, in the detritosphere, we see a larger peak at the transition of phenolic (b) than in the bulk soil treatment, particularly with the Ferrihydrite and Kaolinite. This phenolic peak (b) is similar to that observed by Schaefer *et al*. (Schaefer et al. 2020), where cover crop addition to agricultural soils resulted in a phenolic peak. Schaefer *et al.* interpreted this peak as minimally-degraded plant residue from the cover crops (Schaefer et al. 2020). In our system, this phenolic C is likely derived from the added root litter. The Quartz minerals in the detritosphere do not have a peak at the transition of aromatic C (a) or phenolic C (b). Quartz peaks at the transition of aliphatic C (a) with a broad peak extending to the transition of carboxylic and/or amide C (d) and then dipping slightly at the transition of carbohydrate C (e). The spectra for added root litter resembles that of the rhizosphere soil in **Figure 3.3b**, however the root litter in **Figure 3.3c** has a higher peak at carbohydrate C (e) relative to carboxylic and/or amide C (d), suggesting less oxidized, potentially less microbially-processed C. Total C in the detritosphere soil was similar to the bulk and rhizosphere soil (**SI Table 3.1**).

Overall, what distinguishes the detritosphere from the bulk soil is the presence of phenolic C in the Native Mineral, Ferrihydrite, and Kaolinite and aliphatic C in the Quartz. In the detritosphere, there are more available root-derived macromolecules that can be incorporated into micro- and nano-aggregates. On the minerals capable of micro-aggregation (Kaolinite, Ferrihydrite, and the Native Minerals), the phenolic peak may represent root litter material contained within aggregates and ferrihydrite coatings. Quartz cannot coat small OM fragments or form microaggregates, which could explain the absence of a phenolic peak. Angst *et al.* also found that aggregation and mineral-association may be critical modes of protection for plant-derived C (Angst et al. 2017).

Compared with the root litter, minerals in the detritosphere were lower in carbohydrate-like compounds (e) and higher in carboxylic and/or amide C (d). ^{13}C-NMR analysis of the same root litter, Native Minerals, and Kaolinite from this study in **Chapter 2** also showed a shift from more carbohydrates in the root litter to more aliphatic compounds on Kaolinite. This suggests that the mineral-associated C in the detritosphere is more oxidized, and potentially more microbially-processed, than the root litter. However, as in the bulk soil and rhizosphere, the treatment appears to strongly influence the chemistry of mineral-associated C. Within each treatment, we observed differences across mineral types, but treatment mattered as well.

3.4.4 Linking Carbon Source and Chemistry with Combined NanoSIMS-STXM/NEXAFS

By combining STXM/NEXAFS with NanoSIMS(Keiluweit et al. 2010), it is possible to trace the transformation and fate of root-derived C in the rhizosphere and detritosphere. We examined 15 regions in the rhizosphere and 9 regions in the detritosphere with both STXM/NEXAFS and NanoSIMS. Here we highlight 3 regions with combined STXM/NEXFS and NanoSIMS analysis. **Figure 3.4** is from rhizosphere soil immediately adjacent to the root. **Figure 3.5** is from added root litter with associated soil in the detritosphere. **Figure 3.6** is Ferrihydrite from the rhizosphere treatment.

3.4.4.1 NanoSIMS-STXM/NEXAFS of Rhizosphere Soil

In our rhizosphere soil sample (**Figure 3.4**), 5 sub-regions showed high carbon concentrations in the STXM carbon map (**Figure 3.4b**), labeled Spots 1-5. Only Spot 1 was highly enriched in ^{13}C, with an enrichment level, δ^{13}C 21,606‰, consistent with the average enrichment of *Avena barbata* root material (δ^{13}C 27,278 ± 12,458‰ SE) (**Figure 3.4a**). Spots 2-5 were enriched above natural abundance (δ^{13}C 3,064‰), but not as enriched as the *A. barbata* root. The morphology of Spot 2 is consistent with a saprotrophic fungi (**SI Figure 3.4**), and in both our NanoSIMS analysis and STXM carbon map, showed a higher carbon concentration than Spot 1 or Spots 3-5.

The NEXAFS spectra (**Figure 3.4c**) show that the highly ^{13}C enriched Spot 1 has a small aromatic peak (a), a pronounced peak characteristic of carbohydrate C (d), and then a slight dip around carbonyl C (f). Based on prior work, we interpret the ratio of carbohydrate-like compounds at carboxylic and/or amide C compared with carbohydrate C as an indication of the degree of oxidation (Bhattacharyya and *al. in prep*). From this, based on other spectral characteristics, we can infer whether a C-rich region is likely microbially processed. Compared with the other NEXAFS spectra in the rhizosphere (**Figure 3.4c**), Spot 1 more closely resembles plant-derived compounds that have been minimally microbially-processed.

Spot 2, putatively a fungal cell based on morphology (**Figure 3.4b**), though potentially spatially overlapping other C substrates, has a double peak between carboxylic and/or amide C (d) and carbohydrate C (e), suggesting more oxidation and potential microbially-derived compounds than Spot 1. In fact, the spectra for Spot 2 resembles that of N-acetyl glucosamine (Keiluweit et al. 2012), a common proxy for fungal-derived compounds, 280 – 289 eV, but then the peak at the transition of carbohydrate C at 289.4 eV (e) is higher relative to the transition of carboxylic and/or amide C at 288.3 eV (d). This higher peak at the transition of carbohydrate C at 289.4 eV (e) is characteristic of the fungal cell wall material investigated by Keiluweit *et al.* (Keiluweit et al. 2012). The fungal-like morphology is consistent with a C chemistry that resembles a mix of N-acetyl glucosamine and fungal cell wall material.

Spots 3, 4, and 5 (**Figure 3.4c**) share similar features. All have an aromatic peak, a small phenolic C peak (b), a large peak at carboxylic and/or amide C (d), but no peak at carbohydrate C (e). This shift from more carbohydrate C dominated spectra at Spot 1 to equal carbohydrate C and carboxylic and/or amide C peaks at Spot 2 to a carboxylic and/or amid C dominated spectra in Spots 3-5 indicates a trend toward more oxidized C. Spots 3-5 are likely more microbially processed than Spots 1 and 2, and closely resemble the spectra for *E. coli* bacteria and/or Fe-associated OM investigated by Keiluweit *et al.* (Keiluweit et al. 2012). The interpretation that Spot 1 is less microbially processed and the other spots are more microbially processed is consistent with higher ^{13}C enrichment in Spot 1 than the other spots.

Figure 3.4 highlights the degree of C compositional heterogeneity in soils. In our merged rhizosphere STXM/NEXAFS spectra (**Figure 3.3a**), we observed that the rhizosphere overall imposed a similar chemical signature on all mineral types. However, focusing on a single cluster of particles in **Figure 3.4**, Spots 1, 2, and 5 are all adjacent and yet each have a distinct chemical signature.

3.4.4.2 NanoSIMS-STXM/NEXAFS of Root Litter

The root litter sample was composed of dried ^{13}C-labeled roots from the rhizosphere experiment that were not washed, and thus included attached minerals, microbes, and OM. A total of 9 sub-regions (**Figure 3.5b**) were selected for a comparison of NanoSIMS and STXM/NEXAFS spectra based on their high carbon concentrations in the STXM carbon map. The average ^{13}C enrichment was $\delta^{13}C$ 26,589‰, with spots varying widely from $\delta^{13}C$ 10,044‰ to $\delta^{13}C$ 56,483‰. Spots 1, 2, 6, 7, and 9 were all highly enriched in ^{13}C, while Spots 3, 4, 5, and 8 were less enriched, but still enriched well above natural abundance (**Figure 3.5a**). The variation in enrichment could reflect the differential labeling of different root litter components and/or the presence of root litter attached mineral, microbes, and OM.

The NEXAFS spectra (**Figure 3.5c**) do not show a clear correlation between level of ^{13}C enrichment and chemistry. Spots 1, 2, and 3 have similar NEXAFS spectra, all with very small aromatic peaks (a), then relatively flat until peaking just before the transition of carbohydrate C at 289.4 eV (e) (**Figure 3.5c**). This pattern is generally diagnostic of more carbohydrate-like compounds that have not undergone much oxidation. These spots are compositionally similar to Spot 1 in **Figure 3.4**, and likely represent root litter that is minimally degraded.

Spots 4 and 5 had more carboxylic and/or amide C (d) (**Figure 3.5c**). These spots also only have a small aromatic peak (a). This shift to carboxylic and/or amide C can indicate the degree of oxidation (Bhattacharyya and *al. in prep*). Spots 4 and 5 may be litter that has undergone more microbial processing, or might even contain some microbial products. Spots 6 and 7 start to peak around the transition to carboxylic and/or amide C (d) with a broader, less well-defined peak just before the transition to carbohydrate C at 289.4 eV (e). These spots may represent an intermediate between Spots 1-3 and Spots 4-5, with more oxidation than Spots 1-3, but not as much as Spots 4-5. Spots 6-7 have likely undergone an intermediate level of microbial degradation.

Spots 8 and 9 show distinct NEXAFS spectra from the other sub-regions identified in **Figure 3.5**. Spot 8 has a more defined aromatic peak (a) and then peaks again around the transition of aliphatic C (c) (**Figure 3.5c**). Spot 8 may represent more highly oxidized root litter than Spots 1-7. It is also possible that Spot 8 reflects the heterogeneous composition of root litter, given that 8-12% of root C is aliphatic suberin (Kolattukudy 1980, Lorenz et al. 2007). Spot 9 has a small aromatic peak (a) and a very pronounced peak at the transition to carboxylic and/or amide C (d), with a dip and leveling off after 289 eV. Spot 9 is characteristic of more oxidized C, similar to Spots 4 and 5, but the peak at 288.3 eV at Spot 9 is distinctive and more closely resembles the *E. coli* bacteria spectra in Keiluweit *et al.* (Keiluweit et al. 2012).

Figure 3.5 demonstrates the degree of heterogeneity in root litter C chemistry and ^{13}C enrichment. We did not observe a clear relationship between C chemistry and the degree of ^{13}C enrichment, though all spots were enriched above natural abundance. Overall, the spectra from the root litter materials indicate less oxidized, with more carbohydrate-like compounds, than the rhizosphere soil in **Figure 3.4**. Compared with the merged detritosphere spectra in **Figure 3.3c**, we see that the C that associated with minerals in the mineral bags is more oxidized, and likely more microbially processed, than the initial root litter input.

3.4.4.3 NanoSIMS-STXM/NEXAFS of Ferrihydrite Incubated in Rhizosphere

Figure 3.6 is a sample of ferrihydrite incubated in the rhizosphere. Assuming these particles were not adjacent prior to wet-spotting, we investigated whether there was a correlation between ^{13}C enrichment and C chemistry. We compared and merged the NEXAFS spectra 7 spots that were not ^{13}C enriched to 6 spots that were ^{13}C enriched (**Figure 3.6b**). All the spots we analyzed were thicker than an ideal STXM region, and we believe the high aromatic peaks may, in part, be a relic of this sample thickness. We did not see a clear chemical difference between the ^{13}C enriched and un-enriched merged spectra (**Figure 3.6c**), nor were there any individual spectra with clearly distinct NEXAFS spectra. Both merged spectra have a high peak at the transition of carboxylic and/or amide C (d) and then a dip at the transition of carbohydrate C (e), suggesting oxidation.

When we observed **Figure 3.4**, with soil directly adjacent to the root, we did see a small difference between the spectra of the ^{13}C enriched spot (Spot 1) compared with the other spots, where the ^{13}C enriched spot had less oxidized, possibly less microbially-processed C. However, inside the Ferrihydrite mineral bag, which is approximately 1-2 mm from the root, still within the operationally-defined rhizosphere but further from the immediate zone of root influence, there is no difference between the chemistry of ^{13}C enriched and un-enriched C. One explanation is that

this C is all microbial. The ^{13}C enriched C is derived from microbes consuming root-derived C, while the un-enriched C is derived from microbes consuming other SOM.

3.4.5 Microenvironment Control of Mineral-Associated C Chemistry

The rhizosphere and detritosphere are critical soil microenvironments with higher microbial activity and C transformation than the bulk soil (Blagodatskaya et al. 2014, Finzi et al. 2015, Kuzyakov and Blagodatskaya 2015). In complementary studies of our rhizosphere and detritosphere experiments, we found that mineral type influences total C accumulation and microbial community composition (Whitman et al. 2018). Comparing rhizosphere to bulk soil and detritosphere to bulk soil, we found no significant overall effect of treatment on total C or microbial community composition (**Chapters 1-2**). Here, we find that while mineral type indeed does shape C chemistry within a particular treatment, microenvironment also matters.

The composition of mineral-associated C was influenced by mineral type and C source and environment (rhizosphere, detritosphere, and bulk). STXM/NEXAFS analysis showed that in the detritosphere, mineral-associated C had a distinct phenolic signature. However, the quartz minerals in the detritosphere did not have phenolic C compounds. Microaggregation of kaolinite and ferrihydrite may play an important role in protecting less microbially-degraded litter compounds in the detritosphere. In general, mineral-associated C showed spectroscopic evidence of microbial degradation or resembled published reference spectra for bacterial and fungal material. Overall, we observed that the rhizosphere had a "homogenizing effect" on the chemistry of mineral-associated OM, while the chemistry of mineral-associated OM in bulk and detritosphere soil was influenced more by mineral type.

3.5 TABLES AND FIGURES

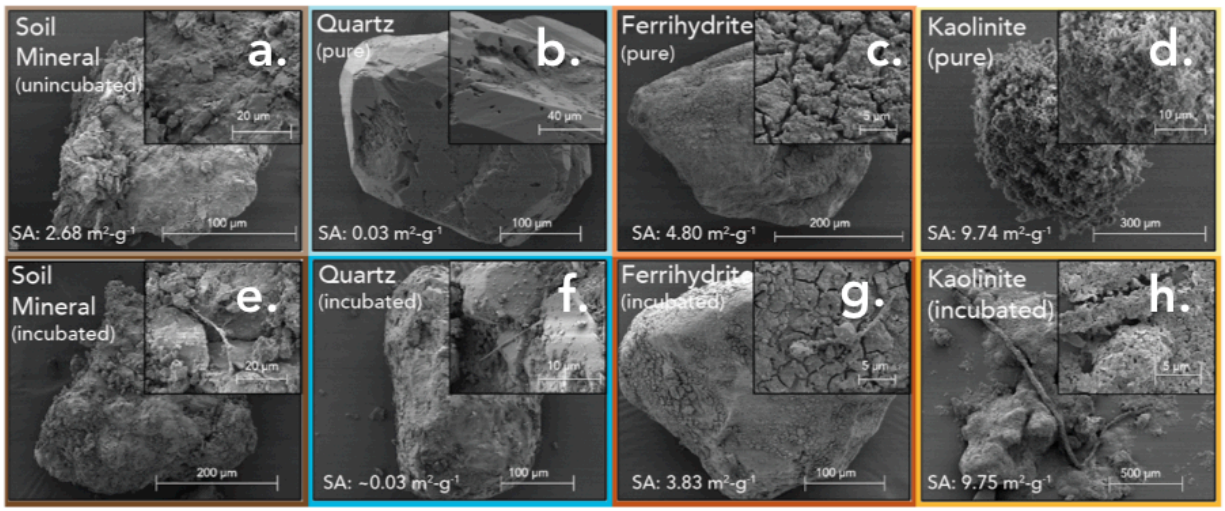

Figure 3.1. Scanning electron microscope (SEM) images (5 eV) of air-dried, gold-coated minerals before (upper row) and after (lower row) incubation in soil microcosms with a growing plant. Pure minerals, shown in the top panels, are of minerals prior to incubation in soil microcosms. Minerals after incubation in the rhizosphere treatment soil microcosms are shown in the bottom panels. Each panel shows an overview of the mineral with an inset panel in the upper right hand corner showing a higher resolution image of the same mineral. Scale bars are in the bottom right of each panel and inset. SA stands for BET surface area, measured with N_2 gas.

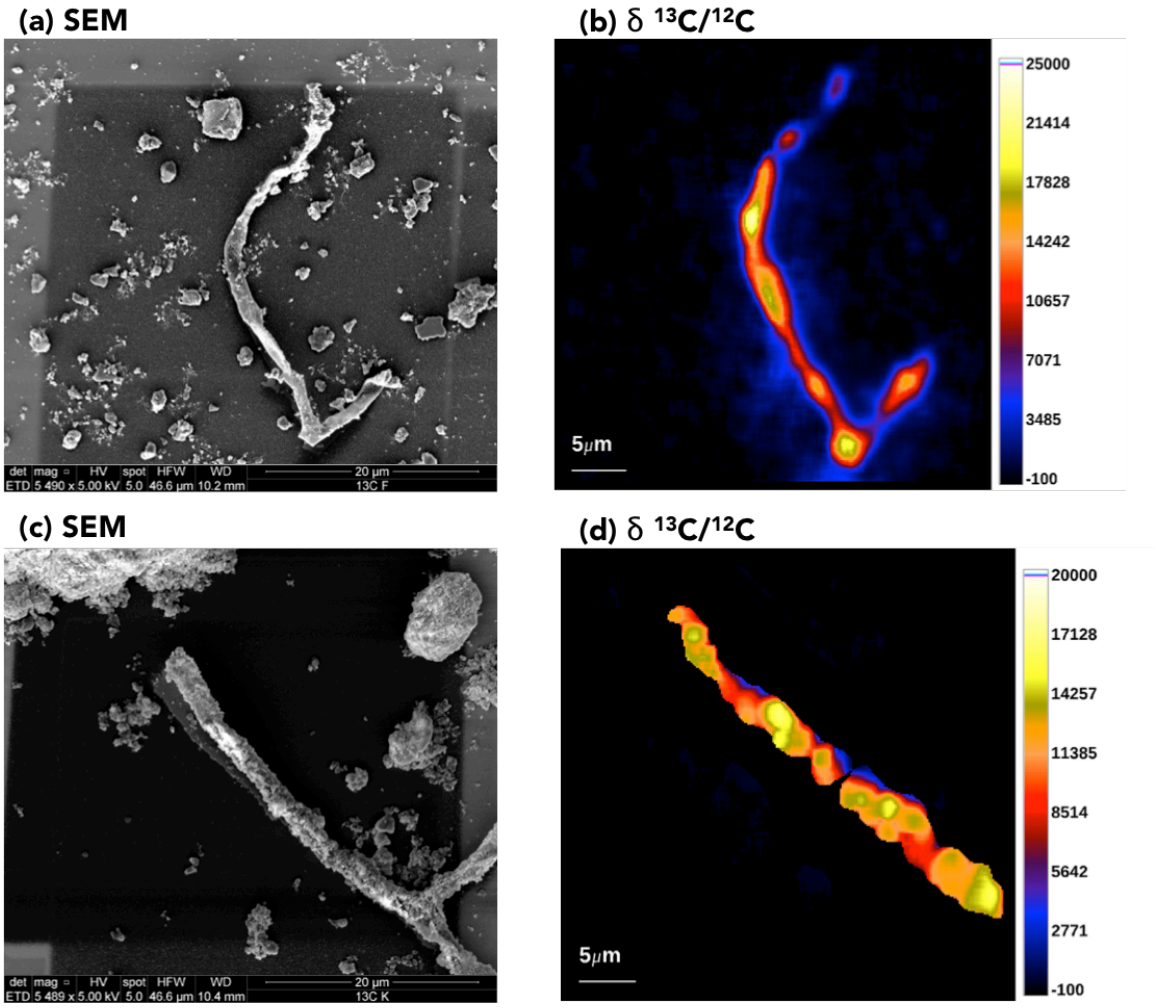

Figure 3.2. SEM images (15 eV) of fungal hyphae from ferrihydrite incubated in the rhizosphere of *A. barbata* (wild oat grass) grown in a $^{13}CO_2$ enriched atmosphere (~10 atm%) (a) and kaolinite incubated in the rhizosphere (c) with complementary NanoSIMS images of ^{13}C enrichment (b and (d), respectively. NanoSIMS images are the delta value of ratios of $^{12}C^{13}C$ to $^{12}C_2$ masses. The background is masked in the NanoSIMS images to highlight the hyphae.

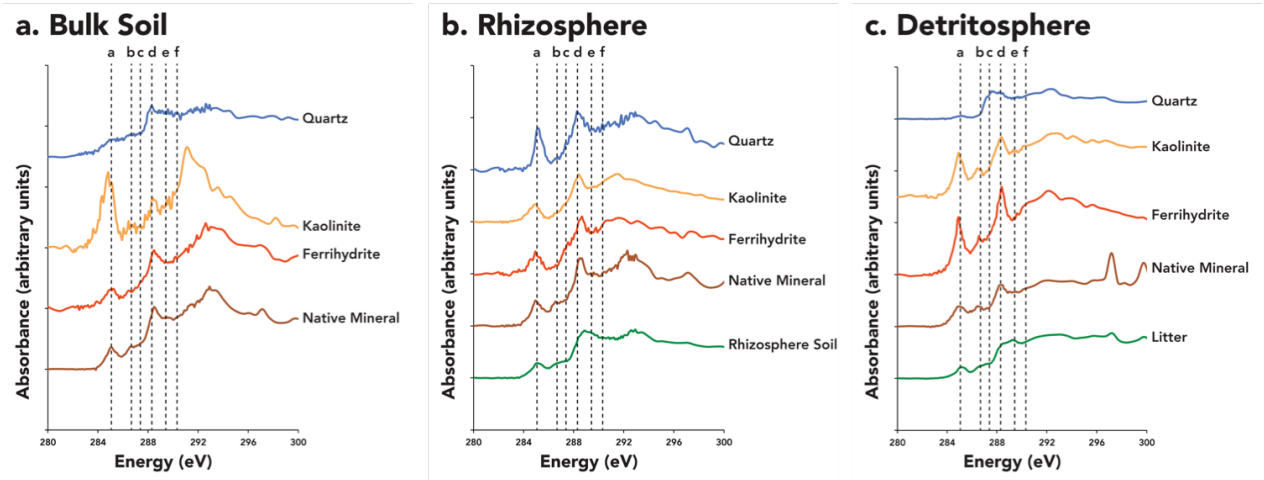

Figure 3.3. NEXAFS spectra for minerals incubated in bulk soil (a), rhizosphere (b), and detritosphere (c). Each spectra is the merged spectra of at least three distinct STXM regions. In the rhizosphere, analysis of the rhizosphere soil is also included as a comparison. On each NEXAFS spectra, carbon adsorption peaks are indicated with dashed lines. Carbon 1s absorption edge peaks are identified as C = C 1s-p * transition of aromatic C at 285.1 eV (a), 1s-p * transition of C"C in ene-ketone at 286.7 eV (b), 1s-3p/r * transition of aliphatic C at 287.4 eV (c), 1s-p * transition of carboxylic and/or amide C at 288.3 eV (d), the 1s-3p/r * transition of alcohol C-OH at 289.4 eV (e), and the 1s-p * transition of carbonyl C at 290.3 eV (f) (Cody et al., 1998; Schumacher et al., 2005; Solomon et al., 2005, 2009; Cody et al., 2011; Kleber et al., 2011). Aromatic peaks (a) are susceptible to distortion due to sample thickness and here are evaluated only according to presence or absence.

Table 3.1. NanoSIMS Analysis of ^{13}C Enriched Regions of Interest in the Rhizosphere

Mineral Type	Indistinct Hotspot	Distinct Hotspot	Hyphae	Hyphosphere
Rhizosphere Soil (n = 5)*	n = 5**	n = 5	n = 1	n = 0
Average $\delta^{13}C \pm SE$	2,943 ± 461	26,144 ± 9728	14,523 ± 35	–
Percent Coverage	55	3.1	0.42	–
Native Mineral (n = 4)	n = 2	n = 0	n = 0	n = 0
Average $\delta^{13}C \pm SE$	782 ± 412	–	–	–
Percent Coverage	0.99	–	–	–
Ferrihydrite (n = 17)	n = 15	n = 7	n = 1	n = 1
Average $\delta^{13}C \pm SE$	432 ± 25	1,613 ± 327	10,574 ± 60	1,914 ± 23
Percent Coverage	3.6	0.07	0.39	0.83
Kaolinite (n = 8)	n = 4	n = 0	n = 2	n = 2
Average $\delta^{13}C \pm SE$	1,207 ± 1,163	–	7,020 ± 5,354	556 ± 62
Percent Coverage	0.36	–	1.09	0.95
Quartz (n = 5)	n = 5	n = 2	n = 0	n = 0
Average $\delta^{13}C \pm SE$	404 ± 30	1,373 ± 270	–	–
Percent Coverage	0.93	0.07	–	–

* The total number of sample areas analyzed is denoted in parentheses

** The number of each ROI denoted in parentheses

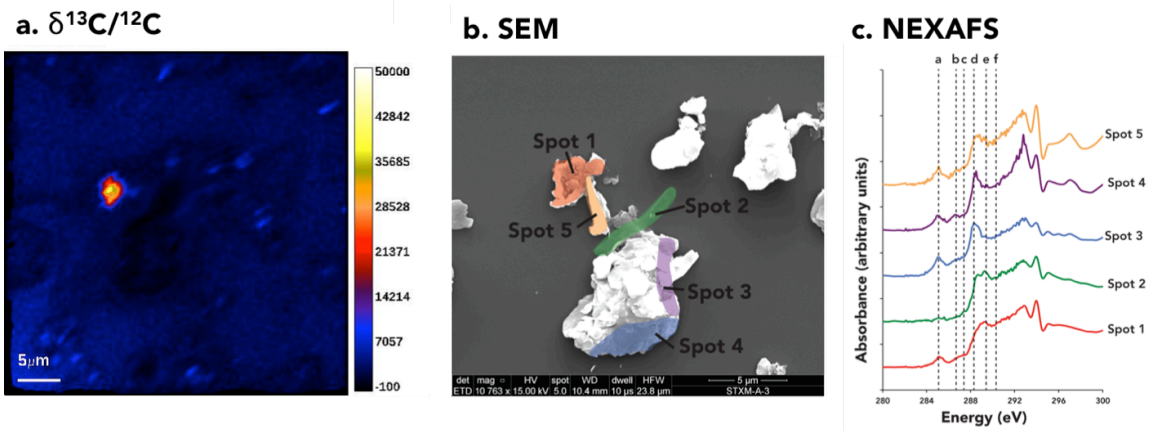

Figure 3.4. Coupled STXM/NanoSIMS imaging and characterization of rhizosphere soil. Alignment of NanoSIMS images (a) with STXM/NEXAFS spectra (b), allows for targeted analysis of the carbon chemistry of ^{13}C labeled regions. In this image from rhizosphere soil, Spot 1 (b), is ^{13}C highly enriched in ^{13}C and Spots 2-5 are enriched above natural abundance (a). We analyzed a total of 5 spots within the NanoSIMS area that had sufficient carbon for STXM/NEXAFS (c). The SEM image shows that Spot 2 is a microbial cell with a rod-shape morphology.

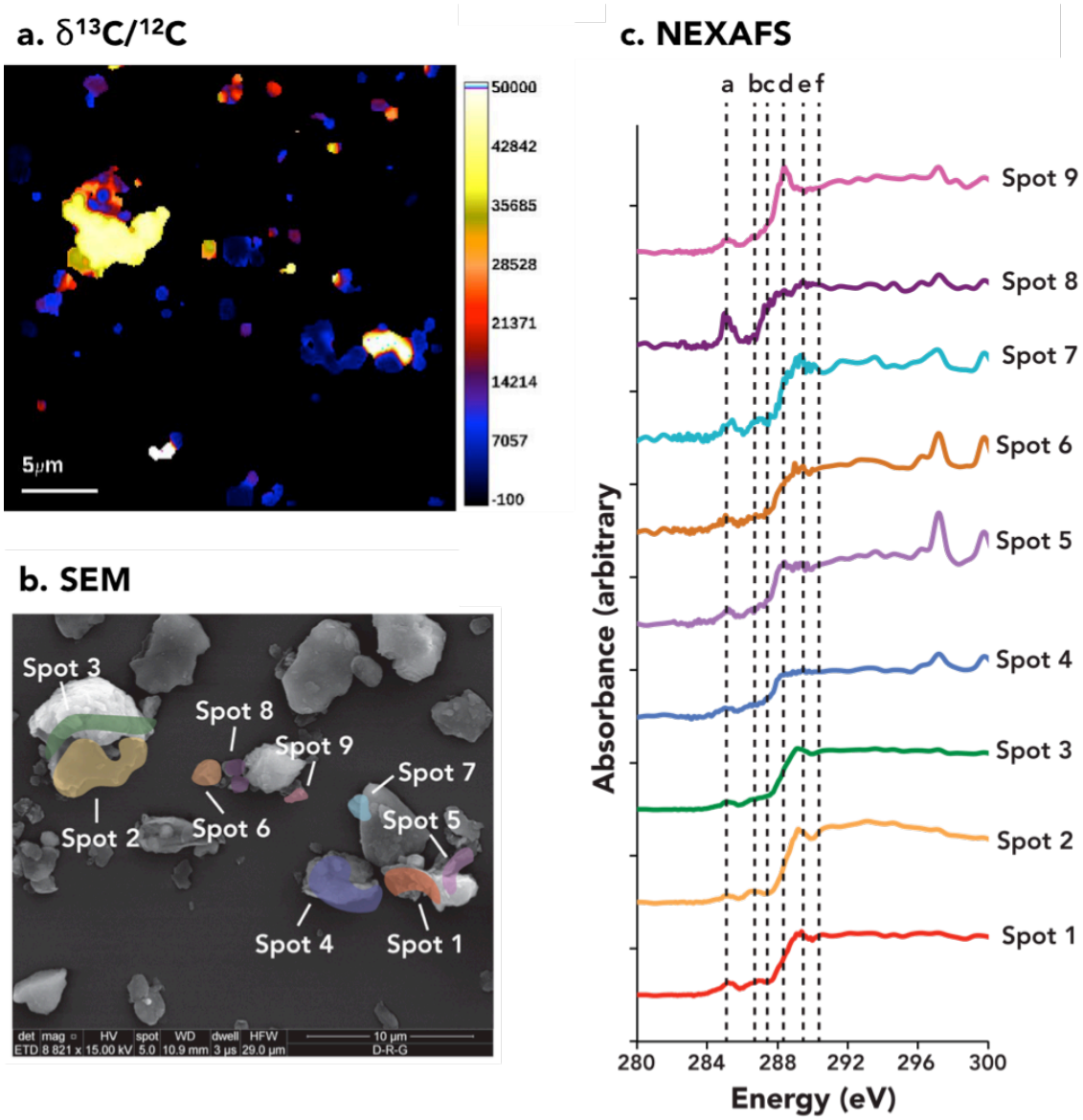

Figure 3.5. Coupled STXM/NanoSIMS imaging and characterization of detritosphere litter. Alignment NanoSIMS images (a) with STXM/NEXAFS spectra (b), allows for targeted analysis of the carbon chemistry of ^{13}C labeled regions. In this image from *Avena barbata root litter*, there is a single area, spot 1 (b), that is ^{13}C labeled (a). We analyzed a total of 9 spots within the NanoSIMS area that had sufficient carbon for STXM/NEXAFS (c). The SEM image shows that all spots are enriched in ^{13}C (a), but some spots are more enriched than others.

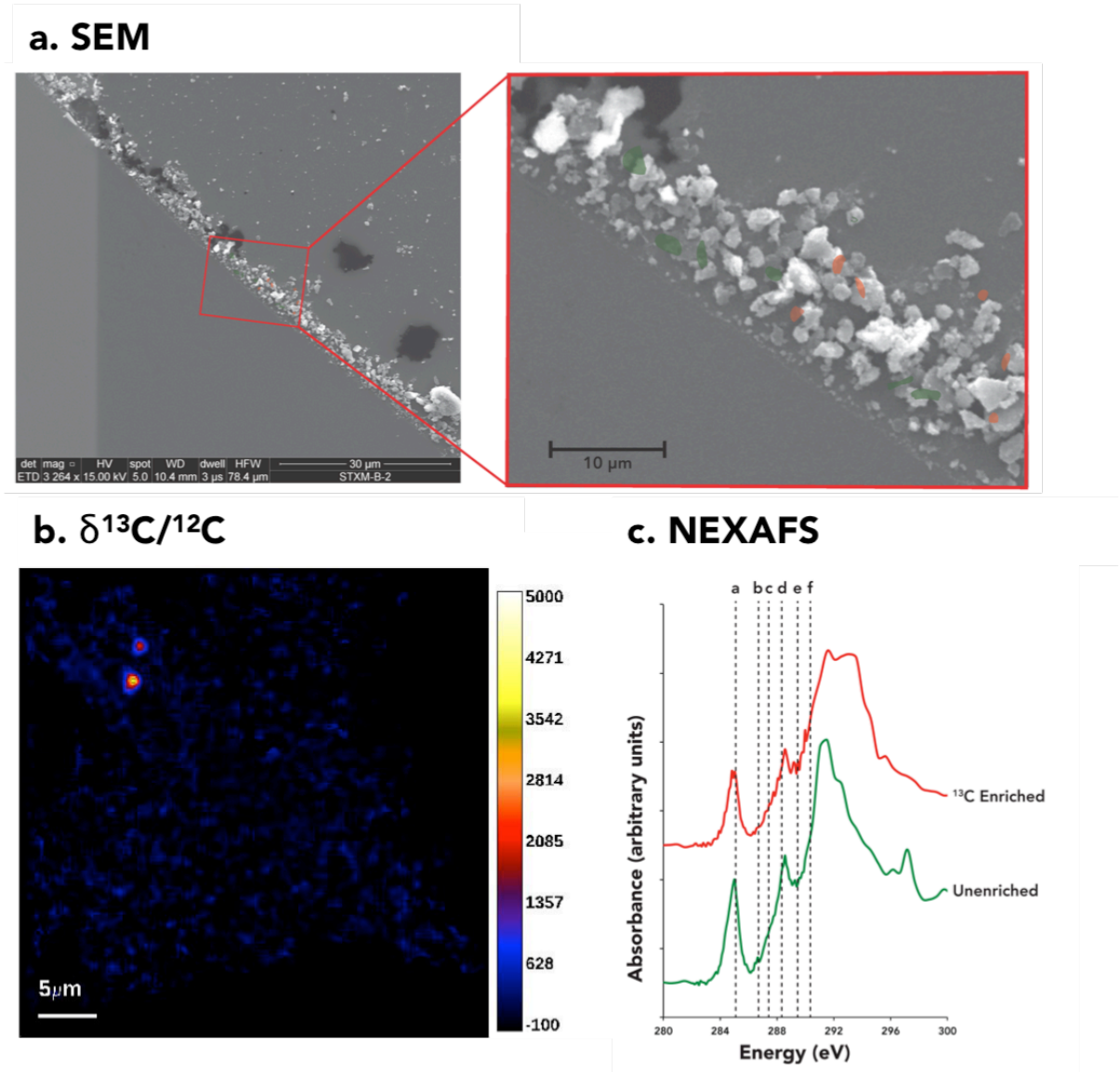

Figure 3.6. Ferrihydrite minerals incubated in rhizosphere. Alignment NanoSIMS images (b) with STXM/NEXAFS spectra (c), allows for targeted analysis of the carbon chemistry of ^{13}C labeled regions. In this image from Ferrihydrite incubated in the rhizosphere of *Avena barbata*, we analyzed 6 spots with ^{13}C enrichment and 7 spots was no ^{13}C enrichment. We show merged NEXAFS for all ^{13}C spots and all unenriched spots (c). Aromatic peaks (a) are susceptible to distortion due to sample thickness and here are evaluated only according to presence or absence.

3.6 SUPPORTING INFORMATION

3.6.1 Supporting Tables and Figures

SI Table 3.1. Total C and ^{13}C on Minerals Across Treatments

Treatment	Mineral	Average Total C (mg C / g mineral)	Standard Error	Average Total C (mg C / m2 mineral)	Standard Error	Average Atom% ^{13}C	Standard Error
Bulk	Native Mineral	14.80	0.84	5.52	0.31	1.09	0.00
	Ferrihydrite	1.14	0.24	0.24	0.05	1.16	0.02
	Kaolinite	1.58	0.54	0.16	0.05	1.17	0.03
	Quartz	0.36	0.07	11.85	2.36	1.20	0.05
Rhizosphere	Native Mineral	17.03	1.01	6.36	0.38	1.53	0.02
	Ferrihydrite	0.87	0.18	0.18	0.04	2.61	0.29
	Kaolinite	0.72	0.11	0.07	0.01	2.77	0.36
	Quartz	0.23	0.03	7.78	1.01	2.05	0.21
Detritosphere	Native Mineral	15.00	2.65	5.60	0.99	1.10	0.00
	Ferrihydrite	0.54	0.09	0.11	0.02	1.14	0.02
	Kaolinite	1.50	0.52	0.15	0.05	1.28	0.10
	Quartz	0.23	0.07	7.51	2.43	1.18	0.05

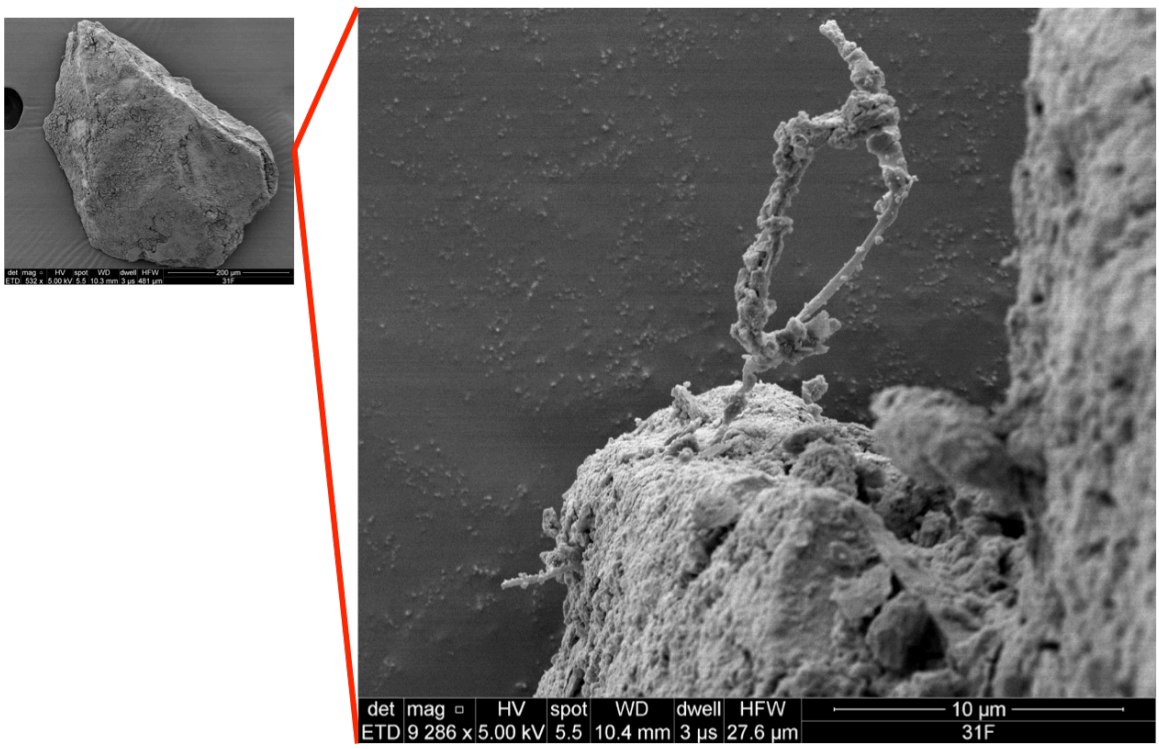

SI Figure 3.1. SEM images of Ferrihydrite incubated in the rhizosphere. A microbial cell that morphologically resembles a fungal hyphae is coated in ferrihydrite.

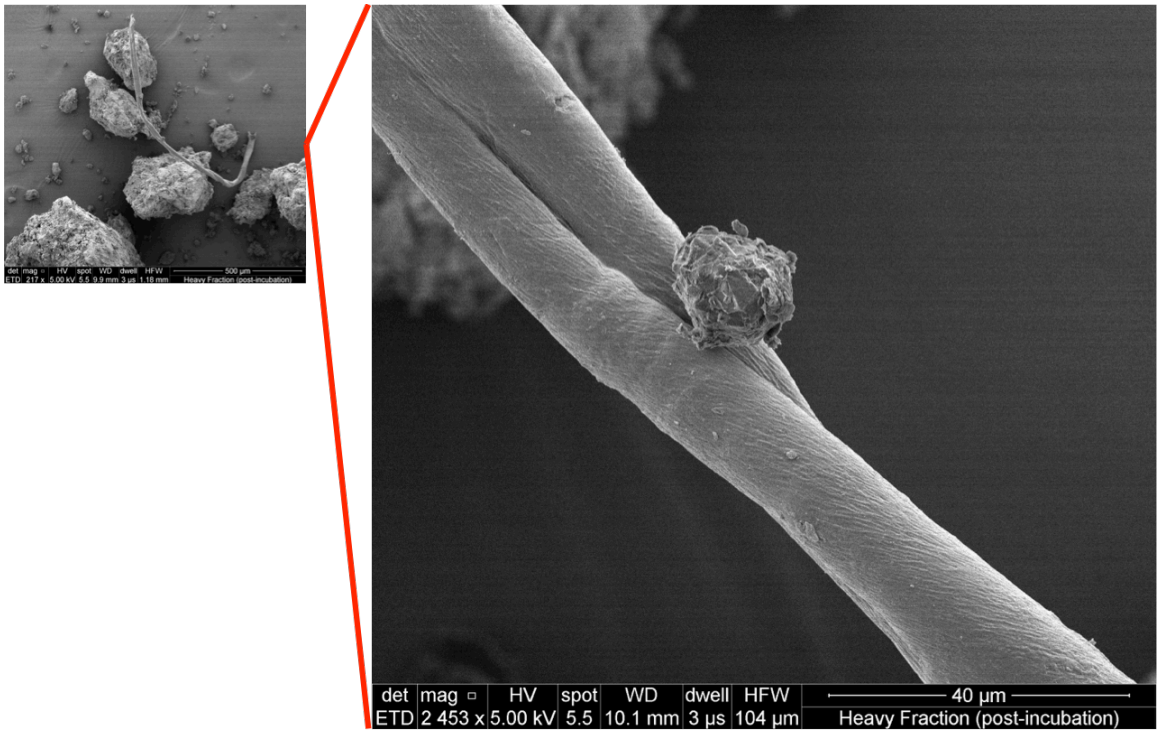

SI Figure 3.2. SEM images of the Native Mineral incubated in the rhizosphere. Perched on a fungal hyphae, there is a sphere of kaolinite minerals resembling a "clay hutch" (Lunsdorf *et al.*, 2000).

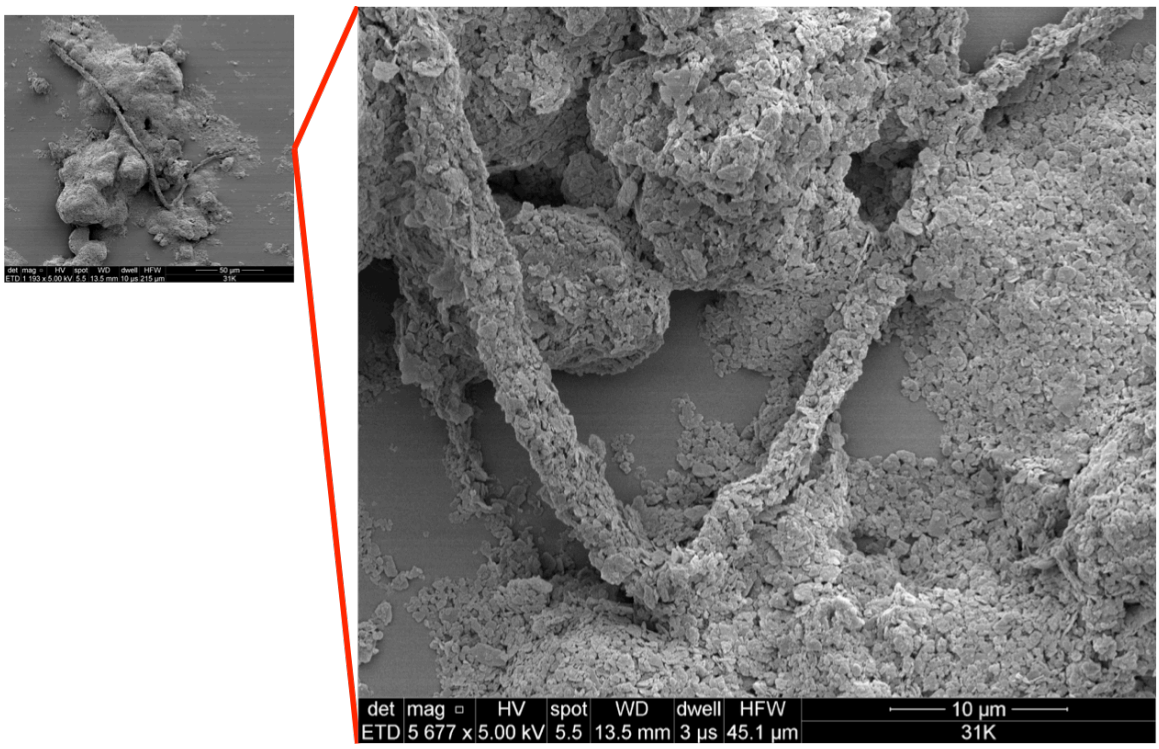

SI Figure 3.3. SEM images of Kaolinite incubated in the rhizosphere. A fungal hyphae is completely encapsulated in kaolinite minerals.

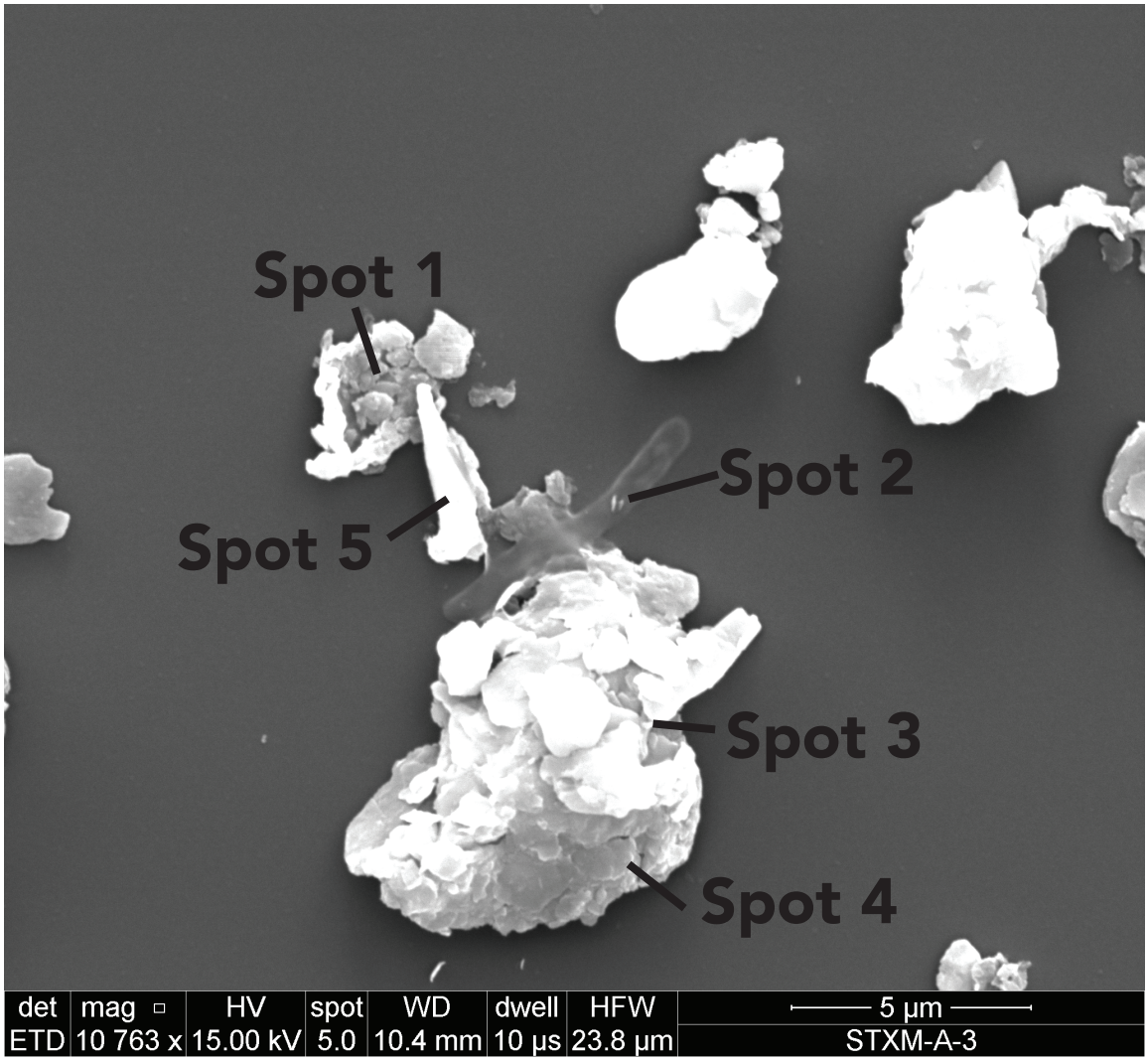

SI Figure 3.4. SEM images of rhizosphere soil, same as Figure 4 in main text, with color removed to show fungal cell morphology of Spot 2.

Conclusion

The primary objective of this dissertation research was to track the fate of C that associates soil minerals, focusing on the influence of mineralogy, plant growth, and the microbial community. Using a stable isotope-enabled approach (^{13}C), we traced mineral-associated C, coupled with next generation sequencing (Illumina MiSeq), high resolution isotopic imaging (NanoSIMS, SEM), and chemical characterization of C compounds (^{13}C-NMR, FTCIR-MS, Lipidomics, and STXM-NEXAFS) to build a mechanistic understanding of the controls on mineral-associated C. This was the first study to explicitly link rhizosphere and detritosphere C transformations to understand the interactions between plant C source and environment, microbial community composition, and mineral-associated C. Our work lends important insights to a broad effort to understand how soil C persists, and whether it might be possible to increase global C storage.

In all three chapters, we saw evidence of the importance of mineral type. In both the rhizosphere and detritosphere experiments, total C varied significantly by mineral type. Microbial community composition Bray-Curtis dissimilarities were significantly correlated with mineral type. We saw this both in the detritosphere in Chapter 2, as well as in Whitman *et al*., 2018, *Environmental Microbiology*, which was based on samples from the rhizosphere experiment in Chapter 1. FTICR-MS analysis of water-extracted OM from minerals and Lipidomic analysis of chloroform-methanol extracted OM from minerals also significantly correlated with mineral type. Despite the consistent influence of mineral type, we made a critical finding that in the rhizosphere, total C accumulation was greatest on ferrihydrite-coated quartz, while in the detritosphere and bulk soil, total C accumulation was greatest on the kaolinite. Therefore, mineral type matters, but *in the context of* C source and environment. In the rhizosphere, the strength of mineral-OM associations may be the most important factor in total C accumulation. In the detritosphere, microaggregation of kaolinite may play a more important role. Further work is needed to disentangle the exact cause for these differences, and how they might apply to different soil systems, but the elucidation of an *interaction* between mineral type and C source and environment is a critical finding.

In Chapters 1 and 2, we saw evidence that C accumulation on minerals is dynamic. In the rhizosphere, kaolinite accumulated no C after 1 month, but the atom% ^{13}C continued to increase, suggesting an *exchange* of root-derived C for soil-derived C. In both the rhizosphere and detritosphere, there was no significant change in total C after an initial period, but root-derived ^{13}C (exudate-derived in the rhizosphere and litter-derived in the detritosphere) did exchange with mineral-associated OM. We also observed that total C accumulation on specimen minerals was slow and only linear for ferrihydrite in the rhizosphere. For all other specimen minerals, as well as ferrihydrite in the detritosphere, most total C accumulation occurred rapidly and then there was little or no change in total C. By the time the plant senesced in the rhizosphere, and after 3 months in the detritosphere, specimen minerals accumulated an order of magnitude less C than that associated with the native minerals. In Chapter 3, NanoSIMS analysis showed that distribution of ^{13}C on minerals is sparse in the rhizosphere, and total C distribution is also likely patchy and sparse. Patchy, sparse C distribution on minerals was also observed from STXM/NEXAFS analysis of the same minerals. On the native minerals, there was no significant change in total C in the rhizosphere or detritosphere although ^{13}C plant C did associate with the

native minerals. Increased C addition to soil through actively growing plants or litter additions are considered potential methods of increasing soil C storage. Our work suggests that significant changes in the quantity mineral-associated C from increased C input may take longer than a single season, if it happens at all. Further work is needed to determine whether studies of a longer timeframe would see significant changes in mineral-associated C.

The composition of mineral-associated C was influenced by mineral type and C source and environment (rhizosphere, detritosphere, and bulk). In the rhizosphere, mineral-associated C had a more diverse compositional profile of C functional groups than the bulk soil, as shown by ^{13}C-NMR. STXM/NEXAFS analysis showed that in the detritosphere, mineral-associated C had a distinct phenolic signature. However, the quartz minerals in the detritosphere did not have phenolic C compounds. Microaggregation of kaolinite and ferrihydrite nanoaggregates may play an important role in protecting less microbially-degraded litter compounds in the detritosphere. In general, mineral-associated C showed spectroscopic evidence of microbial degradation or resembled published reference spectra for bacterial and fungal material.

We identified certain microbes that appear to play a particularly important role in mineral-associated C dynamics. Minerals had associated bacterial, archaeal, and fungal microbial communities, as indicated by sequencing of extracted DNA. While there were some similarities, likely originating from the background soil, the phylogenetic composition of the communities differed between the rhizosphere and detritosphere. Most notably, in the rhizosphere there was a high relative abundance of arbuscular mycorrhizal fungi (AMF, *Glomerales* order), particularly on ferrihydrite-associated quartz (Whitman *et al*., 2018). In Chapter 2, we see that putative AMF account for a large fraction of rhizosphere-derived ^{13}C on minerals. Based on the ^{13}C enrichment and surface area occupied by hyphae, we estimated as much as 77% of the ^{13}C enrichment observed on our Ferrihydrite samples and 95% of the ^{13}C enrichment in our observed Kaolinite samples came from hyphae. Plant symbiotic fungal hyphae such as AMF may act as large conduits of plant C to mineral surfaces. In the detritosphere experiment in Chapter 3, we noted the potential importance of the lipid-rich fungal order *Mucorales* and bacterial order *Streptomyces*, which may play an important role in mineral-associated lipid formation. Based on our ^{13}C-NMR analysis of minerals in the rhizosphere, lipids may be more persistent on minerals than other C functional groups. If so, mineral-associated lipids could have important implications for the persistence of soil OM.

Following a mineral through seasons, we might expect a mineral that starts in bulk soil, coated in more lipid and aliphatic C compounds. Then a root grows past, and the flow of low molecular weight C compounds from the rhizosphere stimulates microbial growth and activity. While a few root exudates may directly associate with the mineral, most are likely processed by microbes. Some microbial products associate with the mineral. Some microbes colonize the mineral. Others die and their necromass attaches to the mineral surface. An arbuscular mycorrhizal fungi extends from the root to the mineral, pumping C directly to the mineral surface. High microbial activity and organic acids from the rhizosphere cause rapid exchange of both new and old C compounds on the mineral. If the mineral is ferrihydrite, with a high surface reactivity, it might hold onto more C than its neighboring quartz. The chemistry of the mineral-associated C has changed, even though the total amount of C may remain the same. Eventually, the root dies. As it begins to decay, the microbial community shifts to more saprotrophic bacteria and fungi. With a pulse of

rainfall after a dry season, a large fraction of the litter is released as CO_2. Some of what remains associates with soil minerals. Those minerals that form aggregates can protect the litter. Lipid-rich microbes may leave a mark on the mineral-associated C chemistry. After the initial pulse of activity after rainfall, there is less C association with minerals. Then a new plant grows and a root once again extends past the minerals. New C associates with the mineral, and those compounds from the detritosphere that are not strongly bound or aggregated may exchange, once again shifting the chemical profile of the C on the mineral surface, even if the total C may not significantly change.

Our work emphasizes the importance of modeling plant-microbe-mineral interactions in concert to understand the mechanisms of C transformation and persistence in soil. We see critical differences between the bulk soil, rhizosphere soil, and detritosphere soil, which are likely particularly important in a seasonal system such as our model annual grassland ecosystem growing under a Mediterranean-type climate. While further work is needed to examine these systems over a longer time scale, our work provides a snapshot of C flow from plants to minerals over the course of a year as *Avena barbata* grows, senesces, and decays. Carbon association with minerals is dynamic, particularly so in the rhizosphere. Our work suggests that increasing C supply to the soil does not necessarily result in increased C association with minerals over a short timescale. However, differences in C source and environment do impact mineral-associated C composition, which in turn could influence longer-term persistence. The potential importance of particular fungal (*Glomerales* in the rhizosphere and *Mucorales* in the detritosphere) and bacterial (*Streptomyces* in the detritosphere) orders is intriguing, and could be an interesting topic for future research. Soils are complex, and our work emphasizes that so, too, are the mechanisms of C persistence.

References

Aamot, H. U., I. S. Hofgaard, and E. Lysøe. 2016. Complete genome sequence of Luteibacter rhizovicinus strain LJ96T, isolated from the rhizosphere of barley (Hordeum vulgare L.) in Denmark. Genomics data **11**:104-105.

Allen, P. J. 1965. Metabolic Aspects of Spore Germination in Fungi. Annual Review of Phytopathology **3**:313-342.

Alvarez, H. M., and A. Steinbuchel. 2002. Triacylglycerols in prokaryotic microorganisms. Applied Microbiology and Biotechnology **60**:367-376.

Angst, G., K. E. Mueller, I. Kögel-Knabner, K. H. Freeman, and C. W. Mueller. 2017. Aggregation controls the stability of lignin and lipids in clay-sized particulate and mineral associated organic matter. Biogeochemistry **132**:307-324.

Bailey, V. L., C. H. Pries, and K. Lajtha. 2019. What do we know about soil carbon destabilization? Environmental Research Letters **14**.

Baisden, W. T., R. Amundson, A. C. Cook, and D. L. Brenner. 2002. Turnover and storage of C and N in five density fractions from California annual grassland surface soils. Global Biogeochemical Cycles **16**.

Banfield, J. F., W. W. Barker, S. A. Welch, and A. Taunton. 1999. Biological impact on mineral dissolution: Application of the lichen model to understanding mineral weathering in the rhizosphere. Proceedings of the National Academy of Sciences **96**:3404.

Banfield Jillian, F., and J. Hamers Robert. 1997. Chapter 3. Processes at minerals and surfaces with relevance to microorganisms and prebiotic synthesis. GeomicrobiologyInteractions between Microbes and Minerals.

Barnard, R. L., S. J. Blazewicz, and M. K. Firestone. 2020. Rewetting of soil: Revisiting the origin of soil CO2 emissions. Soil Biology and Biochemistry **147**:107819.

Barnard, R. L., C. A. Osborne, and M. K. Firestone. 2013. Responses of soil bacterial and fungal communities to extreme desiccation and rewetting. The ISME Journal **7**:2229-2241.

Barnard, R. L., C. A. Osborne, and M. K. Firestone. 2015. Changing precipitation pattern alters soil microbial community response to wet-up under a Mediterranean-type climate. The ISME Journal **9**:946-957.

Bertin, C., X. H. Yang, and L. A. Weston. 2003. The role of root exudates and allelochemicals in the rhizosphere. Plant and Soil **256**:67-83.

Bhattacharyya, A., and *e. al. in prep*.

Birch, H. F. 1958. The effect of soil drying on humus decomposition and nitrogen availability. Plant and Soil **10**:9-31.

Blagodatskaya, E., S. Blagodatsky, T.-H. Anderson, and Y. Kuzyakov. 2014. Microbial Growth and Carbon Use Efficiency in the Rhizosphere and Root-Free Soil. PLos One **9**:e93282.

Blazewicz, S. J., B. A. Hungate, B. J. Koch, E. E. Nuccio, E. Morrissey, E. L. Brodie, E. Schwartz, J. Pett-Ridge, and M. K. Firestone. 2020. Taxon-specific microbial growth and mortality patterns reveal distinct temporal population responses to rewetting in a California grassland soil. The ISME Journal **14**:1520-1532.

Blazewicz, S. J., E. Schwartz, and M. K. Firestone. 2014. Growth and death of bacteria and fungi underlie rainfall-induced carbon dioxide pulses from seasonally dried soil. Ecology **95**:1162-1172.

Bramer, L., and A. White. 2018. fticRanalysis: Analysis and visualization tools for ICR data. R package.

Bray, J. R., and J. T. Curtis. 1957. An Ordination of the Upland Forest Communities of Southern Wisconsin. Ecological Monographs **27**:325-349.

Bresciani, F. R., L. Santi, A. J. Macedo, W.-R. Abraham, M. H. Vainstein, and W. O. Beys-da-Silva. 2014. Production and activity of extracellular lipase from Luteibacter sp. Annals of Microbiology **64**:251-258.

Callahan, B. J., P. J. McMurdie, M. J. Rosen, A. W. Han, A. J. A. Johnson, and S. P. Holmes. 2016. DADA2: High-resolution sample inference from Illumina amplicon data. Nature Methods **13**:581-583.

Caporaso, J. G., J. Kuczynski, J. Stombaugh, K. Bittinger, F. D. Bushman, E. K. Costello, N. Fierer, A. G. Peña, J. K. Goodrich, J. I. Gordon, G. A. Huttley, S. T. Kelley, D. Knights, J. E. Koenig, R. E. Ley, C. A. Lozupone, D. McDonald, B. D. Muegge, M. Pirrung, J. Reeder, J. R. Sevinsky, P. J. Turnbaugh, W. A. Walters, J. Widmann, T. Yatsunenko, J. Zaneveld, and R. Knight. 2010. QIIME allows analysis of high-throughput community sequencing data. Nature Methods **7**:335-336.

Castellano, M. J., K. E. Mueller, D. C. Olk, J. E. Sawyer, and J. Six. 2015. Integrating plant litter quality, soil organic matter stabilization, and the carbon saturation concept. Global Change Biology **21**:3200-3209.

Chang, Y. Y., and J. E. Cronan. 1999. Membrane cyclopropane fatty acid content is a major factor in acid resistance of Escherichia coli. Molecular Microbiology **33**:249-259.

Chapman, S. J. 2010. Carbon Sequestration in Soils. Pages 179-202 *in* R. E. Hester and R. M. Harrison, editors. Carbon Capture: Sequestration and Storage.

Chaudhary, S., A. Shankar, A. Singh, and V. Prasad. 2018. Chapter 16 - Usefulness of Penicillium in Enhancing Plants Resistance to Abiotic Stresses: An Overview. Pages 277-284 *in* V. K. Gupta and S. Rodriguez-Couto, editors. New and Future Developments in Microbial Biotechnology and Bioengineering. Elsevier, Amsterdam.

Chen, C. M., J. J. Dynes, J. Wang, and D. L. Sparks. 2014. Properties of Fe-Organic Matter Associations via Coprecipitation versus Adsorption. Environmental Science & Technology **48**:13751-13759.

Cismasu, A. C., C. Levard, F. M. Michel, and G. E. Brown. 2013. Properties of impurity-bearing ferrihydrite II: Insights into the surface structure and composition of pure, Al- and Si-bearing ferrihydrite from Zn(II) sorption experiments and Zn K-edge X-ray absorption spectroscopy. Geochimica Et Cosmochimica Acta **119**:46-60.

Compant, S., J. Nowak, T. Coenye, C. Clément, and E. Ait Barka. 2008. Diversity and occurrence of Burkholderia spp. in the natural environment. FEMS Microbiol Rev **32**:607-626.

Cotrufo, M. F., M. D. Wallenstein, C. M. Boot, K. Denef, and E. Paul. 2013. The Microbial Efficiency-Matrix Stabilization (MEMS) framework integrates plant litter decomposition with soil organic matter stabilization: do labile plant inputs form stable soil organic matter? Global Change Biology **19**:988-995.

Courchesne, F., and M.-C. Turmel. 2008. Extractable Al, Fe, Mn, and Si. Pages 307-316 *in* M. R. Carter and E. G. Gregorich, editors. Soil Sampling and Methods of Analysis. Canadian Society of Soil Science, Boca Raton, FL.

Creamer, C. A., A. L. Foster, C. Lawrence, J. McFarland, M. Schulz, and M. P. Waldrop. 2019. Mineralogy dictates the initial mechanism of microbial necromass association. Geochimica Et Cosmochimica Acta **260**:161-176.

DeAngelis, K. M., E. L. Brodie, T. Z. DeSantis, G. L. Andersen, S. E. Lindow, and M. K. Firestone. 2009. Selective progressive response of soil microbial community to wild oat roots. Isme Journal **3**:168-178.

DeAngelis, K. M., S. E. Lindow, and M. K. Firestone. 2008. Bacterial quorum sensing and nitrogen cycling in rhizosphere soil. FEMS Microbiology Ecology **66**:197-207.

Dolatabadi, S., G. S. de Hoog, J. F. Meis, and G. Walther. 2014. Species boundaries and nomenclature of Rhizopus arrhizus (syn. R. oryzae). Mycoses **57 Suppl 3**:108-127.

Doncaster, C. P., and A. J. H. Davey. 2007. Analysis of Variance and Covariance. [electronic resource] : How to Choose and Construct Models for the Life Sciences. Cambridge : Cambridge University Press, 2007.

Dungait, J. A. J., D. W. Hopkins, A. S. Gregory, and A. P. Whitmore. 2012. Soil organic matter turnover is governed by accessibility not recalcitrance. Global Change Biology **18**:1781-1796.

Dwivedi, D., W. J. Riley, M. S. Torn, N. Spycher, F. Maggi, and J. Y. Tang. 2017. Mineral properties, microbes, transport, and plant-input profiles control vertical distribution and age of soil carbon stocks. Soil Biology & Biochemistry **107**:244-259.

Dwivedi, D., J. Tang, N. Bouskill, K. Georgiou, S. S. Chacon, and W. J. Riley. 2019. Abiotic and Biotic Controls on Soil Organo–Mineral Interactions: Developing Model Structures to Analyze Why Soil Organic Matter Persists. Reviews in Mineralogy and Geochemistry **85**:329-348.

Ehrlich, H. L. 1996. How microbes influence mineral growth and dissolution. Chemical Geology **132**:5-9.

Eusterhues, K., T. Rennert, H. Knicker, I. Kogel-Knabner, K. U. Totsche, and U. Schwertmann. 2011. Fractionation of Organic Matter Due to Reaction with Ferrihydrite: Coprecipitation versus Adsorption. Environmental Science & Technology **45**:527-533.

Eusterhues, K., C. Rumpel, and I. Kogel-Knabner. 2005. Organo-mineral associations in sandy acid forest soils: importance of specific surface area, iron oxides and micropores. European Journal of Soil Science **56**:753-763.

Eusterhues, K., F. E. Wagner, W. Hausler, M. Hanzlik, H. Knicker, K. U. Totsche, I. Kogel-Knabner, and U. Schwertmann. 2008. Characterization of Ferrihydrite-Soil Organic Matter Coprecipitates by X-ray Diffraction and Mossbauer Spectroscopy. Environmental Science & Technology **42**:7891-7897.

Farrar, J., M. Hawes, D. Jones, and S. Lindow. 2003. How roots control the flux of carbon to the rhizosphere. Ecology **84**:827-837.

Fenn, J. B., M. Mann, C. K. Meng, S. F. Wong, and C. M. Whitehouse. 1989. Electrospray ionization for mass-spectrometry of large biomolecules. Science **246**:64-71.

Finzi, A. C., R. Z. Abramoff, K. S. Spiller, E. R. Brzostek, B. A. Darby, M. A. Kramer, and R. P. Phillips. 2015. Rhizosphere processes are quantitatively important components of terrestrial carbon and nutrient cycles. Global Change Biology **21**:2082-2094.

Frostegard, A., A. Tunlid, and E. Baath. 1993. Phospholipid fatty-acid composition, biomass, and activity of microbial communities from 2 soil types experimentally exposed to different heavy-metals. Applied and Environmental Microbiology **59**:3605-3617.

Garcia, C., P. Nannipieri, and T. Hernandez. 2018. The Future of Soil Carbon.

Glaeser, S. P., and P. Kämpfer. 2014. The Family Sphingomonadaceae. Springer, Berlin Heidelberg

Glassman, S. I., K. G. Peay, J. M. Talbot, D. P. Smith, J. A. Chung, J. W. Taylor, R. Vilgalys, and T. D. Bruns. 2015. A continental view of pine-associated ectomycorrhizal fungal spore banks: a quiescent functional guild with a strong biogeographic pattern. New Phytol **205**:1619-1631.

Glöckner, F. O., P. Yilmaz, C. Quast, J. Gerken, A. Beccati, A. Ciuprina, G. Bruns, P. Yarza, J. Peplies, R. Westram, and W. Ludwig. 2017. 25 years of serving the community with ribosomal RNA gene reference databases and tools. Journal of Biotechnology **261**:169-176.

Gregory, P. J. 2006. Roots, rhizosphere and soil: the route to a better understanding of soil science? European Journal of Soil Science **57**:2-12.

Guglielmetti, S., R. Basilico, V. Taverniti, S. Arioli, C. Piagnani, and A. Bernacchi. 2013. Luteibacter rhizovicinus MIMR1 promotes root development in barley (Hordeum vulgare L.) under laboratory conditions. World Journal of Microbiology and Biotechnology **29**:2025-2032.

Hansel, C. M., S. G. Benner, J. Neiss, A. Dohnalkova, R. K. Kukkadapu, and S. Fendorf. 2003. Secondary mineralization pathways induced by dissimilatory iron reduction of ferrihydrite under advective flow. Geochimica Et Cosmochimica Acta **67**:2977-2992.

Hansel, C. M., S. G. Benner, P. Nico, and S. Fendorf. 2004. Structural constraints of ferric (hydr)oxides on dissimilatory iron reduction and the fate of Fe(II). Geochimica Et Cosmochimica Acta **68**:3217-3229.

Harwood, J. L., and N. J. Russell. 1984. Lipids in plants and microbes. G. Allen & Unwin, London ; Boston.

Heckman, K., A. S. Grandy, X. Gao, M. Keiluweit, K. Wickings, K. Carpenter, J. Chorover, and C. Rasmussen. 2013. Sorptive fractionation of organic matter and formation of organo-hydroxy-aluminum complexes during litter biodegradation in the presence of gibbsite. Geochimica Et Cosmochimica Acta **121**:667-683.

Heckman, K., C. R. Lawrence, and J. W. Harden. 2018a. A sequential selective dissolution method to quantify storage and stability of organic carbon associated with Al and Fe hydroxide phases. Geoderma **312**:24-35.

Heckman, K., H. Throckmorton, W. R. Horwath, C. W. Swanston, and C. Rasmussen. 2018b. Variation in the Molecular Structure and Radiocarbon Abundance of Mineral-Associated Organic Matter across a Lithosequence of Forest Soils. Soil Systems **2**.

Heister, K., C. Hoschen, G. J. Pronk, C. W. Mueller, and I. Kogel-Knabner. 2012. NanoSIMS as a tool for characterizing soil model compounds and organomineral associations in artificial soils. Journal of Soils and Sediments **12**:35-47.

Hiemstra, T. 2013. Surface and mineral structure of ferrihydrite. Geochimica Et Cosmochimica Acta **105**:316-325.

Hinsinger, P., A. G. Bengough, D. Vetterlein, and I. M. Young. 2009. Rhizosphere: biophysics, biogeochemistry and ecological relevance. Plant and Soil **321**:117-152.

Hitchcock, A. P. 2009. aXis2000.

Hong, Z. N., W. L. Chen, X. M. Rong, P. Cai, K. Dai, and Q. Y. Huang. 2013. The effect of extracellular polymeric substances on the adhesion of bacteria to clay minerals and goethite. Chemical Geology **360**:118-125.

Hurt, R. J., M. I. Robeson, M. Shakya, J. Moberly, T. Vishnivetskaya, B. Gu, and e. al. 2014. Improved Yield of High Molecular Weight DNA Coincides with Increased Microbial Diversity Access from Iron Oxide Cemented Sub-Surface Clay Environments. PLos One **9**.

Hutchens, E., D. Gleeson, F. McDermott, R. Miranda-CasoLuengo, and N. Clipson. 2010. Meter-Scale Diversity of Microbial Communities on a Weathered Pegmatite Granite Outcrop in the Wicklow Mountains, Ireland; Evidence for Mineral Induced Selection? Geomicrobiology Journal **27**:1-14.

Jilling, A., M. Keiluweit, A. R. Contosta, S. Frey, J. Schimel, J. Schnecker, R. G. Smith, L. Tiemann, and A. S. Grandy. 2018. Minerals in the rhizosphere: overlooked mediators of soil nitrogen availability to plants and microbes. Biogeochemistry **139**:103-122.

Jones, D. L., C. Nguyen, and R. D. Finlay. 2009. Carbon flow in the rhizosphere: carbon trading at the soil-root interface. Plant and Soil **321**:5-33.

Jones, E., and B. Singh. 2014. Organo-mineral interactions in contrasting soils under natural vegetation. Frontiers in Environmental Science **2**.

Kaiser, C., M. R. Kilburn, P. L. Clode, L. Fuchslueger, M. Koranda, J. B. Cliff, Z. M. Solaiman, and D. V. Murphy. 2015. Exploring the transfer of recent plant photosynthates to soil microbes: mycorrhizal pathway vs direct root exudation. New Phytologist **205**:1537-1551.

Kaiser, K., R. Mikutta, and G. Guggenberger. 2007. Increased stability of organic matter sorbed to ferrihydrite and goethite on aging. Soil Science Society of America Journal **71**:711-719.

Kaiser, M., R. H. Ellerbrock, M. Wulf, S. Dultz, C. Hierath, and M. Sommer. 2012. The influence of mineral characteristics on organic matter content, composition, and stability of topsoils under long-term arable and forest land use. Journal of Geophysical Research-Biogeosciences **117**.

Kallenbach, C. M., S. D. Frey, and A. S. Grandy. 2016. Direct evidence for microbial-derived soil organic matter formation and its ecophysiological controls. Nature Communications **7**.

Kallenbach, C. M., A. S. Grandy, S. D. Frey, and A. F. Diefendorf. 2015. Microbial physiology and necromass regulate agricultural soil carbon accumulation. Soil Biology & Biochemistry **91**:279-290.

Kauffman, C. A. 2017. 33 - Fungal Pneumonias. Pages 292-299.e291 *in* J. Cohen, W. G. Powderly, and S. M. Opal, editors. Infectious Diseases (Fourth Edition). Elsevier.

Keiluweit, M., J. J. Bougoure, P. S. Nico, J. Pett-Ridge, P. K. Weber, and M. Kleber. 2015. Mineral protection of soil carbon counteracted by root exudates. Nature Climate Change **5**:588-595.

Keiluweit, M., J. J. Bougoure, L. H. Zeglin, D. D. Myrold, P. K. Weber, J. Pett-Ridge, M. Kleber, and P. S. Nico. 2012. Nano-scale investigation of the association of microbial nitrogen residues with iron (hydr)oxides in a forest soil O-horizon. Geochimica Et Cosmochimica Acta **95**:213-226.

Keiluweit, M., P. S. Nico, L. H. Zeglin, J. Pett-Ridge, P. Weber, D. D. Myrold, and M. Kleber. 2010. C and N dynamics in soil microstructures: A joined STXM/NEXAFS and NanoSIMS approach. Geochimica Et Cosmochimica Acta **74**:A502-A502.

Kieft, T. L., E. soroker, and M. K. firestone. 1987. Microbial biomass response to a rapid increase in water potential when dry soil is wetted. Soil Biology and Biochemistry **19**:119-126.

Kilcoyne, A. L. D., T. Tyliszczak, W. F. Steele, S. Fakra, P. Hitchcock, K. Franck, E. Anderson, B. Harteneck, E. G. Rightor, G. E. Mitchell, A. P. Hitchcock, L. Yang, T. Warwick, and H. Ade. 2003.

Interferometer controlled scanning transmission X-ray microscopes at the Advanced Light Source. J. Synchrotron Radiat **Volume: 10**

Kim, S., R. W. Kramer, and P. G. Hatcher. 2003. Graphical method for analysis of ultrahigh-resolution broadband mass spectra of natural organic matter, the van Krevelen diagram. Analytical Chemistry **75**:5336-5344.

Kinyangi, J., D. Solomon, B. I. Liang, M. Lerotic, S. Wirick, and J. Lehmann. 2006. Nanoscale biogeocomplexity of the organomineral assemblage in soil: Application of STXM microscopy and C 1s-NEXAFS spectroscopy. Soil Science Society of America Journal **70**:1708-1718.

Kleber, M. 2010. What is recalcitrant soil organic matter? Environmental Chemistry **7**:320-332.

Kleber, M., K. Eusterhues, M. Keiluweit, C. Mikutta, R. Mikutta, and P. S. Nico. 2015a. Chapter One - Mineral–Organic Associations: Formation, Properties, and Relevance in Soil Environments. Pages 1-140 *in* D. L. Sparks, editor. Advances in Agronomy. Academic Press.

Kleber, M., K. Eusterhues, M. Keiluweit, C. Mikutta, R. Mikutta, and P. S. Nico. 2015b. Mineral-Organic Associations: Formation, Properties, and Relevance in Soil Environments. Pages 1-140 *in* D. L. Sparks, editor. Advances in Agronomy, Vol 130.

Kleber, M., R. Mikutta, M. S. Torn, and R. Jahn. 2005. Poorly crystalline mineral phases protect organic matter in acid subsoil horizons. European Journal of Soil Science **56**:717-725.

Kleber, M., P. Sollins, and R. Sutton. 2007. A conceptual model of organo-mineral interactions in soils: self-assembly of organic molecular fragments into zonal structures on mineral surfaces. Biogeochemistry **85**:9-24.

Kogel-Knabner, I., G. Guggenberger, M. Kleber, E. Kandeler, K. Kalbitz, S. Scheu, K. Eusterhues, and P. Leinweber. 2008. Organo-mineral associations in temperate soils: Integrating biology, mineralogy, and organic matter chemistry. Journal of Plant Nutrition and Soil Science **171**:61-82.

Kolattukudy, P. E. 1980. Biopolyester membranes of plants: cutin and suberin. Science **208**:990-1000.

Kuzyakov, Y., and E. Blagodatskaya. 2015. Microbial hotspots and hot moments in soil: Concept & review. Soil Biology & Biochemistry **83**:184-199.

Kuzyakov, Y., and G. Domanski. 2000. Carbon input by plants into the soil. Review. Journal of Plant Nutrition and Soil Science **163**:421-431.

Kyle, J. E., K. L. Crowell, C. P. Casey, G. M. Fujimoto, S. Kim, S. E. Dautel, R. D. Smith, S. H. Payne, and T. O. Metz. 2017. LIQUID: an-open source software for identifying lipids in LC-MS/MS-based lipidomics data. Bioinformatics (Oxford, England) **33**:1744-1746.

Lajtha, K., R. D. Bowden, S. Crow, I. Fekete, Z. Kotroczó, A. Plante, M. J. Simpson, and K. J. Nadelhoffer. 2018. The detrital input and removal treatment (DIRT) network: Insights into soil carbon stabilization. Science of the Total Environment **640-641**:1112-1120.

Lajtha, K., K. L. Townsend, M. G. Kramer, C. Swanston, R. D. Bowden, and K. Nadelhoffer. 2014. Changes to particulate versus mineral-associated soil carbon after 50 years of litter

manipulation in forest and prairie experimental ecosystems. Biogeochemistry **119**:341-360.
Lal, R. 2004a. Soil carbon sequestration impacts on global climate change and food security. Science **304**:1623-1627.
Lal, R. 2004b. Soil carbon sequestration to mitigate climate change. Geoderma **123**:1-22.
Lal, R. 2010. Terrestrial sequestration of carbon dioxide (CO2). Pages 271-303 *in* M. M. MarotoValer, editor. Developments and Innovation in Carbon Dioxide.
Lehmann, J. 2007. A handful of carbon. Nature **447**:143-144.
Lehmann, J., C. M. Hansel, C. Kaiser, M. Kleber, K. Maher, S. Manzoni, N. Nunan, M. Reichstein, J. P. Schimel, M. S. Torn, W. R. Wieder, and I. Kögel-Knabner. 2020. Persistence of soil organic carbon caused by functional complexity. Nature Geoscience **13**:529-534.
Lehmann, J., J. Kinyangi, and D. Solomon. 2007. Organic matter stabilization in soil microaggregates: implications from spatial heterogeneity of organic carbon contents and carbon forms. Biogeochemistry **85**:45-57.
Lenth, R. 2019. emmeans: Estimate Marginal Means, aka Least-Squares Means. R package
Lin, D., W. T. Ma, Z. X. Jin, Y. X. Wang, Q. Y. Huang, and P. Cai. 2016. Interactions of EPS with soil minerals: A combination study by ITC and CLSM. Colloids and Surfaces B-Biointerfaces **138**:10-16.
Liu, J., L. Sandaklie-Nikolova, X. M. Wang, and J. D. Miller. 2014. Surface force measurements at kaolinite edge surfaces using atomic force microscopy. Journal of Colloid and Interface Science **420**:35-40.
Liu, X. R., K. Eusterhues, J. Thieme, V. Ciobota, C. Hoschen, C. W. Mueller, K. Kusel, I. Kogel-Knabner, P. Rosch, J. Popp, and K. U. Totsche. 2013. STXM and NanoSIMS Investigations on EPS Fractions before and after Adsorption to Goethite. Environmental Science & Technology **47**:3158-3166.
Lorenz, K., R. Lal, C. M. Preston, and K. G. J. Nierop. 2007. Strengthening the soil organic carbon pool by increasing contributions from recalcitrant aliphatic bio(macro)molecules. Geoderma **142**:1-10.
Lunsdorf, H., R. W. Erb, W. R. Abraham, and K. N. Timmis. 2000. 'Clay hutches': a novel interaction between bacteria and clay minerals. Environmental Microbiology **2**:161-168.
Lynch, J. M., and J. M. Whipps. 1990. SUBSTRATE FLOW IN THE RHIZOSPHERE. Plant and Soil **129**:1-10.
Mackinnon, I. D. R., P. J. R. Uwins, A. Yago, and D. Page. 1993. Kaolinite particle sizes in the less-than-2-mu-m range using laser scattering. Clays and Clay Minerals **41**:613-623.
Martin, B. D., D. Witten, and A. D. Willis. 2020. Modeling microbial abundances and dysbiosis with beta-binomial regression. Ann. Appl. Stat. **14**:94-115.
Martin, M. 2011. Cutadapt removes adapter sequences from high-throughput sequencing reads. EMBnet.journal; Vol 17, No 1: Next Generation Sequencing Data Analysis.
Mbey, J. A., F. Thomas, A. Razafitianamaharavo, C. Caillet, and F. Villieras. 2019. A comparative study of some kaolinites surface properties. Applied Clay Science **172**:135-145.
McMurdie, P. J., and S. Holmes. 2013. phyloseq: An R Package for Reproducible Interactive Analysis and Graphics of Microbiome Census Data. PLos One **8**.
Mikutta, R., M. Kleber, M. S. Torn, and R. Jahn. 2006. Stabilization of soil organic matter: Association with minerals or chemical recalcitrance? Biogeochemistry **77**:25-56.

Miltner, A., P. Bombach, B. Schmidt-Brücken, and M. Kästner. 2012. SOM genesis: microbial biomass as a significant source. Biogeochemistry **111**:41-55.

Mueller, C. W., A. Kolbl, C. Hoeschen, F. Hillion, K. Heister, A. M. Herrmann, and I. Kogel-Knabner. 2012. Submicron scale imaging of soil organic matter dynamics using NanoSIMS - From single particles to intact aggregates. Organic Geochemistry **42**:1476-1488.

Mueller, C. W., P. K. Weber, M. R. Kilburn, C. Hoeschen, M. Kleber, and J. Pett-Ridge. 2013. Advances in the Analysis of Biogeochemical Interfaces: NanoSIMS to Investigate Soil Microenvironments. Pages 1-46 *in* D. L. Sparks, editor. Advances in Agronomy, Vol 121.

Nguyen, N. H., D. Smith, K. Peay, and P. Kennedy. 2015. Parsing ecological signal from noise in next generation amplicon sequencing. New Phytol **205**:1389-1393.

Nuccio, E. E., J. Anderson-Furgeson, K. Y. Estera, J. Pett-Ridge, P. de Valpine, E. L. Brodie, and M. K. Firestone. 2016. Climate and edaphic controllers influence rhizosphere community assembly for a wild annual grass. Ecology **97**:1307-1318.

Nuccio, E. E., A. Hodge, J. Pett-Ridge, D. J. Herman, P. K. Weber, and M. K. Firestone. 2013. An arbuscular mycorrhizal fungus significantly modifies the soil bacterial community and nitrogen cycling during litter decomposition. Environmental Microbiology **15**:1870-1881.

Nuccio, E. E., E. Starr, U. Karaoz, E. L. Brodie, J. Zhou, S. G. Tringe, R. R. Malmstrom, T. Woyke, J. F. Banfield, M. K. Firestone, and J. Pett-Ridge. 2020. Niche differentiation is spatially and temporally regulated in the rhizosphere. ISME J **14**:999-1014.

Oksanen, J., F. G. Blanchet, M. Friendly, R. Kindt, P. Legendre, D. McGlinn, P. R. Minchin, R. B. O'Hara, G. L. Simpson, P. Solymos, M. H. H. Stevens, E. Szoecs, and H. Wagner. 2019. vegan: Community Ecology Package. R package.

Olukoshi, E. R., and N. M. Packter. 1994. Importance of stored triacylglycerols in Streptomyces: possible carbon source for antibiotics. Microbiology **140 (Pt 4)**:931-943.

Palmer, J. M., M. A. Jusino, M. T. Banik, and D. L. Lindner. 2018. Non-biological synthetic spike-in controls and the AMPtk software pipeline improve mycobiome data. PeerJ **6**:e4925-e4925.

Paul, E. A. 2016. The nature and dynamics of soil organic matter: Plant inputs, microbial transformations, and organic matter stabilization. Soil Biology and Biochemistry **98**:109-126.

Pedregosa, F., G. Varoquaux, A. Gramfort, V. Michel, B. Thirion, and e. al. 2011. Scikit-learn: machine learning in python. ournal of machine learning research **12**:2825–2830.

Pett-Ridge, J., and M. K. Firestone. 2017. Using stable isotopes to explore root-microbe-mineral interactions in soil. Rhizosphere **3**:244-253.

Pett-Ridge, J., J. Shi, K. Estera-Molina, E. E. Nuccio, M. Yuan, R. Rijkers, T. Swenson, K. Zhalnina, T. R. Northen, J. Zhou, and M. K. Firestone. 2020 (in press). Rhizosphere carbon turnover from cradle to grave: the role of microbe-plant interactions.*in* V. Gupta and A. K. Sharma, editors. Rhizosphere Biology: Interactions with Plants. Springer Nature Press.

Pett-Ridge, J., and P. K. Weber. 2012. NanoSIP: NanoSIMS Applications for Microbial Biology. Pages 375-408 *in* A. Navid, editor. Microbial Systems Biology: Methods and Protocols. Humana Press, Totowa, NJ.

Philippot, L., J. M. Raaijmakers, P. Lemanceau, and W. H. van der Putten. 2013. Going back to the roots: the microbial ecology of the rhizosphere. Nature Reviews Microbiology **11**:789-799.
Pinheiro, J., D. Bates, S. DebRoy, D. Sarkar, and R. C. Team. 2019. nlme: Linear and Nonlinear Mixed Effects Models. R package version 3.1-139.
Pitt, J. I. 2014. PENICILLIUM | Penicillium and Talaromyces:: Introduction. Pages 6-13 *in* C. A. Batt and M. L. Tortorello, editors. Encyclopedia of Food Microbiology (Second Edition). Academic Press, Oxford.
Placella, S. A., E. L. Brodie, and M. K. Firestone. 2012. Rainfall-induced carbon dioxide pulses result from sequential resuscitation of phylogenetically clustered microbial groups. Proceedings of the National Academy of Sciences **109**:10931.
Pluskal, T., S. Castillo, A. Villar-Briones, and M. Oresic. 2010. MZmine 2: modular framework for processing, visualizing, and analyzing mass spectrometry-based molecular profile data. BMC bioinformatics **11**:395-395.
Poger, D., and A. E. Mark. 2015. A Ring to Rule Them All: The Effect of Cyclopropane Fatty Acids on the Fluidity of Lipid Bilayers. Journal of Physical Chemistry B **119**:5487-5495.
Porras, R. C., C. E. Hicks Pries, M. S. Torn, and P. S. Nico. 2018. Synthetic iron (hydr)oxide-glucose associations in subsurface soil: Effects on decomposability of mineral associated carbon. Science of the Total Environment **613-614**:342-351.
Quast, C., E. Pruesse, P. Yilmaz, J. Gerken, T. Schweer, P. Yarza, J. Peplies, and F. O. Glöckner. 2012. The SILVA ribosomal RNA gene database project: improved data processing and web-based tools. Nucleic Acids Research **41**:D590-D596.
Rasse, D. P., C. Rumpel, and M. F. Dignac. 2005. Is soil carbon mostly root carbon? Mechanisms for a specific stabilisation. Plant and Soil **269**:341-356.
Ravel, B., and M. Newville. 2005. ATHENA, ARTEMIS, HEPHAESTUS: data analysis for X-ray absorption spectroscopy using IFEFFIT. Journal of Synchrotron Radiation **12**:537-541.
Rivers, A. R., K. C. Weber, T. G. Gardner, S. Liu, and S. D. Armstrong. 2018. ITSxpress: Software to rapidly trim internally transcribed spacer sequences with quality scores for marker gene analysis. F1000Research **7**:1418-1418.
Roose, T., and A. C. Fowler. 2004. A mathematical model for water and nutrient uptake by plant root systems. Journal of Theoretical Biology **228**:173-184.
Roose, T., and A. Schnepf. 2008. Mathematical models of plant-soil interaction. Philosophical Transactions of the Royal Society a-Mathematical Physical and Engineering Sciences **366**:4597-4611.
Ross, G. L., and C. Wang. 1993. Extractable Al, Fe, Mn and Si. Pages 239-246 *in* M. R. Carter, editor. Soil Sampling and Methods of Analysis. Lewis Publication, Boca Raton.
Schaefer, M. V., N. A. Bogie, D. Rath, A. R. Marklein, A. Garniwan, T. Haensel, Y. Lin, C. C. Avila, P. S. Nico, K. M. Scow, E. L. Brodie, W. J. Riley, M. L. Fogel, A. A. Berhe, T. A. Ghezzehei, S. Parikh, M. Keiluweit, and S. C. Ying. 2020. Effect of Cover Crop on Carbon Distribution in Size and Density Separated Soil Aggregates. Soil Systems **4**.
Schimel, J. P. 2018. Life in Dry Soils: Effects of Drought on Soil Microbial Communities and Processes. Annual Review of Ecology, Evolution, and Systematics **49**:409-432.
Schimel, J. P., and S. M. Schaeffer. 2012. Microbial control over carbon cycling in soil. Frontiers in Microbiology **3**.

Schlatter, D., A. Fubuh, K. Xiao, D. Hernandez, S. Hobbie, and L. Kinkel. 2009. Resource Amendments Influence Density and Competitive Phenotypes of Streptomyces in Soil. Microbial Ecology **57**:413-420.

Schmidt, M. W. I., M. S. Torn, S. Abiven, T. Dittmar, G. Guggenberger, I. A. Janssens, M. Kleber, I. Kogel-Knabner, J. Lehmann, D. A. C. Manning, P. Nannipieri, D. P. Rasse, S. Weiner, and S. E. Trumbore. 2011. Persistence of soil organic matter as an ecosystem property. Nature **478**:49-56.

Schroth, B. K., and G. Sposito. 1997. Surface charge properties of kaolinite. Clays and Clay Minerals **45**:85-91.

Schweinsberg-Mickan, M. S. Z., R. G. Joergensen, and T. Mueller. 2012. Rhizodeposition: Its contribution to microbial growth and carbon and nitrogen turnover within the rhizosphere. Journal of Plant Nutrition and Soil Science **175**:750-760.

Shi, S., E. Nuccio, D. J. Herman, R. Rijkers, K. Estera, J. Li, U. N. da Rocha, Z. He, J. Pett-Ridge, E. L. Brodie, J. Zhou, and M. Firestone. 2015a. Successional Trajectories of Rhizosphere Bacterial Communities over Consecutive Seasons. Mbio **6**.

Shi, S., A. E. Richardson, M. O'Callaghan, K. M. DeAngelis, E. E. Jones, A. Stewart, M. K. Firestone, and L. M. Condron. 2011. Effects of selected root exudate components on soil bacterial communities. Fems Microbiology Ecology **77**:600-610.

Shi, S. J., E. Nuccio, D. J. Herman, R. Rijkers, K. Estera, J. B. Li, U. N. da Rocha, Z. L. He, J. Pett-Ridge, E. L. Brodie, J. Z. Zhou, and M. Firestone. 2015b. Successional Trajectories of Rhizosphere Bacterial Communities over Consecutive Seasons. Mbio **6**.

Shi, S. J., E. E. Nuccio, Z. J. Shi, Z. L. He, J. Z. Zhou, and M. K. Firestone. 2016. The interconnected rhizosphere: High network complexity dominates rhizosphere assemblages. Ecology Letters **19**:926-936.

Shi, Z., S. D. Allison, Y. He, P. A. Levine, A. M. Hoyt, J. Beem-Miller, Q. Zhu, W. R. Wieder, S. Trumbore, and J. T. Randerson. 2020. The age distribution of global soil carbon inferred from radiocarbon measurements. Nature Geoscience **13**:555-559.

Siliakus, M. F., J. van der Oost, and S. W. M. Kengen. 2017. Adaptations of archaeal and bacterial membranes to variations in temperature, pH and pressure. Extremophiles **21**:651-670.

Six, J., R. T. Conant, E. A. Paul, and K. Paustian. 2002. Stabilization mechanisms of soil organic matter: Implications for C-saturation of soils. Plant and Soil **241**:155-176.

Six, J., S. D. Frey, R. K. Thiet, and K. M. Batten. 2006. Bacterial and fungal contributions to carbon sequestration in agroecosystems. Soil Science Society of America Journal **70**:555-569.

Sohlenkamp, C., and O. Geiger. 2016. Bacterial membrane lipids: diversity in structures and pathways. FEMS Microbiology Reviews **40**:133-159.

Sokol, N. W., S. E. Kuebbing, E. Karlsen-Ayala, and M. A. Bradford. 2019a. Evidence for the primacy of living root inputs, not root or shoot litter, in forming soil organic carbon. New Phytologist **221**:233-246.

Sokol, N. W., J. Sanderman, and M. A. Bradford. 2019b. Pathways of mineral-associated soil organic matter formation: Integrating the role of plant carbon source, chemistry, and point of entry. Global Change Biology **25**:12-24.

Sollins, P., C. Swanston, M. Kleber, T. Filley, M. Kramer, S. Crow, B. A. Caldwell, K. Lajtha, and R. Bowden. 2006. Organic C and N stabilization in a forest soil: Evidence from sequential density fractionation. Soil Biology & Biochemistry **38**:3313-3324.

Solomon, D., J. Lehmann, J. Harden, J. Wang, J. Kinyangi, K. Heymann, C. Karunakaran, Y. S. Lu, S. Wirick, and C. Jacobsen. 2012. Micro- and nano-environments of carbon sequestration: Multi-element STXM-NEXAFS spectromicroscopy assessment of microbial carbon and mineral associations. Chemical Geology **329**:53-73.

Sposito, G. 2008. The chemistry of soils. 2nd edition. Oxford University Press, Oxford ; New York.

Starr, E. P., E. E. Nuccio, J. Pett-Ridge, J. F. Banfield, and M. K. Firestone. 2019. Metatranscriptomic reconstruction reveals RNA viruses with the potential to shape carbon cycling in soil. Proceedings of the National Academy of Sciences of the United States of America **116**:25900-25908.

Starr, E. P., S. J. Shi, S. J. Blazewicz, A. J. Probst, D. J. Herman, M. K. Firestone, and J. F. Banfield. 2018. Stable isotope informed genome-resolved metagenomics reveals that Saccharibacteria utilize microbially-processed plant-derived carbon. Microbiome **6**.

Stewart, C. E., K. Paustian, R. T. Conant, A. F. Plante, and J. Six. 2007. Soil carbon saturation: concept, evidence and evaluation. Biogeochemistry **86**:19-31.

Stockmann, U., M. A. Adams, J. W. Crawford, D. J. Field, N. Henakaarchchi, M. Jenkins, B. Minasny, A. B. McBratney, V. D. de Courcelles, K. Singh, I. Wheeler, L. Abbott, D. A. Angers, J. Baldock, M. Bird, P. C. Brookes, C. Chenu, J. D. Jastrow, R. Lal, J. Lehmann, A. G. O'Donnell, W. J. Parton, D. Whitehead, and M. Zimmermann. 2013. The knowns, known unknowns and unknowns of sequestration of soil organic carbon. Agriculture Ecosystems & Environment **164**:80-99.

Sudderth, E. A., S. B. St Clair, S. A. Placella, S. M. Swarbreck, C. Castanha, D. J. Herman, M. L. Fischer, M. Kleber, E. B. Sudderth, M. S. Torn, M. K. Firestone, G. L. Andersen, and D. D. Ackerly. 2012. Annual grassland resource pools and fluxes: sensitivity to precipitation and dry periods on two contrasting soils. Ecosphere **3**.

Sulman, B. N., J. A. M. Moore, R. Abramoff, C. Averill, S. Kivlin, K. Georgiou, B. Sridhar, M. D. Hartman, G. S. Wang, W. R. Wieder, M. A. Bradford, Y. Q. Luo, M. A. Mayes, E. Morrison, W. J. Riley, A. Salazar, J. P. Schimel, J. Y. Tang, and A. T. Classen. 2018. Multiple models and experiments underscore large uncertainty in soil carbon dynamics. Biogeochemistry **141**:109-123.

Sung, G.-H., N. L. Hywel-Jones, J.-M. Sung, J. J. Luangsa-ard, B. Shrestha, and J. W. Spatafora. 2007. Phylogenetic classification of Cordyceps and the clavicipitaceous fungi. Studies in Mycology **57**:5-59.

Tamura, M., V. Suseela, M. Simpson, B. Powell, and N. Tharayil. 2017. Plant litter chemistry alters the content and composition of organic carbon associated with soil mineral and aggregate fractions in invaded ecosystems. Global Change Biology **23**:4002-4018.

Tang, J. Y., and W. J. Riley. 2015. Weaker soil carbon-climate feedbacks resulting from microbial and abiotic interactions. Nature Climate Change **5**:56-60.

Taylor, D. L., W. A. Walters, N. J. Lennon, J. Bochicchio, A. Krohn, J. G. Caporaso, and T. Pennanen. 2016. Accurate Estimation of Fungal Diversity and Abundance through Improved Lineage-Specific Primers Optimized for Illumina Amplicon Sequencing. Appl Environ Microbiol **82**:7217-7226.

Tfaily, M. M., R. M. Wilson, H. M. Brewer, R. K. Chu, H. M. Heyman, D. W. Hoyt, J. E. Kyle, and S. O. Purvine. 2019. Single-throughput Complementary High-resolution Analytical Techniques for Characterizing Complex Natural Organic Matter Mixtures. J. Vis. Exp. **143**.

Torn, M. S., M. Kleber, E. S. Zavaleta, B. Zhu, C. B. Field, and S. E. Trumbore. 2013. A dual isotope approach to isolate soil carbon pools of different turnover times. Biogeosciences **10**:8067-8081.
Torn, M. S., S. E. Trumbore, O. A. Chadwick, P. M. Vitousek, and D. M. Hendricks. 1997. Mineral control of soil organic carbon storage and turnover. Nature **389**:170-173.
Trumbore, S. 2000. Age of soil organic matter and soil respiration: radiocarbon constraints on belowground c dynamics. Ecological Applications **10**:399-411.
Unger, S., C. Máguas, J. S. Pereira, T. S. David, and C. Werner. 2010. The influence of precipitation pulses on soil respiration – Assessing the "Birch effect" by stable carbon isotopes. Soil Biology and Biochemistry **42**:1800-1810.
Uroz, S., C. Calvaruso, M.-P. Turpault, and P. Frey-Klett. 2009. Mineral weathering by bacteria: ecology, actors and mechanisms. Trends in Microbiology **17**:378-387.
Uroz, S., L. C. Kelly, M.-P. Turpault, C. Lepleux, and P. Frey-Klett. 2015. The Mineralosphere Concept: Mineralogical Control of the Distribution and Function of Mineral-associatec Bacterial Communities. Trends in Microbiology **23**:751-762.
Van Krevelen, D. W. 1950. Graphical-Statistical Method for the Study of Structure and Reaction Processes of Coal. Fuel **29**:269-228.
Vidal, A., J. Hirte, S. F. Bender, J. Mayer, A. Gattinger, C. Hoschen, S. Schadler, T. M. Iqbal, and C. W. Mueller. 2018. Linking 3D Soil Structure and Plant-Microbe-Soil Carbon Transfer in the Rhizosphere. Frontiers in Environmental Science **6**.
Vogel, C., C. W. Mueller, C. Hoschen, F. Buegger, K. Heister, S. Schulz, M. Schloter, and I. Kogel-Knabner. 2014. Submicron structures provide preferential spots for carbon and nitrogen sequestration in soils. Nature Communications **5**.
Wan, J., T. Tyliszczak, and T. K. Tokunaga. 2007. Organic carbon distribution, speciation, and elemental correlations within soil microaggregates: applications of STXM and NEXAFS spectroscopy.
Wang, X. M., M. Q. Zhu, L. K. Koopal, W. Li, W. Q. Xu, F. Liu, J. Zhang, Q. S. Liu, X. H. Feng, and D. L. Sparks. 2016. Effects of crystallite size on the structure and magnetism of ferrihydrite. Environmental Science-Nano **3**:190-202.
Wang, Y., P. Griffin, K. Jin, M. L. Fogel, A. Steele, and G. D. Cody. 2013. Tracing H isotope effects in the dynamic metabolic network using multi-nuclear (1H, 2H and 13C) solid state NMR and GC–MS. Organic Geochemistry **57**:84-94.
Weete, J. D., D. J. Weber, and J. L. Laseter. 1970. Lipids of Rhizopus arrhizus Fischer. Journal of bacteriology **103**:536-540.
Whitman, T., R. Neurath, A. Perera, D. Ning, J. Z. Zhou, P. Nico, J. Pett-Ridge, and M. Firestone. 2018. Microbial community assembly differs across mineral types in a rhizosphere microcosm. Environmental Microbiology **20**:4444-4460.
Willis, A. 2016. Species richness estimation with high diversity but spurious singletons.
Woolet, J., and T. Whitman. 2020. Pyrogenic organic matter effects on soil bacterial community composition. Soil Biology and Biochemistry **141**:107678.
Wright, E. S. 2016. Using DECIPHER v2.0 to Analyze Big Biological Sequence Data in R. The R Journal **8**:352-359.
Wu, L., C. Wen, Y. Qin, H. Yin, Q. Tu, J. D. Van Nostrand, T. Yuan, M. Yuan, Y. Deng, and J. Zhou. 2015. Phasing amplicon sequencing on Illumina Miseq for robust environmental microbial community analysis. BMC Microbiology **15**:125.

Yang, Y., F. Heidari, and B. Hu. 2019. Fungi (Mold)-Based Lipid Production. Methods Mol Biol **1995**:51-89.

Yilmaz, P., L. W. Parfrey, P. Yarza, J. Gerken, E. Pruesse, C. Quast, T. Schweer, J. Peplies, W. Ludwig, and F. O. Glöckner. 2013. The SILVA and "All-species Living Tree Project (LTP)" taxonomic frameworks. Nucleic Acids Research **42**:D643-D648.

Zelles, L. 1997. Phospholipid fatty acid profiles in selected members of soil microbial communities. Chemosphere **35**:275-294.

Zhalnina, K., K. B. Louie, Z. Hao, N. Mansoori, U. N. da Rocha, S. J. Shi, H. J. Cho, U. Karaoz, D. Loque, B. P. Bowen, M. K. Firestone, T. R. Northen, and E. L. Brodie. 2018. Dynamic root exudate chemistry and microbial substrate preferences drive patterns in rhizosphere microbial community assembly. Nature Microbiology **3**:470-480.